Politecnico di Torino

Corso di Laurea Magistrale in Ingegneria per l'Ambiente ed il Territorio
Master course in Industrial Environmental Sustainability
A.Y. 2025/2026
Sessione di Laurea Marzo 2026

# Integrated Water Resources Management with WEAP model application: Assessment of new infrastructures in the Orco Valley


Relatore:
Poggi Davide
Co-relatori
Alfano Maria Elena
Lucca Enrico

Candidato:
Stefano Debernardis
Matricola s332785

# ABSTRACT

Water resources management represents a particularly complex challenge in mountainous contexts, where climate change and increasing water demand exert additional pressure on hydrological systems.
This thesis aims to analyze how water resource management is influenced and reshaped by the construction of new hydraulic infrastructures in the Orco River basin, located in northwestern Piedmont at the foot of the Southern Graian Alps.
The study area was represented and modelled using the WEAP (Water Evaluation and Adaptation Planning) software.
WEAP is a software tool used for hydrological modeling that supports water resource planning through alternative scenarios based on different water allocation strategies.
The implemented scenarios include the introduction of the new Valle Orco aqueduct and a new reservoir on the Soana River.
The climatic data were derived from ARPA meteorological stations within the basin and from the Copernicus ERA5 dataset for the period 2012–2024, according to the hydrological calendar.
The results highlight the impacts generated by the new infrastructures, showing variations in irrigation deficits and hydropower production under different water allocation strategies.
In particular, the construction of the new reservoir led to increased hydropower generation and reduced irrigation deficits during the simulation period.
Overall, the study confirms the validity and practical relevance of integrated hydrological modelling as a support tool for new infrastructures assessment and improvement of different water allocation strategies in complex mountain environments subjected to hydrological pressures.

# LIST OF TABLES

# LIST OF FIGURES

# SUMMARY

# 1) Introduction

Nowadays, water resources management is one of the most important challenges we face.
In fact, climate change, rapid expansion of irrigation, increasing water demand for industrial purposes, land use and hydroelectric energy production pose many risks about the availability of water supply and security in a large part of the world *(Mekonnen and Getu, 2025)*.
These combined factors have increased the pressure on this topic, pushing researchers for new approaches and techniques.
For these reasons, traditional methods give way to modern approaches like Integrated Watershed modeling and simulation.

In fact, according to *Loucks and van Beek (2017)*, water systems are both characterized by a purely hydrological section and a human based one, which is defined following the water allocation rules, sectorial water resource competition, regional regulations and water demand for human purposes.
To this end, many software tools, like WEAP, MODSIM-DSS, MIKE HYDRO and SWAT-MODFLOW, have been developed through years to support these new analysis approaches.
In this way, it is possible to find a compromise between water use and the preservation of environmental flows and ecosystems.

However, the modeling of a mountainous basin poses additional complexity to this challenge.
Their hydrological behavior is strongly affected by its heterogeneous and steep topography, sudden and rapid changes in elevation, glacier melting routines, snow accumulation and melting process and finally by climate conditions.
Furthermore, more complexity is characterized by the presence of lakes, artificial reservoirs and hydropower infrastructures, like dams, forced conducts and gauge stations along the river's course.

To deal with these challenges, the use of modeling software such as WEAP (Water Evaluation and Planning System) is a solid resource.
WEAP is an integrated water resources software tool that includes modules used to simulate hydrological processes and infrastructure operations (*Yates et al., 2005a, Yates et al., 2005b*), giving the possibility of building a hydrological model

that can be used to simulate and evaluate the trade-offs between the internal sectors implemented in the watershed.
WEAP's structure is particularly useful also for the possibility of analyzing different scenarios simply by changing demand priorities or modifying the water supply according to the climate conditions.

This thesis has a dual goal.
Firstly, the main aim is to carry out a detailed analysis of the possible water resource management dynamics characterizing the Orco Valley catchment, located in the North-Western part of the Piedmont region, and the evaluation of the impacts generated by the introduction of new infrastructures within the basin. Secondly, it also aims to verify if a different watershed and Hydrological Response Units (HRUs) configuration compared to the methodology approach adopted by *Lucca (2025)*, which follows the methodology used by *Young et al. (2009)*, can equally lead to satisfactory and consistent results.

The hydrological model developed using WEAP will be calibrated through a comparison between the modeled data and the observed data from the hydrological gauge stations located along Orco river, the snow gauge stations and the observed volume of Ceresole reservoir.

Finally, different scenarios characterized by the introduction of new infrastructures and different water allocation strategies will be simulated in order to evaluate water availability for energetic, urban and agricultural purposes and for environmental sustainability.

# 2) Study Area

## 2.1) Orco Valley general description

The Orco Valley river basin is an alpine catchment located in the Graian Alps, within the Piedmont region of northwestern Italy (*Figure 1*).
It covers an area of approximately 910 km² and follows the eastward course of the Orco River, extending from the Colle del Nivolet (2,612 m a.s.l.) down to the Canavese plain (about 181 m a.s.l.).
The basin is bounded to the north by the alpine ridge that separates it from the Aosta Valley, and to the south by the mountain chain dividing it from the Lanzo Valleys.
Its altitudinal range is wide, spanning from 181 m a.s.l. at the confluence of the Orco River with the Po River, up to 3,672 m a.s.l. in the western mountainous sector that borders with France and the Aosta Valley.

From the climatic point of view, the Orco Valley exhibits significant variability driven primarily by altitude. In the higher sections of the valley, such as around Ceresole Reale, winters are long and cold, with frequent snowfall and extended periods of sub-zero temperatures. In contrast, the lower-altitude areas experience milder conditions, typically showing a temperature increase of about 2–3 °C (*Arpa Piemonte, historical data series*).
Summer climate patterns follow a similar gradient: the upper valley remains fresh even at the peak of the season, while the eastern lower portion of the valley becomes progressively drier and warmer.

Looking at the hydrological aspect, the main river of the basin is the Orco stream, which as previously mentioned, crosses the valley from the west to the east side of the valley.
The other waterways of the basin are mainly the Orco's tributaries like Soana stream, which flows into the Orco river at Ronco Canavese.
The basin has also many glaciers, like Ciardoney, which take part to the hydrological aspect of the valley with a total surface area of 5.64 km^2 (Smiraglia and Azzoni, 2015).

The hydrological aspect of the basin has a relevant role in energy production.
In fact, from the first years of the 1930's until the 1960's, several artificial reservoirs were developed with a total storage capacity around 86 million m^3 and a total

installed capacity around 300 MW. All the reservoirs and the hydroelectric stations are managed by IREN (Iren S.p.A., 2022).

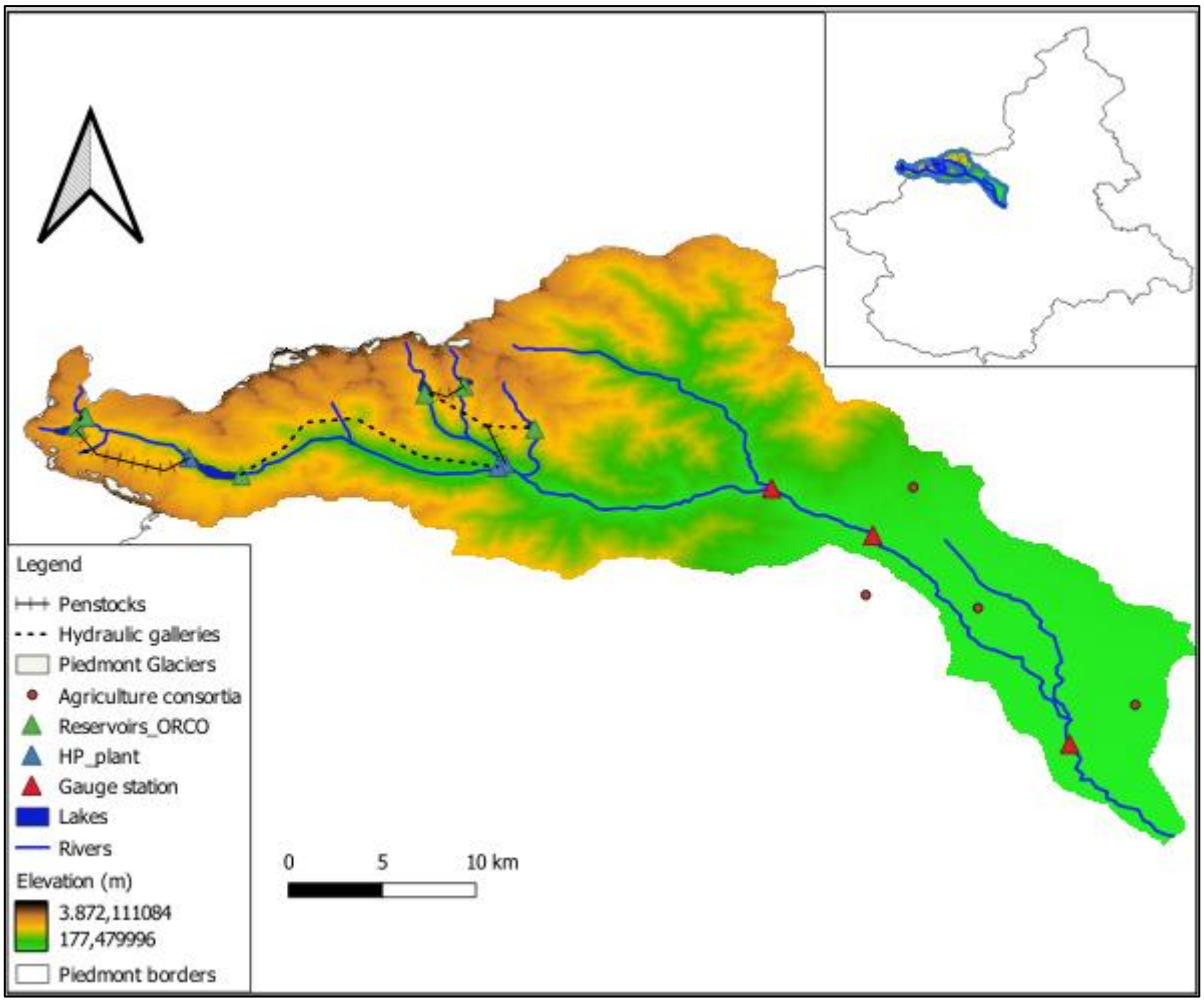


*Figure 1: Valle Orco river basin.*

Finally, in terms of land cover, the valley is mainly characterized by larch and spruce woods, bare soil in the higher elevation areas and range lands.
There is also a small percentage of soil which is covered by wetlands, medium density urban areas and agricultural fields.

## 2.2) Description of Valle Orco's Hydroelectric system

As previously mentioned, Valle Orco basin has many advantages for hydroelectric energy production.
The hydroelectric system of the valley that falls under IREN administration is characterized by three main plant complexes:

- Agnel-Serrù-Villa;
- Ceresole-Rosone;
- Telessio-Eugio-Rosone;

The total capacity of the whole reservoirs is around 86 million m^3, and a total installed power of 300 MW.
Considering seasonal variations, the total energy system can produce around 670 GWh each year.
The plant complex is composed of 6 different reservoirs, whose volume data are reported in the table below:

| **Reservoir** | **Volume ($Mm^3$)** | **Elevation (m.a.s.l.)** |
|---|---|---|
| Agnel | 2,1 | 2300 |
| Serrù | 14,5 | 2250 |
| Teleccio | 23,5 | 1918 |
| Eugio | 5,14 | 1908 |
| Ceresole | 36,2 | 1520 |
| Valsoera | 7,77 | 2414 |

*Table 1: Volume of main Orco Valley reservoirs.*

## 2.3) Working principle of the plant complex system

The plant complex is based on a system of hydraulic galleries that connect the reservoirs to convey the stored water to the power stations (*Figure 2*).
To convey water to the stations, firstly, a system of free surface galleries and pressurized galleries is used.
This gallery system is necessary to collect additional water that comes from runoff water or other secondary waterways.
Then, water is conveyed into penstocks to the local power station.

In the first part of the plant complex, water is transferred from Agnel reservoir to Serrù reservoir through a free-surface tunnel.
From Serrù reservoir, water enters in a pressurized water tunnel, collecting water from nearby secondary waterways.
Then, water is conveyed into penstocks to the Villa's power station, where it is turbinated and discharged into Ceresole reservoir.
At this point, another free-surface gallery starts its path from the reservoir to reach Rosone's power station.
Here, water can be directly discharged into the Orco river or conveyed at Bardonetto's run-of-river-plant.

On the other hand, the second part of the plant complex is composed by Valsoera, Telessio and Eugio reservoir.
Water is first conveyed from Valsoera reservoir to Telessio's power station, then is released in the homonymous reservoir.
A pumping system was installed to take water back to the Valsoera's reservoir, making water reusable for producing more energy to satisfy the peak demand of energy.
Water coming from Telessio and Eugio reservoir is conveyed through a diversion gallery into a single penstock section towards Rosone's power station.
This configuration produces a relevant hydraulic jump of 1192,82 m.

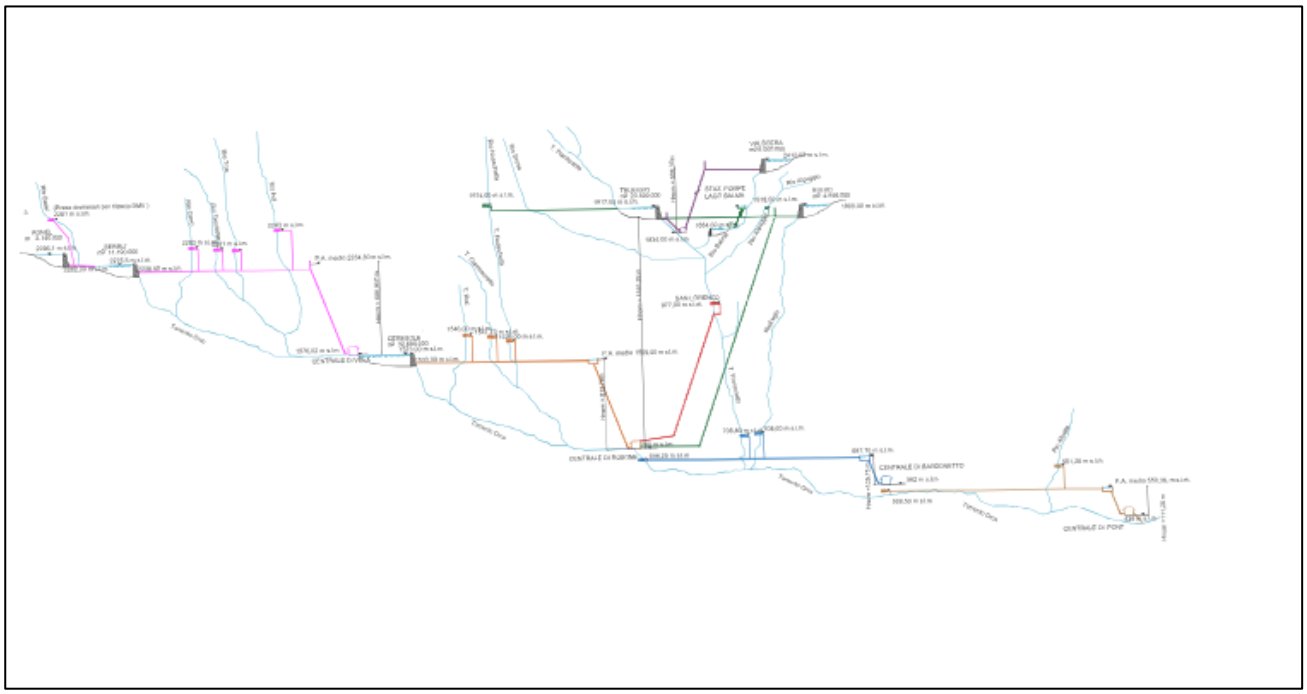

*Figure 2: Orco Valley hydraulic scheme elaborated by Maria Elena Alfano according to Iren S.p.A. technical reports (2022).*

# 3) Building the hydrological model

To perform the assessment analysis and evaluate new alternative strategies for trade-offs for water management, a hydrological simulation model has been built using software WEAP.
The building process of the model, however, took many steps and additional tasks in order to make it as realistic and functional as possible.
In this chapter, all the operations and processes that contributed to the model building are explained and shown in detail.
The definition of some model modules was based on the methodological approach adopted by *Lucca (2025)*.

## 3.1) Delineation of the Sub-basins and hydrological response units.

The first step in building the hydrological model consists in identifying the sub-basins that characterize the catchment and the assignment of the respective Hydrologic Response Units to each of them.
To do this, the QGIS software was used for its practicality in carrying out this preliminary operation.
To extract the sub-basins, a DEM (Digital Elevation Model) raster file of the valley was used, allowing the different elevation bands of the basin to be identified. Subsequently, the DEM was overlaid with a map taken from Google Earth in order to precisely locate the main surface water bodies and the rivers flowing through the valley.

Then, to identify the various sub-basins that characterize the valley, the *Upslope Area* function was used.
By using this function, QGIS recognizes and assigns all the values located at an elevation higher than the selected point.
In this case, the points selected for applying the *Upslope Area* function mainly correspond to the emissaries of the main surface water bodies, as well as the locations where the tributaries of the Orco River flow into it.

At the end of the procedure, a total of 11 sub-basins were identified, whose names and areas are reported in *Table 2*.

| Sub basin name | Extension ($km^2$) |
|---|---|
| Gauge_sub_basin | 116,470 |
| Sub_basin_eugio_diff | 9,228 |
| Sub_basin_Final | 309,578 |
| Sub_basin_Agnel | 10,999 |
| Sub_basin_Eugio | 9,816 |
| Sub_basin_Valsoera | 8,775 |
| Sub_basin_Serrù | 6,064 |
| Sub_basin_Teleccio | 15,536 |
| Sub_basin_Rosone | 139,120 |
| Sub_basin_Soana | 214,543 |
| Sub_basin_Ceresole | 68,51 |

Table 2: Valle Orco sub-basins and relative extension.

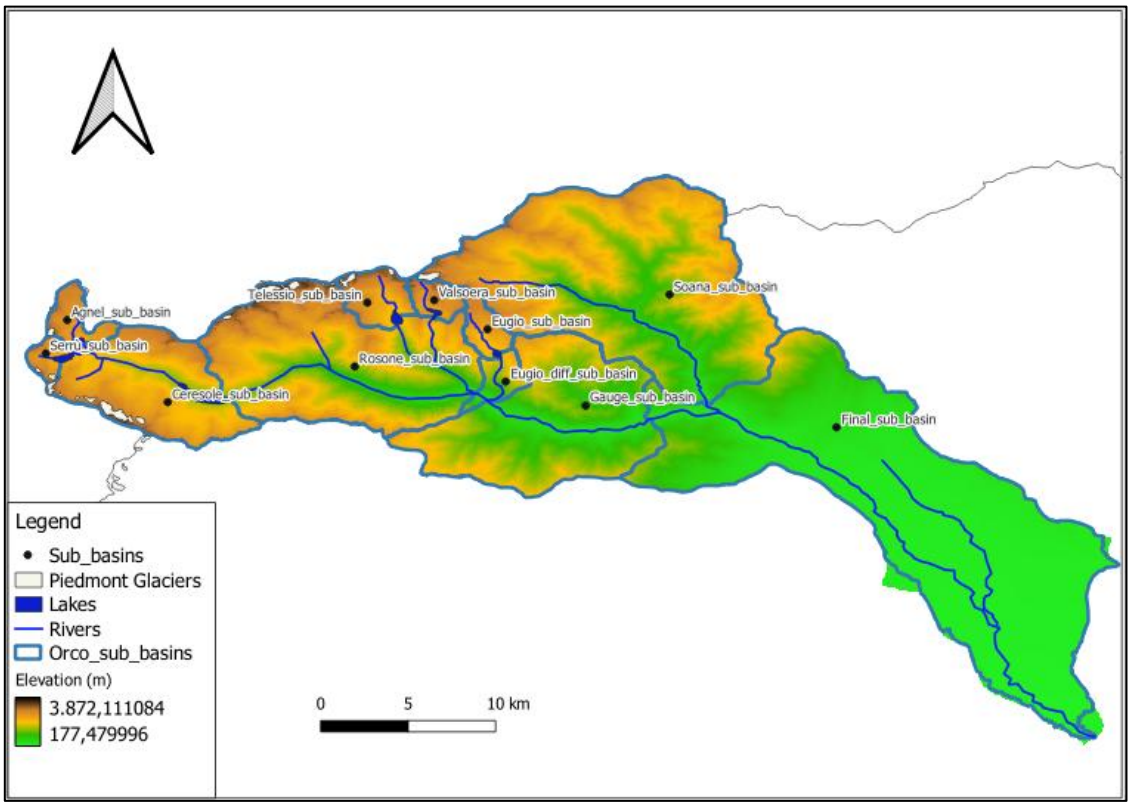


*Figure 3: Valle orco sub-basins delineated.*

As for the assignment of the Hydrological Response Units (HRUs), it is firstly necessary to define what they are. A Hydrological Response Unit represents an area within the basin where the hydrological response is homogeneous within its defined boundaries.

The subdivision of the basin into HRUs was carried out by importing into QGIS a shapefile generated using the SWAT software.
The *Soil and Water Assessment Tool (SWAT*) is a software tool used for hydrological modeling within a catchment area.
Its working principle is based on the simulation of hydrological processes that occur in the sub-basins and in the HRUs by using topographic, land use, soil type information and meteorological data based on their spatial position (*Arnold et al., 2012*).

The SWAT shapefile represents the surface of the entire Orco Valley, divided into a total of 1601 areas that share the same hydrological response.
For each of these areas, the land cover type, soil type, slope, and area are defined.
The following tables show the various soil types, slopes and land uses, and for each category the number of HRUs in which that characteristic was identified is reported.

| **Land use** | **Number of HRUs** |
|---|---|
| Agriculture (AGRL) | 72 |
| Forests (FRST) | 649 |
| Bare Soil (BARR) | 190 |
| Wetland (SWRN) | 55 |
| Range Land (RNGE) | 551 |
| Medium density urban areas (URMD) | 57 |
| Water (WATR) | 27 |

*Table 3: table with Land use categories and their respective HRUs in the catchment*

| **Soil Type** | **Number of HRUs** |
|---|---|
| Loam (L) | 945 |
| Clay I | 6 |
| Clay Loam (CL) | 317 |
| Sandy Loam (SL) | 52 |
| Sandy Clay Loam (SCL) | 72 |
| Silty Clay Loam (SICL) | 18 |
| Silty Loam (SIL) | 186 |
| Silty Clay (SIC) | 5 |

*Table 4: table that lists soil types and their respective HRUs in the catchment*

| Slope (%) | Number of HRUs |
|---|---|
| 0-10 | 417 |
| 10-20 | 146 |
| 20-25 | 105 |
| 25-30 | 106 |
| 30-35 | 127 |
| 35-50 | 271 |
| >50 | 429 |

*Table 5: table that lists the slope classes and their respective HRUs in the catchment*

The SWAT file from which the HRU information was derived (such as slope, area, soil type, and land use) did not contain data regarding HRU elevation. Elevation is an important parameter for the correct assignment of the most appropriate climatic variables.

Therefore, in order to obtain this additional information, the *Zonal Statistics* tool in QGIS was used.
This tool allows the assignment of values corresponding to a selected statistical measure to the attribute table of a shapefile.
By using the SWAT shapefile together with the DTM representing the Orco Valley as inputs to the tool, a new shapefile was obtained that also included the elevation of each HRU.
In this way, it was possible to derive the mean elevation of each sub-basin and to subdivide the valley into elevation bands.

Finally, the assignment of the HRUs to their respective sub-basins was carried out manually, since there was no correspondence between the sub-basins identified using QGIS and those into which the SWAT file had already been subdivided.

Specifically, the procedure was performed by selecting the cells representing the Hydrological Response Units in the attribute table of the SWAT file and then visualizing them on the map in order to assign each HRU to the sub-basin in which it was located.

### 3.2) Problems during the HRUs assignment

During the assignment of the HRUs, two main issues emerged:

- Some cells did not belong entirely to a single sub-basin;
- The total area of the HRUs contained in the SWAT file was smaller than the overall area of the basin.

Regarding the first issue, several HRUs were located in an intermediate position between two adjacent sub-basins, making their assignment more complex. To address this problem, it was ultimately decided to assign each HRU to the sub-basin containing the largest portion of its area.
Although this approach simplified the issue related to assigning the cell to a specific sub-basin, it resulted in a slight reduction in the total area of the adjacent sub-basin.

On the other hand, when comparing the areas reported in *Table 2* with the total area obtained by summing the HRUs within their respective sub-basins, discrepancies were observed.
This mismatch is mainly due to the fact that the SWAT shapefile reports a total valley area smaller than that derived from the DTM file.
Additional area differences also arise from the issue previously described.

To resolve the problem, it was decided to increase the area of the various HRUs by adding a value calculated as follows:

- Computation of the area difference between the values reported in *Table 2* and the sum of the HRUs within the respective basins;
- Calculation of the percentage of the total missing area;
- Calculation of the percentage of basin area represented by each individual HRU;
- Multiplication of the latter by the total missing area;
- Addition of the resulting value to the area of the corresponding HRU.

In this way, the summed areas are now consistent and completely matched.

## 3.3) WEAP's hydrological model.

### 3.3.1) Introduction to WEAP software

WEAP is a software tool designed for planning purposes and allows the adoption of an integrated approach to water resources management. The model implemented within the software is intended to bridge the gap between water resources management and basin-scale hydrology, while meeting the requirement that an effective Integrated Water Resources Management (IWRM) model should be reliable, user-friendly, and readily available to the scientific and technical community (*Yates et al., 2005a*).

In its WEAP21 version, the tool integrates a comprehensive set of hydrological processes with the management of water demand and infrastructure installed within the watershed, ensuring a coherent representation of the system (*Yates et al., 2005a*).
A relevant advantage of the software is the possibility of analyzing the river basin through the implementation of different scenarios. These scenarios can be multiple and include various types of changes, such as climate-related variations, land-use changes, increases or decreases in water demand, and particularly the assignment of different priority levels.

Of particular importance in scenario analysis is the concept of priority.
Through this functionality, the model assigns numerical values to define which demand sites have the highest priority. Essentially, the higher the numerical value, the lower the priority assigned to a specific demand node, and vice versa.

However, the concept of priority will be further discussed in *Section 4*, where the scenarios implemented in the hydrological model developed for this thesis will be introduced and described.

### 3.3.2) Catchment organization.

WEAP operates according to the principle of water mass balance within a river basin, in which the components of the system are represented through nodes and links. Water sources, such as reservoirs, are represented as nodes, while locations where water supply is required, such as hydroelectric plants or urban areas, are represented as demand sites. Demand sites are connected to water resource nodes through specific connection links.

The structure of the model related to the organization of the river basin is arranged according to a tree-based scheme, in which each branch is subdivided into further sub-branches. According to this organization, the model is mainly developed through two main tree structures:

- ***Key Assumptions***;
- ***Demand Sites and Catchments***.

Within the *Key Assumptions* section, in addition to climatic data from meteorological stations, all hydrological variables that determine and influence the hydrological behavior of the Hydrological Response Units (HRUs) within each sub-catchment are reported (*Section 3.3.4*). The *Demand Sites and Catchments* section, on the other hand, includes all sub-basins with their respective HRUs, as well as the demand sites that have been implemented within the model.

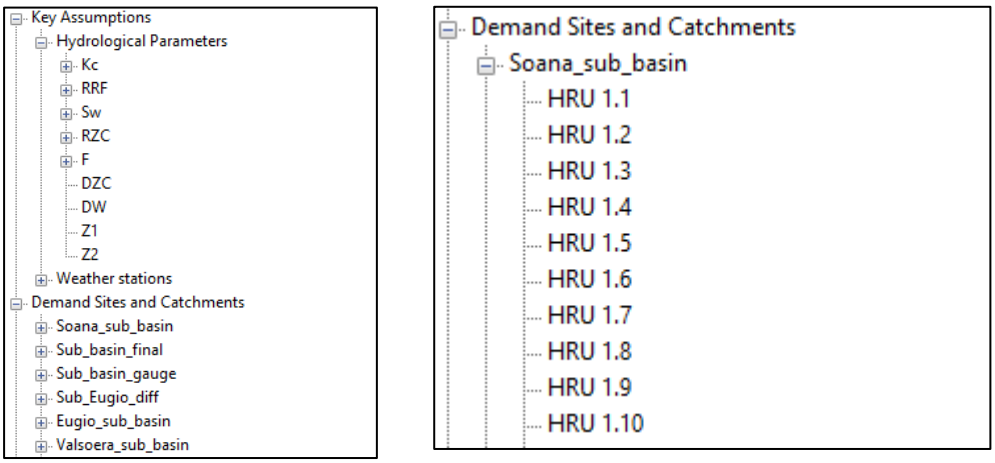


*Figure 4 (left) and Figure 5 (right): data view window of WEAP software tool. On the left it is shown the tree structure organization of Key assumptions and Demand Sites and Catchments, while on the right, the schematization of each sub-basin is shown.*

### 3.3.3) Catchment Hydrology module

The physical hydrology module consists of several conceptually simple components that are combined to ensure high computational efficiency, while maintaining a sufficient level of detail to represent the main hydrological processes and to address key issues related to water resources management (*Yates et al., 2005a*). For each timestep, the hydrological module is executed first, updating the hydrological state of the analyzed river basin. The hydrological module adopts the **Soil Moisture Method** approach.

The **Soil Moisture Method** is based on a one-dimensional scheme that includes two soil layers (or "buckets"), relying on empirical functions to describe evapotranspiration, surface runoff, and deep percolation for each unit of the watershed (*Yates, 1996*). Thanks to this configuration, the method can highlight how soil type and land use influence the aforementioned hydrological processes.

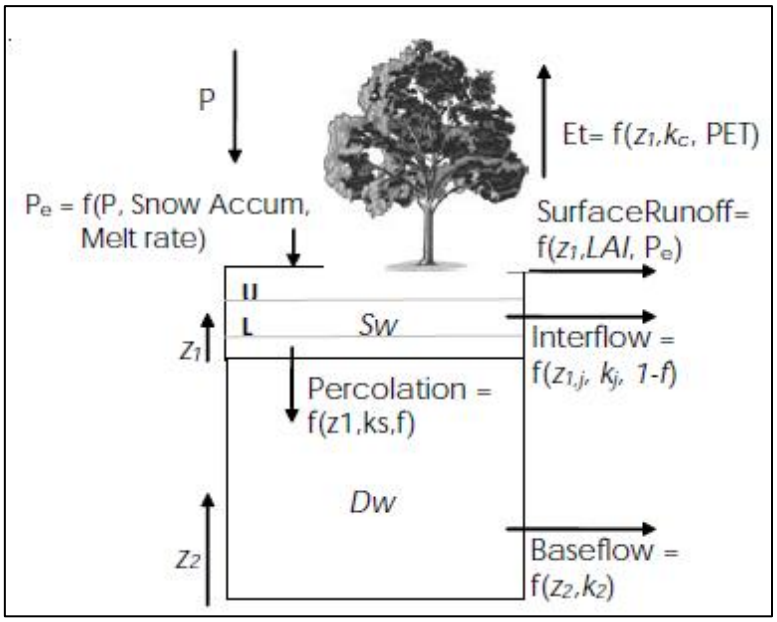


*Figure 6: Schematic representation of the 2-layers soil moisture store, showing the hydrologic inputs and outputs for a specific land cover or soli type (Yates et al. 2005a).*

To ensure optimal model performance and obtain more detailed results, the river basin can be subdivided first into sub-catchments and subsequently into Hydrological Response Units (HRUs), each characterized by a specific soil category and a different land use (*Section 3.1*).

Under standard conditions, climatic variables are assumed to be homogeneous within each sub-catchment. However, this assumption is difficult to apply in mountainous environments, where HRUs may exhibit a wide range of elevations. For this reason, in the model developed for this thesis the assignment of climatic variables was modified so that they are attributed to each individual HRU, thereby allowing for more realistic results.

The mass balance of the first layer of soil for each individual HRU is calculated according to the following equation:

$$Rd_j \frac{dz_{1,j}}{dt} = P_e(t) - PET(t)k_{c,j}(t)\left(\frac{5z_{1,j} - 2z_{1,j}^2}{3}\right) - P_e(t)z_{1,j}^{RFFj} - f_j k_s z_{1,j}^2 - (1 - f_j)k_{s,j}z_{1,j}^2$$

Eq. 3.1

where:

- $z_{1,j}$ = [1,0] is the relative storage given as a function of the total effective storage of the root zone, which is expressed as $Rd_j(mm)$ for land cover fraction, j;
- $P_e(t)$ is the effective precipitation;
- $PET$ is the Potential Evapotranspiration calculated by using the modified FAO Penman-Monteith equation;
- $k_{c,j}(t)$ is the crop evapotranspiration coefficient;
- $RFFj$ is the Runoff Resistance Factor of the fraction j;
- $f_j$ is the preferred flow direction;
- $k_{s,j}$ is the hydraulic conductivity of the upper soil layer $(mm/timestep)$;

The effective precipitation $P_e(t)$ is computed by the model through a simple temperature-index model (*Yates et al.,2005a*).
In this way, $P_e(t)$ takes account of the snow water equivalent and snowmelt from the accumulated snowpack in the sub-catchments.
To do so, the model calculates a melting coefficient $m_c$, which can be expressed as follows:

$$m_c = \begin{cases} 0 & T_i < T_s \\ 1 & if \quad T_i < T_l \\ \frac{T_i - T_s}{T_l - T_s} & T_s \leq T_i \leq T_s \end{cases}$$

Eq. 3.2

where $T_i$ is the measured temperature for month I, while $T_s$ and $T_l$ are the freezing and melting thresholds.

The snow accumulation of a specific catchment is function of the observed total precipitation $P_i$ and the melting coefficient $m_c$.
It is expressed as:

$$Ac_i = Ac_{i-1} + (1 - m_c)P_i - m_{i-1} \qquad \text{Eq. 3.3}$$

where $m_i$ is the melt rate, that can be defined as:

$$m_i = \min(Ac_i m_c, Em) \qquad \text{Eq. 3.4}$$

where $Em$ is the available melt energy converted to an equivalent water depth/time.
Finally, the hydrological module calculates the effective precipitation $P_e(t)$ as:

$$P_e(t) = P_i m_c + m_i \qquad \text{Eq. 3.5}$$

Regarding the second soil layer, since the model developed in this thesis does not include groundwater modeling, the mass balance equation can be expressed in a simplified form as follows:

$$Dw \frac{dz_{2,j}}{dt} = (1 - f_i)k_j z_{1,j}^2 - k_2 z_{2,j}^2 \qquad \text{Eq. 3.6}$$

where:

- $Dw$ is the deep percolation from the upper storage given in *Eq. 3.1* and it represents the inflow to the 2nd layer storage;
- $k_2$ is the saturated conductivity of the lower storage (mm/time) which is a single value for the catchment.

The modeling timestep, denoted in the previous equations as $t$, can be defined according to different temporal intervals. WEAP allows simulations to be performed with a temporal resolution ranging from daily to annual scales. The time step therefore defines the temporal resolution of the model (*Lucca, 2025*).

In the case of the model developed in this thesis, a weekly time step was adopted, mainly due to the limited extension of the analyzed watershed and the morphology of the study area. In particular, the presence of pronounced altitudinal gradients makes the weekly time scale more suitable for capturing

significant temperature variations, which strongly influence snow and glacier accumulation and melt processes (*Lucca,2025*).

The weekly time-step structure adopted by WEAP for the model is shown in *Figure 7*.

| Title | Abbrev. | Length | Begins | Ends |
|---|---|---|---|---|
| Week 1 | Wk 1 | 7 | 1 Jan | 7 Jan |
| Week 2 | Wk 2 | 7 | 8 Jan | 14 Jan |
| Week 3 | Wk 3 | 7 | 15 Jan | 21 Jan |
| Week 4 | Wk 4 | 7 | 22 Jan | 28 Jan |
| Week 5 | Wk 5 | 7 | 29 Jan | 4 Feb |
| Week 6 | Wk 6 | 7 | 5 Feb | 11 Feb |
| Week 7 | Wk 7 | 7 | 12 Feb | 18 Feb |
| Week 8 | Wk 8 | 7 | 19 Feb | 25 Feb |
| Week 9 | Wk 9 | 8 | 26 Feb | 4 Mar |

*Figure 7: WEAP weekly scheduled organization. It is possible to notice the title and length of each week, considering also when it begins and when it ends.*

For the development of the model, the hydrological year calendar was adopted, thus starting at week 40 (1st October to 7th October) and ending at week 39 (24th September to 30th September) of the following year.

### 3.3.4) Hydrological Parameters

As introduced in *Section 3.3.2*, hydrological parameters are indicators that determine how, and to what extent, they influence the hydrological behavior of the HRUs within the watershed.

These parameters mainly depend on soil type, land use, and the slope characteristics of the area. Based on the WEAP User Guide (*Sieber & Purkey, 2015*), *Table 6* was compiled, listing all the hydrological parameters included in the equations described in *Section 3.3.3.*.

| Name of parameter | Description | Characteristics of influence |
|---|---|---|
| Crop coefficient (kc) | It is relative to the reference crop. | Land use |
| Soil Water Capacity (Sw) | The effective water holding capacity of the top layer of soil, represented in mm | Soil type, depth |
| Deep water Capacity (DWC) | Effective water holding capacity of lower, deep soil layer, represented in mm. This value is given for the entire catchment and does not vary by land class type. Baseflow will increase if this parameter increases. | Catchment |
| Deep Conductivity (DC) | Is the conductivity rate (length/time) of the deep layer at full saturation (z2 = 1). It controls the transmission of the baseflow. This value is given for the whole catchment and does not vary by land type. | Catchment |
| Runoff Resistance Factor (RRF) | This parameter is used to control the surface runoff response. It is related to factors such as leaf area index and land slope. Runoff increases with high values. It varies among the land classes | Slope, Land use |
| Root Zone Conductivity (RZC) | It indicates the root zone conductivity rate at full saturation (z1=1) which will be partitioned according to Preferred Flow Direction, between interflow and flow to the lower soil layer. It varies among land classes | Soil type |
| Preferred Flow Direction (f) | If this value is 1, flow is horizontal, 0 if flow is vertical. It is used to partition the flow out of the root zone layer between the interflow and flow to the lower soil layer. | Slope |
| Initial Z1 | It is the value assumed at the beginning of simulation. It represents the percentage of relative storage with respect to the total effective storage of the root water capacity | |
| Initial Z2 | It represents the initial value of Z2 at the beginning of the simulation. It is the relative storage given as percentage of the total effective storage of the lower soil bucket | |

*Table 6: list of hydrological parameters applicable to the WEAP hydrological module (Sieber & Purkey,2015)*

The hydrological parameters defined in the previous table are assumed to remain constant over time and do not vary on a weekly basis, except for the *crop coefficient*.
This parameter, in fact, is subject to seasonal variations.

*Table 7* reports the initial values adopted for each land-use type defined within the model for the Crop Coefficient parameter according to *Nistor (2018)*.

| Crop coefficient (Kc) | | | |
|---|---|---|---|
| **Soil Use** | **Kc initial-season** | **Kc mid-season** | **Kc end-season** |
| AGRL | 0,5 | 1,1 | 0,6 |
| BARR | 0,4 | 0,6 | 0,5 |
| FRST | 0,35 | 0,55 | 0,4 |
| RNGE | 0,7 | 0,7 | 0,7 |
| SWRN | 1 | 1 | 1 |
| URMD | 0,3 | 0,3 | 0,3 |
| WATR | 1,2 | 1,2 | 1,2 |

*Table 7: Kc values reported for model's first calibration (Nistor, 2018).*

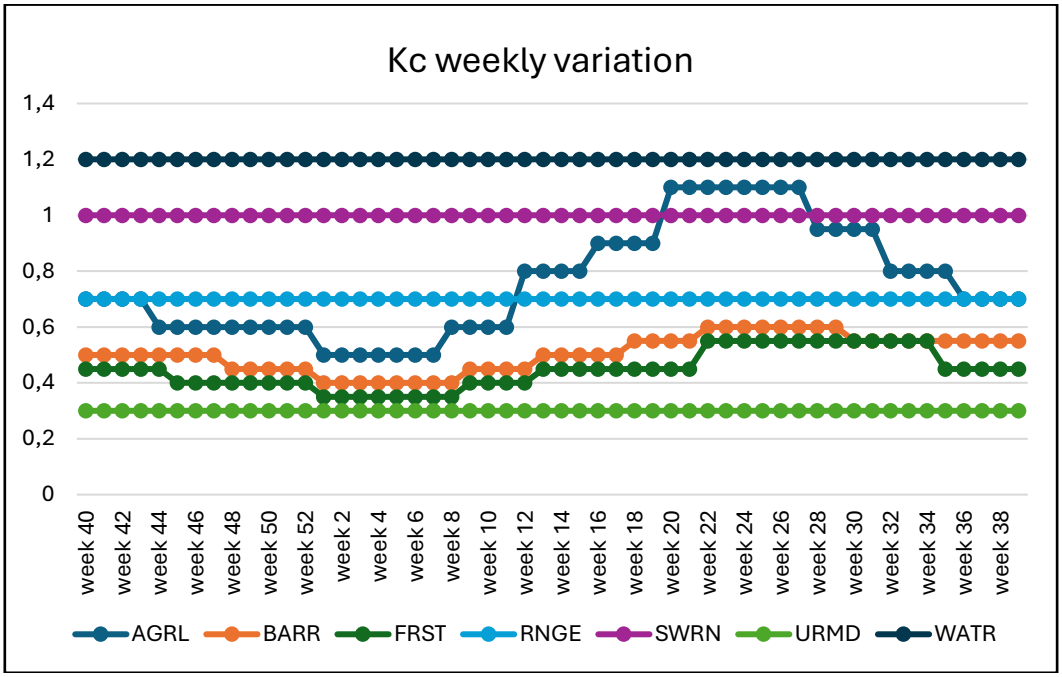


*Figure 8: representation of Kc weekly variation according to the land use class (initial values).*

The initial hydrological parameters assumed, and the final values calibrated are reported in *Section 8*.

### 3.3.5) Climate data review and analysis

The climatic data required by WEAP for the simulation of the hydrological module implemented in the model are the following:

- Temperature;
- Precipitation;
- Humidity;
- Wind;
- Cloudiness Fraction.

As reported in ***Section 3.3.3***, temperature and precipitation measurements are required to calculate the effective precipitation $P_e(t)$ (*Eq. 3.2* and *Eq. 3.5*), while the remaining climatic variables are used to compute the potential evapotranspiration $P_e(t)$.

According to the *WEAP User Guide* (*Sieber & Purkey, 2015*), $PET(t)$ is calculated using a simplified form of the Penman–Monteith equation (*Allen et al., 1998*), appropriately modified for a standardized grass crop with a height of 0.12 m and a surface resistance of 69 $m/s$.
In this formulation, the main modifications implemented with respect to the standard version of the equation are the following:

- Albedo varies over a range from 0,15 to 0,25 as a function of snow cover;
- Soil Heat Flux has been ignored.

The meteorological data used within the model had been downloaded from the website of the Regional Agency for Environmental Protection of the Piedmont Region (*Arpa Piemonte*).
For the purposes of the analyses carried out using the hydrological model, a temporal period ranging from 01/01/2011 to 31/12/2024 was considered.
This choice is driven by the adequate duration of the period analyzed, ensuring representative results, and by the good availability of data from the meteorological stations.

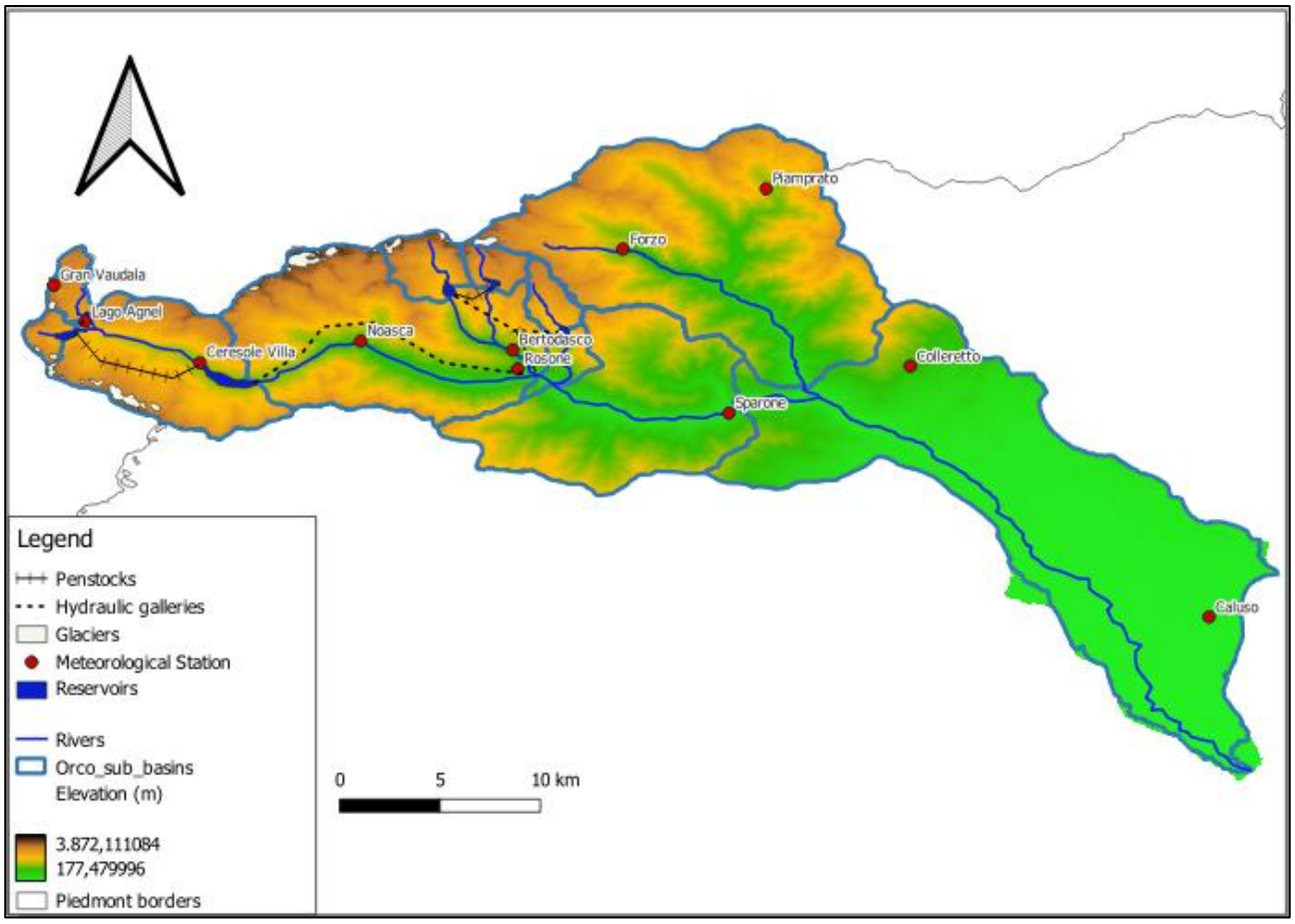


*Figure 9: Orco Valley map with representation of meteorological stations locations.*

| Meteorological station | Elevation (m.a.s.l.) | Parameters |
|---|---|---|
| Bertodasco | 1137 | P-H-T |
| Gran Vaudala | 3272 | SR-W-T |
| Ceresole Villa | 1581 | P-T |
| Forzo | 1162 | P-T |
| Lago Agnel | 2304 | P-T |
| Noasca | 1055 | P-T |
| Piamprato | 1555 | P-T-H |
| Rosone | 701 | P-T |
| Caluso | 257 | SR-W-T-P-H |
| Colleretto | 1240 | P-T |
| Sparone | 524 | P-T |

*Table 8: Meteorological stations elevation and parameters measured.*

In the parameter section of *Table 8*: P= precipitation, H=Humidity, T=Temperature, SR=Solar Radiation; W=Wind.

As shown in *Figure 8*, the study area is characterized by a good distribution of meteorological stations, which ensures adequate data coverage, particularly with respect to temperature and precipitation measurements.
Indeed, as reported in *Table 8*, data related to these climatic variables are recorded at all meteorological stations, except Gran Vaudala for precipitation.

For this reason, in order to assign temperature and precipitation data in a proper way to the different hydrological units within the study area, specific analyses were carried out.

### Temperature Analysis.

With regard to temperature, a graph representing the monthly average temperature over the entire analysis period was first constructed.
The result of this processing is shown in *Figure 10*.

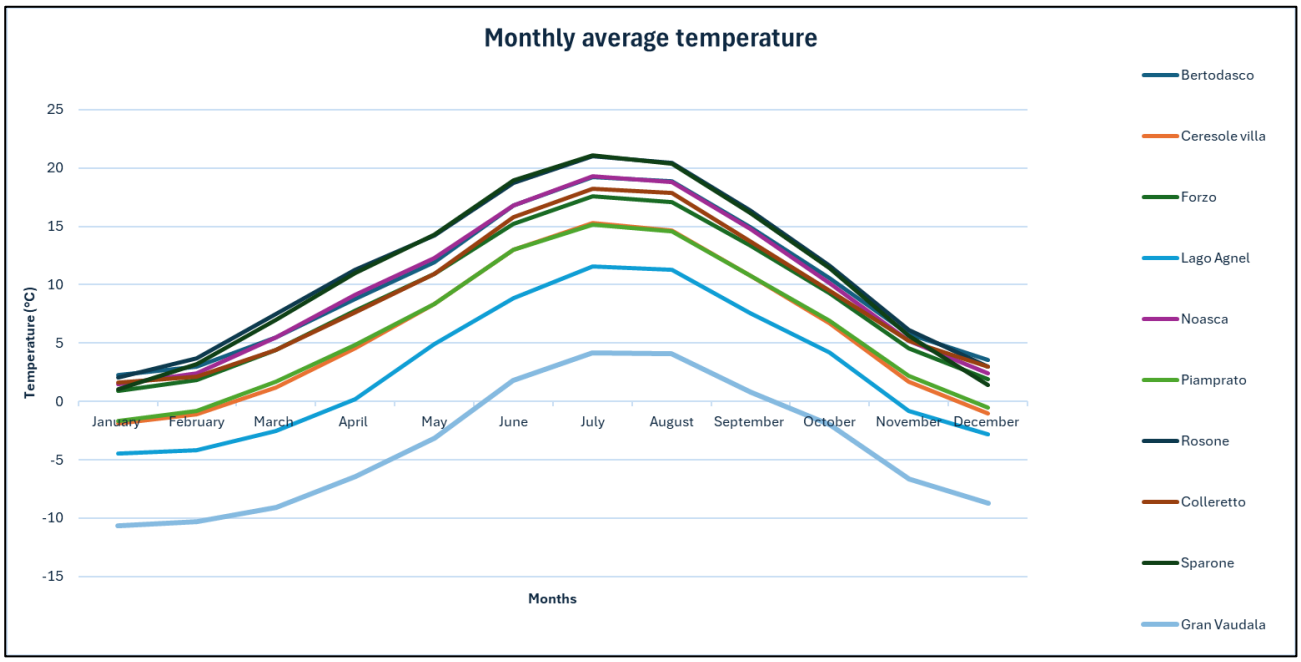


*Figure 10: monthly average temperature plot for the analyzed period.*

By observing the graph, a clear decrease in temperature with increasing elevation within the catchment can be identified.

It can also be noticed that temperatures recorded at stations located at similar elevations exhibit comparable trends.
Once this relationship has been identified, temperature measurements were assigned to the individual HRUs by considering the following characteristics:

- average elevation of the *Hydrological Response Unit*;
- position relative to the nearest meteorological station characterized by a similar altitude.

### Precipitation Analysis.

Regarding precipitation, a graph showing the monthly cumulative values over the entire analysis period was constructed, as shown in *Figure 11*.

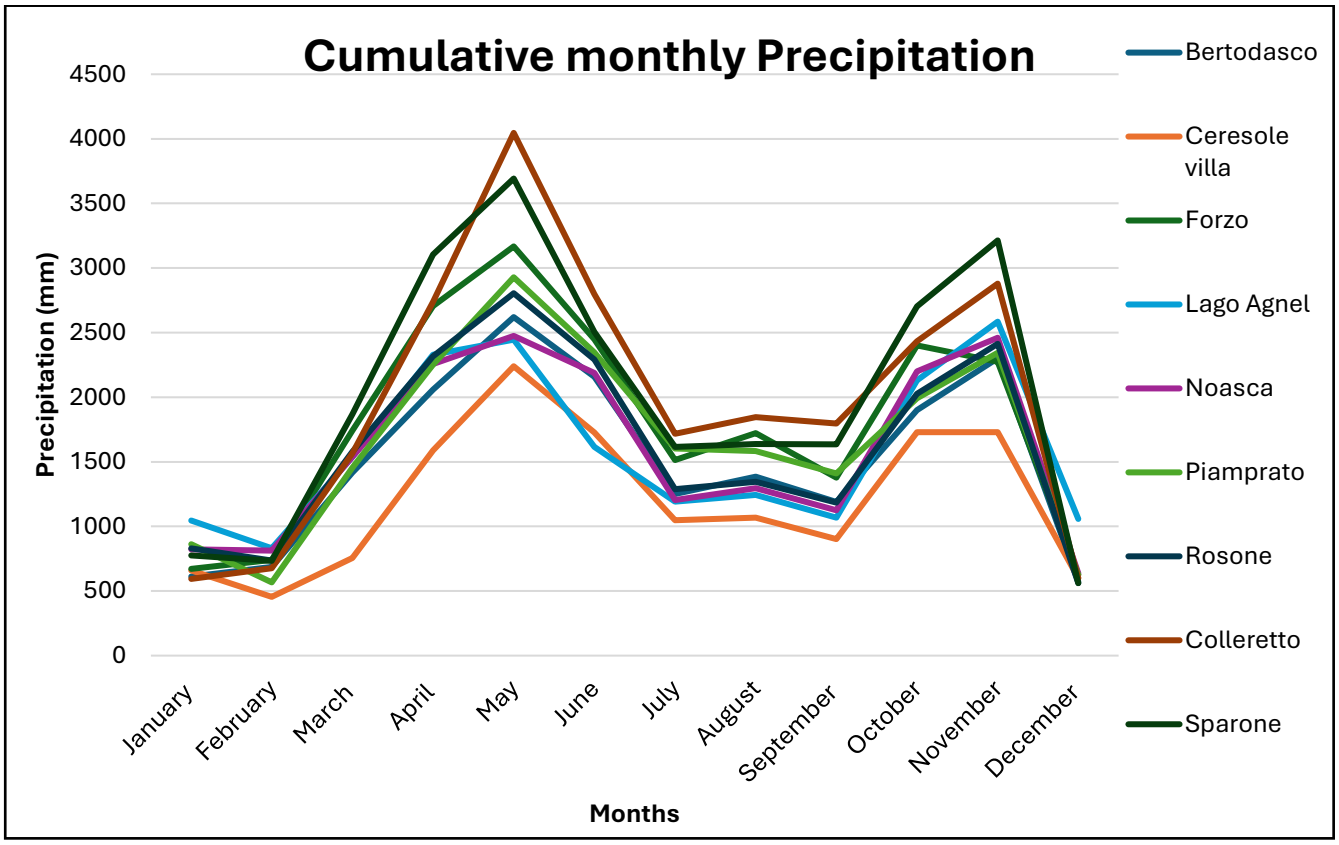


*Figure 11: cumulative monthly precipitation for the analyzed period.*

As can be observed from the graph, the precipitation analysis does not reveal a well-defined trend with respect to the elevation of the meteorological stations. The data instead show a significant variability mainly related to the spatial location of the stations rather than to their elevation.
From a seasonal perspective, by observing the position of the peaks for each station reported in the graph, May and November emerge as the wettest months.

Precipitation data were assigned to the HRUs within the individual sub-catchments based on the spatial position of each HRU relative to the available reference meteorological station.

Therefore, each HRU was associated with the geographically closest station, assuming that it is sufficiently representative of the analyzed hydrological unit.

### Assignment of the remaining climatic variables.

About the remaining climatic variables, the limited availability of meteorological stations (only two for wind and solar radiation and three for humidity) does not allow for a detailed analysis aimed at identifying the factors influencing these variables, either in terms of elevation or spatial location.

For this reason, the assignment of climatic data related to the remaining parameters was carried out by associating each HRU with the values recorded at the nearest meteorological station.

However, it is important to provide some clarifications concerning the cloudiness fraction and wind measurements:

- The cloudiness fraction is not a directly measurable parameter and is used within the WEAP solver to calculate net solar radiation (*Sieber & Purkey, 2015*).
  To this end, a Python script (*Lucca, 2025*) was developed to estimate this parameter by inverting the Ångström formula (*Chapter 4.2.6*, *Handbook of Hydrology*, *Gray and Prowse, 1992*), relating extraterrestrial solar radiation to net solar radiation.
  Extraterrestrial solar radiation was calculated using the FAO-56 formulation (*Allen et al., 1998*).
- Wind measurements presented several critical issues, particularly with respect to the Gran Vaudala meteorological station.
- The daily data provided by this station show numerous gaps, with a maximum discontinuity of 92 consecutive missing days.
  An additional limitation is related to the location of the meteorological station, situated at an elevation of 3272 m a.s.l., which results in very high average wind speed values that are not applicable to the surrounding sub-catchments, as they would not provide realistic estimates.

  To overcome these issues, it was decided to use data available from the *Copernicus ERA5* platform (*C3S*).

A major advantage of this platform is the availability of data dating back to 1940 for any area of the world; however, its main drawback lies in its spatial resolution.

The minimum spatial resolution that can be downloaded is 0.1° × 0.1°, corresponding to an area of approximately 121 km², which makes it more difficult to identify local-scale fluctuations and microclimates within the study area. Therefore, four ERA5 pixels were downloaded, representing a total area of 484 km². The downloaded pixels were subsequently overlapped with the study area map developed in QGIS, and the values contained within each pixel were assigned to the underlying and adjacent catchments based on spatial coordinates.

Finally, for the downstream catchments, wind data from the Caluso meteorological station were used, due to the good continuity of the time series and the consistency in the order of magnitude of the values compared to those obtained from ERA5.

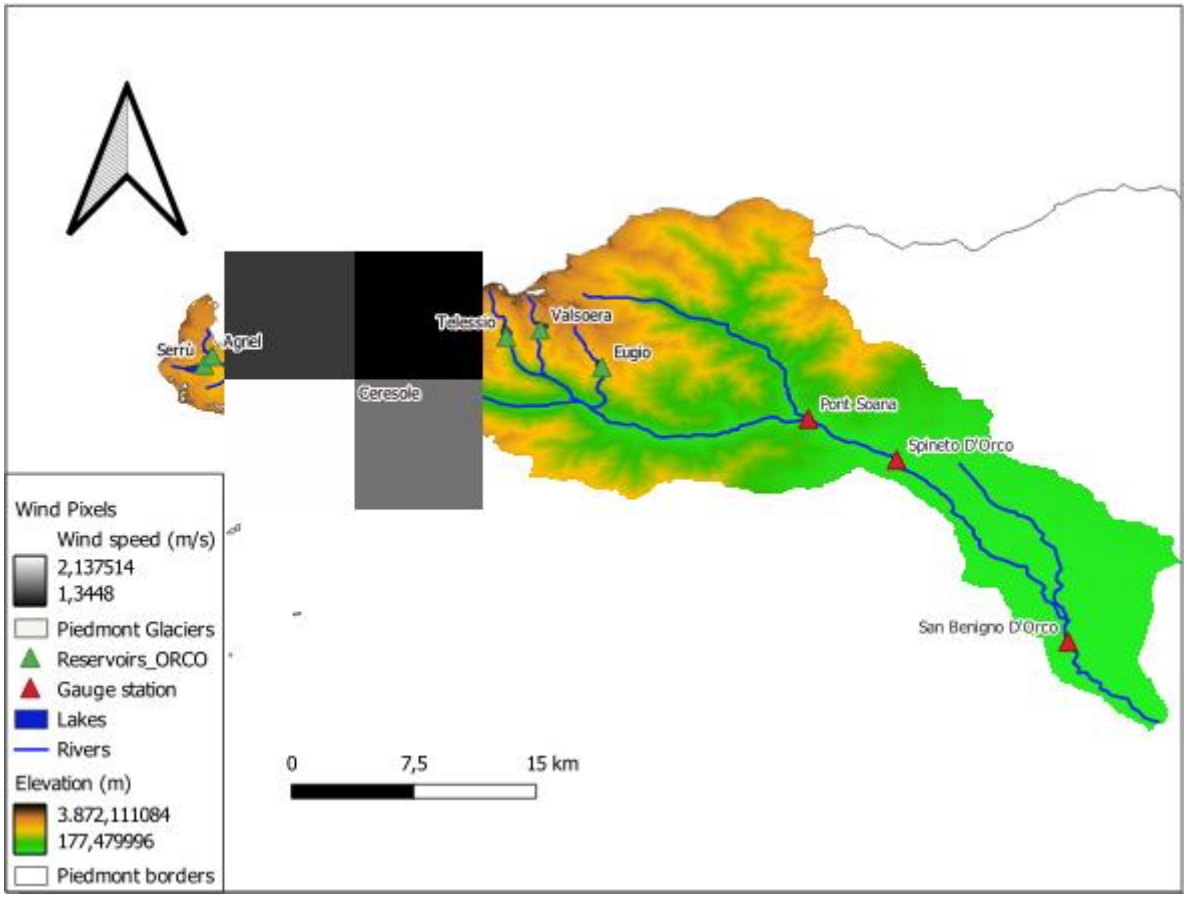


*Figure 12: Representation of ERA5 (CS3) pixels extracted for wind data analysis.*

### 3.3.6) Snow data

According to what was previously defined in *Section 3.3.3*, the *Soil Moisture Method* implemented within the model accounts for the processes of accumulation and melting of the snowpack within the catchment area.

Specifically, WEAP computes a *melting coefficient* (Eq. 3.2, *Section 3.3.3*), which allows for an appropriate estimation of $P_e(t)$.

Within the study area, several stations provide measurements related to the snow layer accumulated throughout the year. The snow monitoring stations from which the data were extracted are also managed by the Regional Environmental Protection Agency (*ARPA Piemonte, historical data series*) of the Piedmont Region.

The location and the list of the aforementioned stations from which the data were obtained are reported and described in *Figure 13* and *Table 9*.

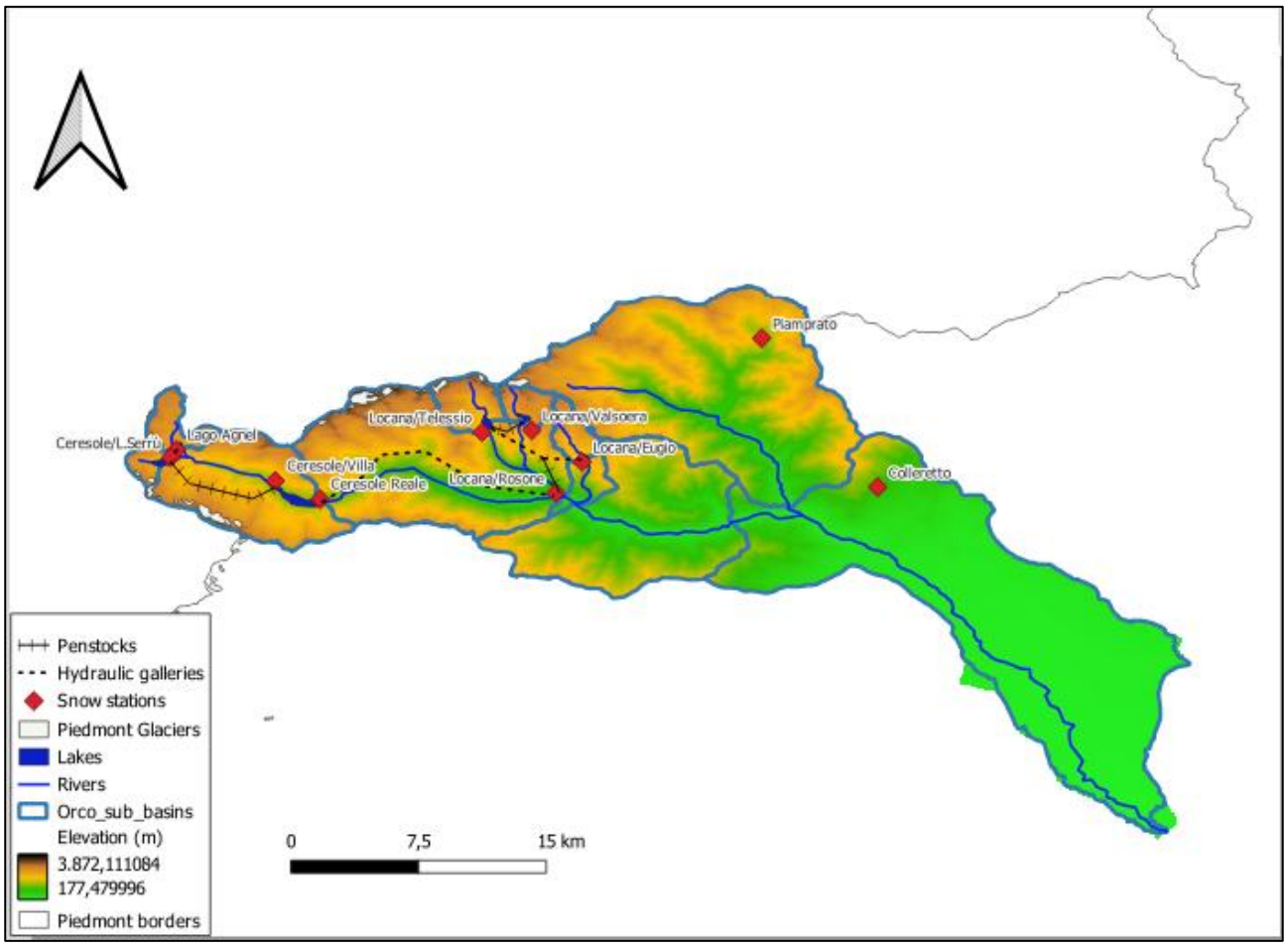


*Figure 13: Representation of snow gauge stations across the Orco Valley.*

| Snow gauge station | Elevation (m.a.s.l.) |
|---|---|
| Ceresole/Lago Serrù | 2283 |
| Ceresole/Villa | 1581 |
| Ceresole Reale | 1573 |
| Locana/Telessio | 1940 |
| Locana/Valsoera | 2412 |
| Locana/Eugio | 1900 |
| Locana/Rosone | 700 |
| Piamprato | 1555 |
| Colleretto | 1240 |
| Lago Agnel | 2304 |

*Table 9: List of snow gauge stations used for the model.*

All the snow gauge stations considered show a high degree of data continuity and are therefore suitable for use within the model. However, some stations exhibit missing days within the dataset, with measurements interrupted from the end of May and resuming in October.

Nevertheless, this issue was not considered critical for the purposes of the analysis, since the temporal gaps occur during the summer period, when the snowpack is generally absent. Consequently, the missing dates were integrated into the dataset by assigning zero value to the snowpack depth.

The WEAP model requires snow-related input data to be expressed in millimeters of water equivalent. Since the measurements provided by the stations are reported in centimeters, a conversion to *Snow Water Equivalent* (SWE), expressed in millimeters, was therefore performed.

For the calculation of the *Snow Water Equivalent*, the following equation was used:

$$SWE = Hs * \rho b \qquad \text{Eq. 3.7}$$

where $Hs$ represents the local snow depth while $(m)$ $\rho b$ represents the bulk density of snow $(kg\ m^{-3})$.

Snow density was calculated according to the methodology proposed by *Guyennon et al. (2019)*, which accounts for seasonal variability and the location of the stations within the Alpine region. The equation used to estimate snow density is reported below:

$$\rho b = n_0 + n_1 * (DOY + 61) + n_2 * (DOY + 61)^2 \quad \text{Eq. 3.8}$$

where:

- $n_0$ is a calibrated parameter and its value for South-Western Italian Alps is 285,9;
- $n_1$ is a calibrated parameter which value for South-Western Italian Alps is 0,13;
- $n_2$ is a calibrated parameter which value for South-Western Italian Alps is -0,0001;
- $DOY$ expresses the day of the year starting by 1st of November.

In this way, the adopted formulation allows seasonal variations in snow density to be considered, thus showing a gradual increase in density over time *(Guyennon et al., 2019)*.

Subsequently, for each snow monitoring station, the corresponding *Snow Water Equivalent* was calculated and expressed in millimeters and then averaged on a weekly basis. During the analysis, a graph was produced, shown in *Figure 14*, which illustrates the temporal evolution of the mean SWE values over the entire analysis period.

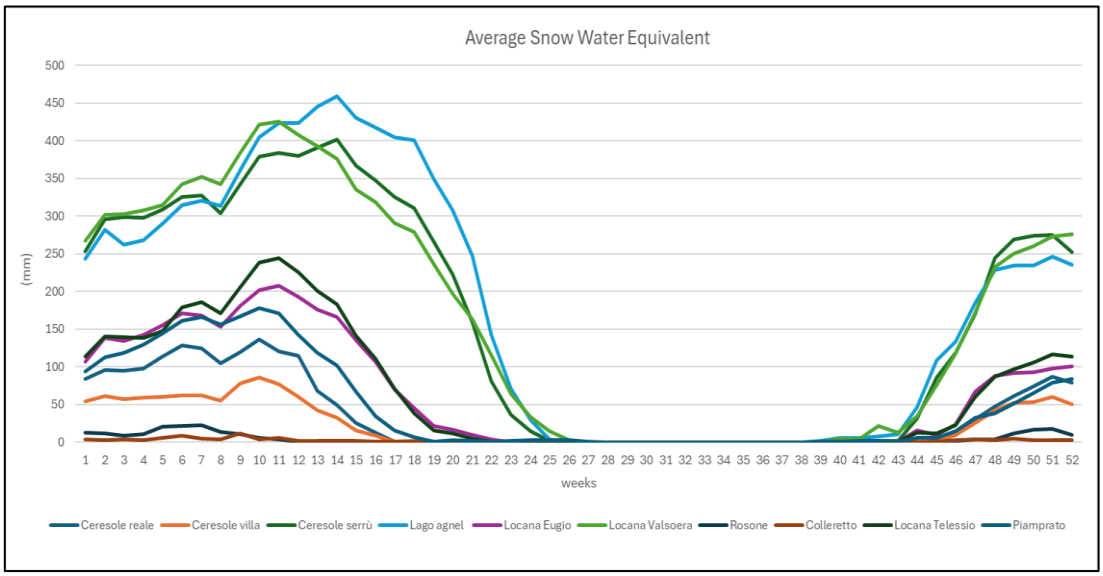


*Figure 14: Average snow water equivalent for the snow gauge stations*

By observing the graph, the periods characterized by the highest SWE values occur within the time interval between week 10 and week 19, with an absolute peak around week 14. This period therefore corresponds to the phase of maximum snowpack accumulation and the subsequent onset of the melting phase.

In general, a clear tendency can also be observed, showing an increase in SWE values with increasing station elevation, in agreement with what is typically expected in mountainous environments.

Finally, with regard to data assignment within the model, the values recorded by the snow monitoring stations were assigned to the individual *Hydrologic Response Units* (HRUs) in which each meteorological station is located.
To this end, the map produced in QGIS shows the location of the snow monitoring stations (*Figure 13*) was used and subsequently overlaid with the SWAT shapefile.

To ensure greater accuracy, it was also verified that the mean elevation value of the selected HRUs was approximately similar or equal to the values reported in *Table 9*.

### 3.3.7) Glacier module

Within the hydrological model, the optional module related to the *glacier routine* has been implemented, aimed at simulating the processes of glacier accumulation and melting on the ground surface.

The accumulation of the glacier layer occurs through the conversion of the existing snow into ice. In addition, snow that has not melted within a period of 12 months is automatically converted into ice.
The ice begins the melting phase when it is no longer covered by snow and when the recorded temperature exceeds a predefined threshold *(Sieber & Purkey, 2015)*.

The following equations describe the processes of ice accumulation and melting implemented within the ***Glacier Module***:

$$IceMelt = Rnet * GRf * \frac{\frac{Days}{\lambda f}}{\frac{\rho w}{1.1}} \quad if\ snowdepth = 0\ and\ T_t \geq T_{icemelt} \qquad \text{Eq. 3.9}$$

$$IceMelt = 0 \quad if\ snowdepth > 0\ or\ T_t < T_{icemelt} \qquad \text{Eq. 3.10}$$

where:

- $IceMelt$ is the depth of ice that melts, expressed in millimeters;
- $Rnet$ is the Net Radiation $[Mj/days/m\text{^}2]$;
- $GRf$ is the fraction of net radiation that contributes to ice melting;
- $Days$ is referred to the number of days within the timestep;
- $\lambda f$ is the the latent heat required for ice fusion = $0{,}334\ MJ/kg$;
- $\rho w$ is the density of water = $1000\ kg/m\text{^}3$;
- $1.1$ is a conversion factor that is used to take account of the lower density of ice with respect to water;
- $T_t$ is the Temperature of air expressed in °C;
- $T_{icemelt}$ is the temperature threshold at which ice starts melting, expressed in °C.

Regarding the melting and freezing temperatures, WEAP uses default values of 1 °C and 0.5 °C, respectively, while the predefined value of $GRf$ is set to 70%. These parameters will subsequently be subject to calibration within the model by performing a comparison with the available data for the Ciardoney Glacier. (*Società Meterologica Italiana, 2025*).

### Glaciers data

According to the Italian National Glacier Inventory for the year 2010 *(Smiraglia and Azzoni, 2015)*, the Orco Valley hosts 27 glaciers with a total surface area of approximately 5.64 km².

In order to simplify data assignment within the WEAP model, an additional HRU named *"Glacier"* was created within the sub-basins containing glaciers. This HRU represents the cumulative area of all glaciers located within the same sub-basin, along with the average ice thickness derived from *Mercalli and Cat Berro (2005)*.

The values used in this module are reported in *Table 10*.

| Sub basin | Glacier Surface (m^2) | Ice Depth (m) |
|---|---|---|
| Serrù_sub_basin | 250000 | 5 |
| Agnel_sub_basin | 200000 | 10 |
| Ceresole_sub_basin | 1900000 | 10 |
| Teleccio_Valsoera sub_basin | 2080000 | 10 |
| Teleccio_sub_basin | 600000 | 7 |
| Valsoera_sub_basin | 50000 | 5 |
| Soana_sub_basin | 560000 | 25 |

*Table 10: Glaciers data used for each sub basin.*

### 3.3.8) Agricultural sites

In the eastern portion of the watershed, corresponding to the lower-elevation sector of the valley, four different agricultural consortia withdraw water from the Orco River. Only a part of the areas served by these consortia falls within the study area, covering a total surface of approximately 54 km² (*Lucca,2025*).

With respect to agricultural land use, maize represents the predominant crop, while soybean and wheat are also present, as reported in the Geoportal of Piedmont region (*Regione Piemonte, 2025*).
This information is particularly relevant for the definition of the **Crop Coefficient (Kc)**; for this reason, in this study, Kc values characteristic of maize cultivation were adopted (see *Section 3.3.4*).

Nevertheless, there is a significant lack or total absence of information regarding the actual withdrawal rates of the individual agricultural consortia, as well as their seasonal variability associated with irrigation practices.
Considering this data limitation and ensuring a realistic estimation of the water withdrawals for each consortium (*Lucca, 2025*), reference was made to the maximum authorized or abstractable discharge values, reported as follows:

- 11 m³/s for the Caluso Consortium;
- 5 m³/s for the East Orco Consortium;
- 7.4 m³/s for the West Orco Consortium;
- 2.6 m³/s for the Reirola–San Marco Consortium.

Based on these maximum values, the weekly withdrawals patterns were manually reconstructed, assuming a temporal distribution consistent with the periods of higher irrigation water demand (*Figure 15*).

The withdrawals values obtained are used for the whole analysis period of the model.

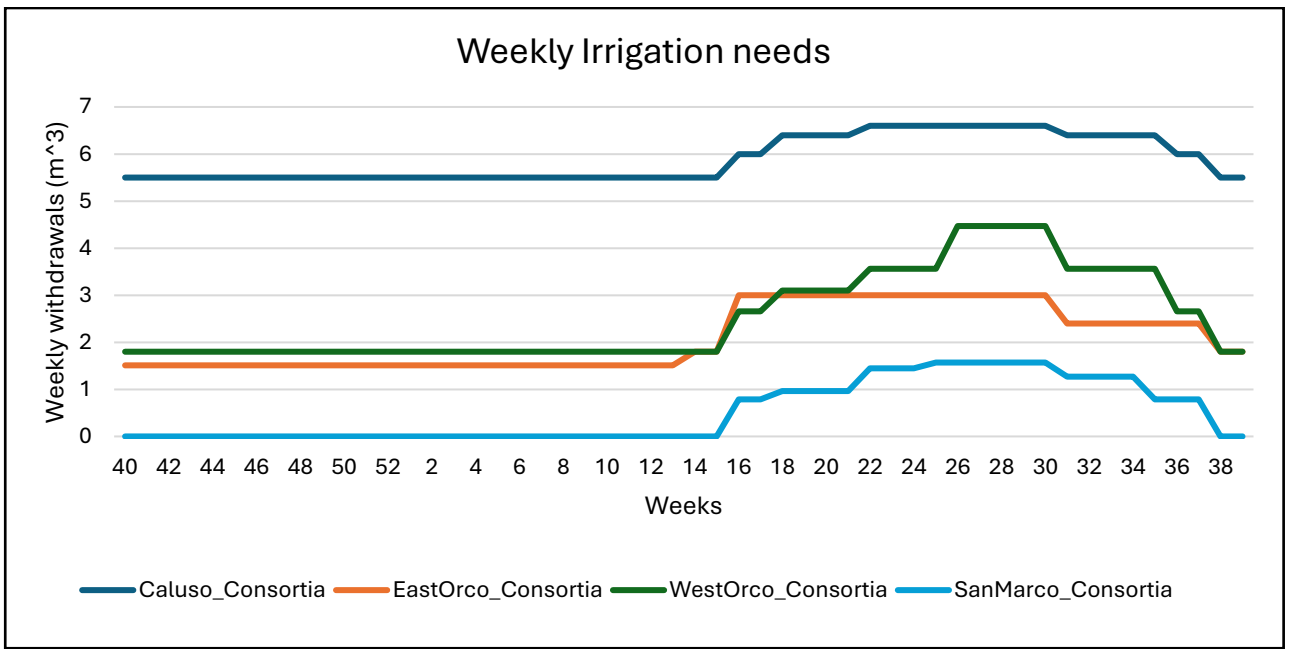


*Figure 15: weekly withdrawals for Valle Orco Consortia.*

From the graph reported above, it can be observed that the periods of highest water demand of the agricultural consortia coincide with the time interval between weeks 24 and 30 of the year, corresponding to the months of June and July.

The magnitude of the water abstractions was determined based on the information reported in *Section 5.2.3.7* of PhD Thesis "*The Water-Energy-Food-Ecosystems Nexus", Lucca, (2025).*

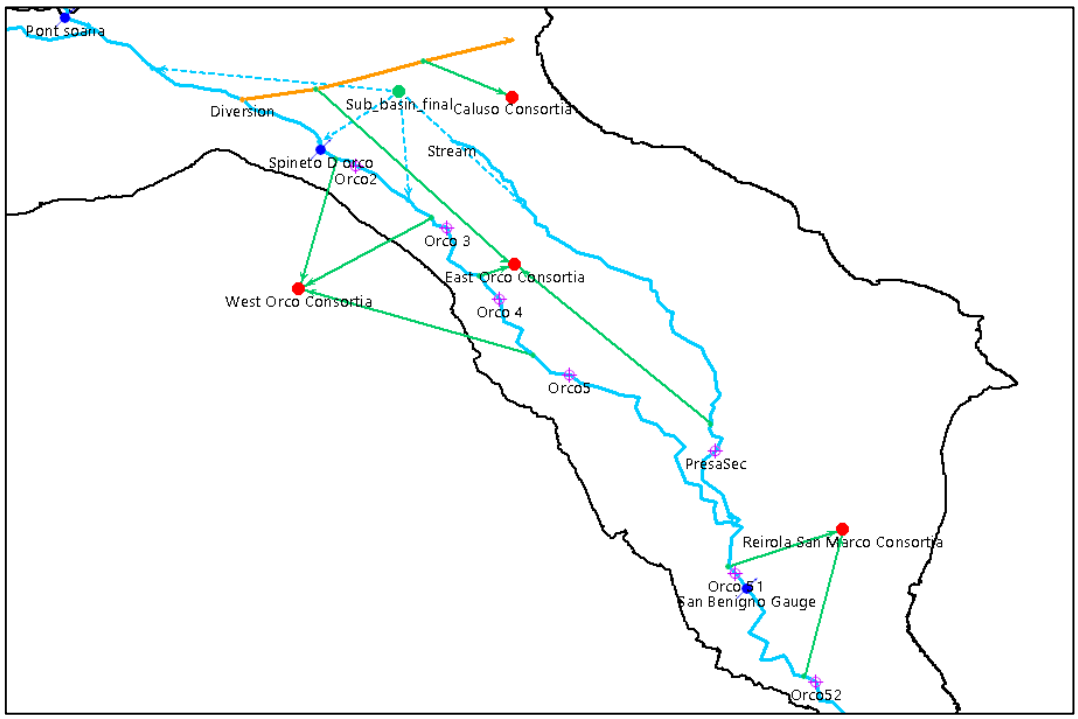


*Figure 16: Schematic representation from WEAP model of agricultural consortia and their withdrawals sites*

### 3.3.9) Reservoir Module

As previously described *in Section 2.2*, six artificial reservoirs for hydropower purposes are located within the Orco Valley.
Their storage capacities and elevations are reported in *Table 1* (page 5).

However, to simplify the management of the reservoir module and considering the operational schemes described in the technical reports provided by Iren S.p.A. (2022), the Agnel reservoir was not explicitly represented in the model. According to these reports, this reservoir is kept completely empty during the winter months and primarily serves to supply the nearby Serrù reservoir.

Based on these considerations, the storage capacity of the Agnel reservoir was aggregated with that of the Serrù reservoir, and the runoff generated from the Agnel sub-basin was directly diverted into the latter.

An additional modeling choice concerned the representation of the Telessio and Valsoera reservoirs.
As discussed in *Section 2.3*, the Valsoera reservoir does not directly supply water to the Rosone power plant but instead transfers its flows to the Telessio reservoir. To accurately reproduce this dynamic within the model, a diversion link connecting the two reservoirs was therefore introduced.

With regard to reservoir characterization within the WEAP module, each reservoir is divided into four operational zones (*Sieber & Purkey, 2015*), defined as follows:

- ***Flood Control Zone***, representing the portion of the reservoir reserved for flood management, whose upper limit coincides with the maximum storage capacity;
- ***Conservation Zone***, dedicated to regular releases aimed at meeting downstream water demands; its upper boundary is defined by the *Top of Conservation* parameter;
- ***Buffer Zone***, an intermediate zone in which releases are more limited compared to the Conservation Zone; its upper boundary is identified by the *Top of Buffer*, below which releases are regulated according to the *Buffer Coefficient*;
- ***Inactive Zone***, corresponding to the storage volume below which no water releases are allowed; this zone is defined by the *Top of Inactive* and requires a refilling phase before any further releases can occur.

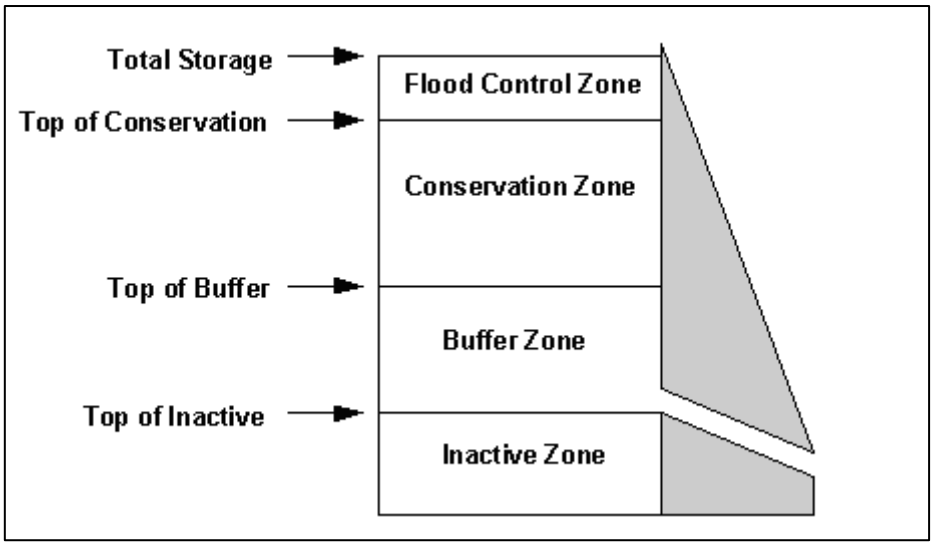


*Figure 17: Schematization of Reservoir's zones (Sieber & Purkey, SEI, 2015)*

To realistically represent the dynamics within each reservoir, WEAP requires the input of specific parameters for every reservoir present in the study area. The main parameters considered are:

- ***Max Storage Volume*** $(Mm^3)$***;***
- ***Initial Storage Volume*** $(Mm^3)$ ,which is the initial volume assumed by WEAP at the start of the simulation;
- ***Volume-Elevation Curve*** for each reservoir, derived from a global dataset (Zhen Hao, 2023) and cross-checked with values reported in the technical reports of each reservoir;
- ***Net Evaporation*** $(mm/week)$***,*** representing the amount of water evaporated from the reservoir. This parameter was calculated using a Python script (*Lucca, 2025*), following the methodology presented in Chapter 4 of the *Handbook of Hydrology* (*Gray and Prowse, 1992*);
- ***Top of Conservation Volume*** $(Mm^3)$***;***
- ***Top of Buffer Volume*** $(Mm^3)$***;***
- ***Top of Inactive Volume*** $(Mm^3)$***;***
- ***Buffer Coefficient***, which regulates releases when the reservoir volume falls within the Buffer Zone. This coefficient can range from 0 (no release) to 1 (regular release);
- ***Observed Volume*** $(Mm^3)$***.*** When available, observed volumes are used to calibrate the variations of storage within the reservoir. Within the study area, only the Ceresole reservoir has observed volume data, reported in a technical report related to a reservoir lining project. However, the measured data are only available up to 2022.

*Table 11* summarizes the parameters described above for each reservoir, derived from the respective technical reports provided by Iren up to 2022.

| ***Reservoir name*** | ***Total Storage*** $(Mm^3)$ | ***Initial Storage year 2010*** $(Mm^3)$ | ***Top of conservation*** $(Mm^3)$ | ***Top of Buffer*** $(Mm^3)$ | ***Top of Inactive*** $(Mm^3)$ | ***Buffer coefficient*** |
|---|---|---|---|---|---|---|
| ***Ceresole*** | 36,2 | 26 | 35,5 | 10 | 1,1 | 0,3 |
| ***Serrù*** | 17 | 12 | 16,7 | 5 | 0,5 | 0,4 |
| ***Telessio*** | 23,5 | 16 | 22,1 | 3 | 0,9 | 0,2 |
| ***Valsoera*** | 8,1 | 7 | 7,7 | 1,5 | 0,5 | 0,2 |
| ***Eugio*** | 5,1 | 3,5 | 4,9 | 0,3 | 0,1 | 0,2 |

*Table 11: list of parameters that have been used for the reservoir's definition within the model.*

### 3.3.10) Hydropower plants representation

With regard to the representation of hydropower plants within the model, the Ceresole Villa, Ceresole–Rosone, and Telessio–Eugio–Rosone plants were included.

Within WEAP, there are two main approaches for modeling hydropower plants:

- the use of the reservoir module;
- the use of the run-of-river hydro module.

For the case study under analysis, the second approach was considered more appropriate, as the power plants are located separately from the reservoirs and are supplied through penstocks or hydraulic tunnels.
This configuration does not allow direct representation using the reservoir module alone.

However, the run-of-river hydro module is primarily designed to represent hydropower plants located directly along a river course; therefore, on its own, it is insufficient to adequately reproduce the hydraulic scheme of the implemented plants.

To overcome this limitation, a demand site node was introduced for each plant and connected to the corresponding run-of-river hydro node through a return flow link.

This configuration allows the water volume to be withdrawn and subsequently turbined by each plant to be represented as a demand within the node.
Data related to the water withdrawals of each hydropower plant were obtained from the section dedicated to the Water Protection Plan on the official website of the Piedmont Region.

In order to represent the connections between the power plants, the supplying reservoirs, and the secondary intakes located along tributary streams, transmission links were used.

Information concerning the main technical characteristics of the modeled hydropower plants were derived from the technical reports provided by IREN S.pa. (2022).

| Power plant | Max. turbine flow (m^3/s) | Fixed Head (m) | Turbine efficiency (%) |
|---|---|---|---|
| Ceresole-Villa | 6,84 | 686 | 82 |
| Ceresole-Rosone | 7 | 812 | 86 |
| Telessio-Eugio-Rosone | 8 | 1152 | 83 |

*Table 12: Technical informations of Orco Valley Hydropower plants.*

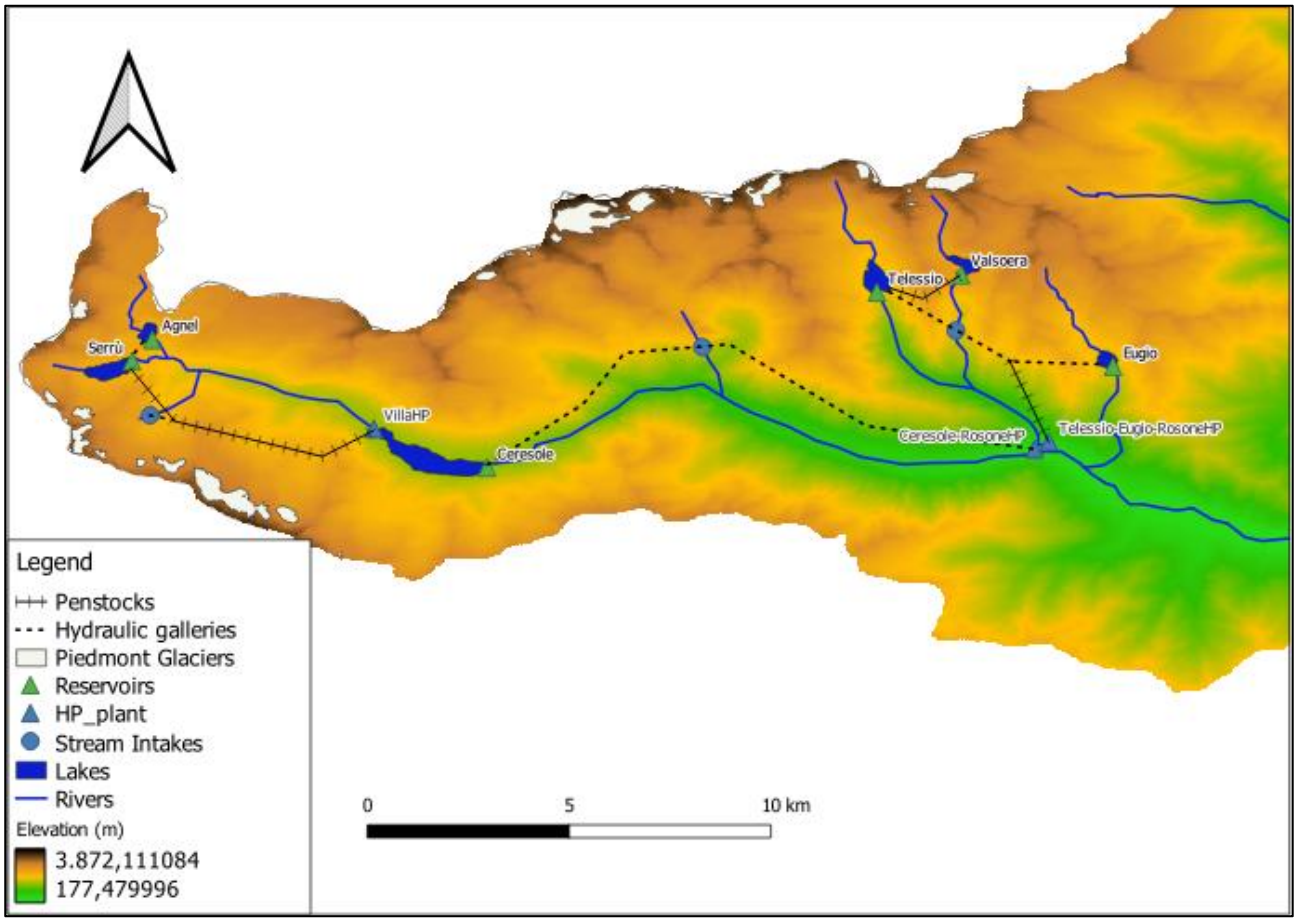


*Figure 18: Schematic representation of hydropower scheme modelled in WEAP.*

### 3.3.11) Environmental Flows check nodes

Finally, within the hydrological model, specific nodes were introduced with the purpose of verifying the maintenance of the Minimum Environmental Flow Requirement (EFR).
The Minimum Environmental Flow is defined as the minimum discharge that must be preserved within the watercourse in order to maintain its ecological functions and to prevent significant damage to the fluvial ecosystem.

According to *Lucca* (*2025*), nodes related to the EFR were placed immediately downstream of the abstraction points, both agricultural and hydropower-related, originating from reservoirs or from secondary intakes along the streams.
This configuration allows for verifying whether the withdrawn water volumes are compatible with ensuring compliance with the EFR.

Within the study area, the EFR values to be guaranteed exhibit a very wide range, with values varying from 0.041 m³/s at the Serrù reservoir up to 5.7 m³/s in the vicinity of the Reiola San Marco agricultural consortium, thus highlighting a progressive increase in EFR values from upstream to downstream.
In total, 16 EFR control points were included in the model.

The EFR values adopted in the model were determined based on multiple sources: partly derived from the technical reports of the reservoirs provided by *Iren S.p.A (2022)* and partly obtained from the documentation available in the section dedicated to regional regulations on the official website of the *Piedmont Region (2025)*.

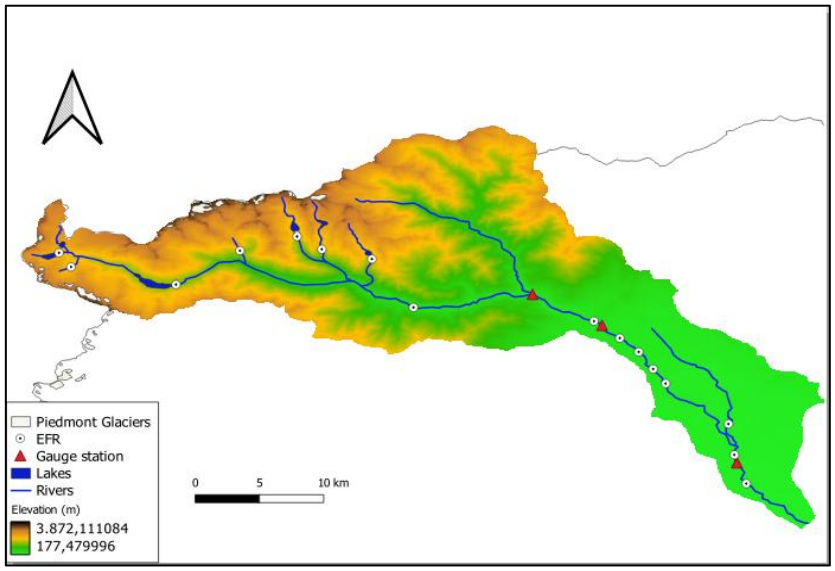


*Figure 19: Position of EFR points inside the Orco Valley.*

## 3.4) Calibration of the Model

Once the model building phase was completed, a calibration procedure was carried out in order to verify that the developed system is able to represent in a realistic and reliable way the hydrological dynamics occurring within the study area. A model that is not able to faithfully reproduce past conditions cannot therefore be considered reliable in representing future scenarios (*WEAP Tutorial, SEI, 2023*).

In order to ensure an adequate calibration of the model, simulated values were compared with observed data over the period 2013–2024. The years 2011–2012 were excluded from the analysis, as reported in the *WEAP Tutorial* (SEI, 2023), since the first two years are used as a *warm-up* period, necessary for the stabilization of the model's initial conditions.

The observed data used for the model calibration phase are listed below:

- observed streamflow at the gauge stations of Pont Soana, Spineto d'Orco, and San Benigno d'Orco (used for the calibration of the hydrological module);
- total ice thickness loss over the entire period from the Ciardoney Glacier (used for the calibration of the glacier module);
- observed volume of the Ceresole reservoir from 2012 to 2022 (used for the calibration of the hydrological module and the snow module for the higher-elevation basins);
- snow level measured at the stations located within the valley, converted into Snow Water Equivalent (SWE) as described in Section 3.3.6.

Nevertheless, it is necessary to introduce some specific considerations regarding the calibration of the snow module. Given the large number of snow stations within the valley and the significant variability in snowpack thickness measured at each station, achieving an optimal calibration for all snow stations proved to be particularly challenging. As a result, 8 stations exhibited excellent calibration performance, while 2 stations showed less satisfactory results, highlighting a general tendency to obtain better calibration outcomes at higher elevations.

In particular, the Colleretto (1240 m a.s.l.) and Rosone (701 m a.s.l.) stations, due to their location and the relatively low snowpack thickness observed, exhibited

calibration results that were not fully satisfactory. Nevertheless, this limitation does not significantly affect the overall water balance of the model.

To assess the degree of calibration achieved, WEAP performs a statistical analysis of the simulation results during model execution. The main statistical performance indicators considered in this study are as follows:

- ***Nash–Sutcliffe Efficiency (NSE)***, which describes how well modeled streamflow matches observed streamflow;
- ***Root Mean Square Error (RMSE)***, which indicates the degree to which modeled and observed flows match;
- ***Ratio of the Root Mean Squared Error to the Standard Deviation (RSR)***, which measures how much simulated flows deviate from observed hydrographs;
- ***Pearson correlation coefficient (r)***, which describes the degree of collinearity between simulated and observed data;
- ***Percent Bias (PBIAS)***, which expresses the tendency toward consistent over- or underestimation of flows.

*Table 13* presents a summary scheme showing which coefficients and parameters are involved within each model module.

| Module | Parameters calibrated | Statistical metric of reference |
|---|---|---|
| *Catchment hydrology (Streamflow and Reservoirs module)* | Hydrological Parameters:<br>• Kc.<br>• Sw.<br>• RZC.<br>• Dw.<br>• F.<br>• RRF. | NSE, PBIAS, RSR |
| *Snow melting and accumulation* | • Melting point temperature (ºC).<br>• Freezing Point Temperature (ºC).<br>• Albedo Lower Boundary.<br>• Albedo Upper Boundary. | r, RMSE |
| *Glacier* | • Radiation coefficient (effective percentage of radiation that contributes to ice melting).<br>• Freezing point temperature (ºC).<br>• Melting point Temperature (ºC). | None.<br>Only total melted depth was considered in order to calibrate the glacier module. |

*Table 13: Summary of calibrated parameters and statistical metrics adopted referred to their specific module.*

# 4) Scenarios

## 4.1) Concept of supply priority and scenarios introduction

To enable a comparison and to evaluate the different impacts that alternative water resource management strategies may have within the mountainous Orco Valley basin, also considering possible changes related to the construction of new infrastructures, four different scenarios were planned and implemented within the developed hydrological model.

However, before proceeding with the description of the scenarios, it is necessary to define how WEAP organizes and structures water resource allocation within the hydrological basin.

Within the model, each node included in the hydrological model, such as demand sites, run-of-river hydropower plants and reservoirs, as well as the related transmission links, a priority is assigned.
This priority ranges from 1 to 99, where the value 1 represents the highest possible priority, while 99 represents the lowest priority that can be assigned.
According to this framework, WEAP first attempts to satisfy the water demand of nodes with higher priority and subsequently those characterized by lower priority.
Transmission links are also characterized by a supply preference based on priority.
If the water resources are not sufficient to satisfy the demand of a specific demand site, a water deficit will be generated.
This dynamic is particularly relevant for lower supply preference nodes.

This concept is particularly relevant in the case of hydropower.

Where multiple supply options are available, a higher supply preference was assigned to intakes located along secondary streams and creeks compared to conduits directly supplied by the reservoir.

## 4.2) Scenario 1: Reference conditions.

The first scenario was defined to represent the reference conditions, which can subsequently be compared with the following three scenarios.

In this case, within the study area, the priority system is organized in order to replicate the water allocation management strategy adopted in the Orco catchment for the analyzed period.
According to this logic, the reservoirs in the valley are managed to optimize hydropower production.
This dynamic influences the allocation of water resources to the agricultural consortia, which have a lower supply priority compared to hydropower (*Lucca,2025*).

| **Node (Reservoir or Demand Site)** | **Priority** |
|---|---|
| Serrù Reservoir | 3 |
| Ceresole Reservoir | 5 |
| Teleccio Reservoir | 3 |
| Eugio Reservoir | 3 |
| Valsoera Reservoir | 3 |
| Ceresole Villa Power Plant | 2 |
| Ceresole Rosone Power Plant | 4 |
| Teleccio-Eugio-Rosone Power Plant | 2 |
| Caluso Consortium | 6 |
| Ovest-Orco Consortium | 7 |
| Est-Orco Consortium | 7 |
| Reirola San Marco Consortium | 8 |
| All Environmental Flow Requirements | 1 |

*Table 14: Representation of supply priorities for Reference Scenarios*

As shown in *Table 14*, the highest priority is assigned to the maintenance of the environmental minimum flow at each location described in *Section 3.3.10*, while hydropower plants are in second position. This is followed by the filling operations of reservoirs and, finally, agricultural consortia.

## 4.3) Scenario 2: Introduction of the new Valle Orco aqueduct.

Through the implementation of this scenario, the objective is to evaluate the impact that the introduction of the new acqueduct, currently under construction, could have within the Orco Valley.

According to information reported on the website of the Ministry of the Environment and Energy Security (2018) and on the SMAT website (2025), the construction of the new water supply system is necessary to address water shortages by using water from reservoirs located at high elevation within the valley.

The intake structure will be located near Locana town, specifically in the Hamlet of Bardonetto. The water will then be conveyed to the new water treatment plant in Locana, which is also under construction phase, and subsequently distributed to 43 different municipalities, serving a total of approximately 150000 people.

Based on the available project data, the nominal discharge of the water supply system will be approximately 0,6 cubic meters per second, with a maximum withdrawal capacity, in case of necessity, of up to 0,8 cubic meters per second. However, since the system is still under construction, according to information reported by SMAT, as of 31 December 2024 the works were completed by 49.1 percent, data on the actual volumes of water withdrawn are not currently available.
For this reason, in order to represent this scenario within the model, a theoretical water demand was assumed based on the average and maximum flow rates potentially withdrawable from the river (*Figure 20*).

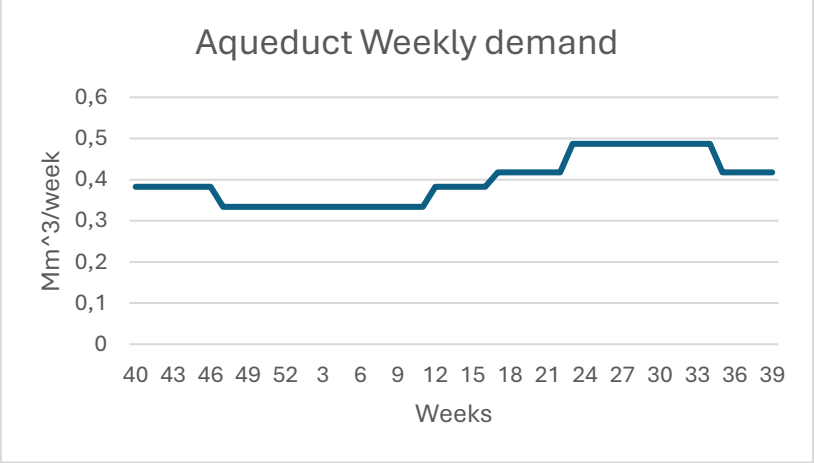


*Figure 20: weekly demand calculated for each week of the year.*

For the calculation of the weekly withdrawal values shown in *Figure 20*, a constant demand of 0,6 cubic meters per second was not assumed, but to vary the demand according to the season and the period of the year.

According to this approach, the assumed withdrawal flow rate values are:

- 0,55 $m^3/s$ from week 40 to week 46 and week 12 to week 16;
- 0,48 $m^3/s$ from week 47 to week 11;
- 0,6 $m^3/s$ from week 17 to week 22 and week 36 to week 39;
- 0,7 $m^3/s$ from week 23 to week 35;

However, the absence of possible peak events or irregularities during the year may represent a limitation for a fully realistic representation of the impacts that these could have within the model.

The table below represents the hierarchy of priorities assigned within the scenario.

| **Node (Reservoir or Demand Site)** | **Priority** |
|---|---|
| Serrù Reservoir | 3 |
| Ceresole Reservoir | 5 |
| Teleccio Reservoir | 3 |
| Eugio Reservoir | 3 |
| Valsoera Reservoir | 3 |
| Ceresole Villa Power Plant | 2 |
| Ceresole Rosone Power Plant | 4 |
| Teleccio-Eugio-Rosone Power Plant | 2 |
| Caluso Consortium | 6 |
| Ovest-Orco Consortium | 7 |
| Est-Orco Consortium | 7 |
| Reirola San Marco Consortium | 8 |
| All Environmental Flow Requirements | 1 |
| Valle Orco's Aqueduct | 1 |

*Table 15: Representation of supply priorities for scenario 2.*

### 4.4) Scenario 3: Different water allocation with aqueduct.

The purpose of this scenario is to evaluate the effects within the model by changing the water allocation priority values, while still considering the presence of the new aqueduct system under construction.

In this specific case, the nodes related to downstream agricultural consortia will be assigned a higher priority compared to the upstream hydropower plants. As a result, the expected outcome of the simulation for this scenario should show a reduction in hydropower production during the irrigation season and an increased tendency of the model to release water from the reservoirs to satisfy the water demand of the downstream agricultural consortia.

The aqueduct system will always maintain the highest priority, given the importance of the water resource for human use.

| **Node (Reservoir or Demand Site)** | **Priority** |
|---|---|
| Serrù Reservoir | 7 |
| Ceresole Reservoir | 8 |
| Teleccio Reservoir | 7 |
| Eugio Reservoir | 7 |
| Valsoera Reservoir | 7 |
| Ceresole Villa Power Plant | 6 |
| Ceresole Rosone Power Plant | 7 |
| Teleccio-Eugio-Rosone Power Plant | 6 |
| Caluso Consortium | 3 |
| Ovest-Orco Consortium | 4 |
| Est-Orco Consortium | 4 |
| Reirola San Marco Consortium | 5 |
| All Environmental Flow Requirements | 1 |
| Valle Orco's Aqueduct | 1 |

*Table 16: Representation of supply priorities for scenario 3.*

### 4.5) Scenario 4: Influence of the new reservoir in Soana sub-basin.

The Department of Environmental, Land and Infrastructure Engineering (DIATI) of the Politecnico of Turin has conducted a research study to verify the technical pre-feasibility for the construction of a new reservoir within the Val Soana *(Iren S.p.A. Press Release, 2024)*.

The reservoir will be located near Stroba, between the municipalities of Pont Canavese and Ingria. According to the IREN press release, the reservoir is expected to have a total capacity of approximately 35 million cubic meters and a height of about 145 meters. The reservoir would be primarily used for hydropower and agricultural purposes, but also to supply water for firefighting services and for flood management and control.

However, to date, the project is still at the preliminary stages of feasibility studies and information regarding the realization of the reservoir is very limited or almost entirely absent.

Despite the limitations due to the lack of data on the reservoir, it was decided to include the reservoir in the model and to evaluate its potential impact within the valley in terms of water resource management.

Since no information is available regarding technical components, such as the maximum turbine flow, hydropower withdrawals, and especially the elevation-volume curves, numerous assumptions were made within the model.

Given the similarity in total capacity, the main characteristics of the Ceresole reservoir were used as a reference for the modeling of the new reservoir.

Despite the difference in dam height and structure between the two reservoirs (52 meters for Ceresole and around 145 meters for the new reservoir), it was decided to use the same Elevation-Volume curve, adjusted in terms of elevation.

The motivation for this choice is based on three considerations:

- The goal is not to evaluate the variations in the free surface elevation of the reservoir, but only the volumes released from it according to the demand that must be satisfied;
- Net evaporation has a minimal influence on the variations in reservoir volume, since the losses or gains caused by this parameter are on the order of millimeters;

- The elevation-volume curve is useful for calculating energy production only if the Reservoir module is used.

Since the hydropower plants within the model are represented and simulated according to the procedure described in *Section 3.3.10,* this curve will have no influence on energy production.

Based on these assumptions, *Table 17* shows the characteristics of the reservoir and its corresponding hydropower plant.

| **Reservoir Soana** | **Assumed Value** |
|---|---|
| Maximum storage $(Mm^3)$ | 35 |
| Top of Conservation $(Mm^3)$ | 34 |
| Top of Buffer $(Mm^3)$ | 9 |
| Top of Inactive $(Mm^3)$ | 1,2 |
| Buffer Coefficient | 0,2 |
| Initial Storage at year 2010 $(Mm^3)$ | 0 |
| **Soana Power Plant** | **Assumed Value** |
| Max Turbine Flow $(m^3/s)$ | 10 |
| Fixed Head $(m)$ | 300 |
| Turbine efficiency $(\%)$ | 85 |

*Table 17: Parameters used for Soana reservoir modelling and assumed values for Soana Power Plant*

As shown in *Table 17*, the reservoir was assumed to be empty in the year 2010, allowing it to fill naturally over-time.

Regarding the choices related to the hydropower plant, it was decided to use a fixed head slightly higher than the dam height, assuming that the power plant is located downstream respect to the reservoir.

Furthermore, for the withdrawal values assigned to the plant for electricity production, it was assumed a water withdrawal demand modeled on the Ceresole-Rosone power plant demand.
The power plant turbine was designed in order to operate at optimal efficiency levels, thereby maximizing the flow rate withdrawn (*Table 17*).

Along the course of the Soana stream, immediately downstream of the reservoir, an EFR check point was included, reporting the values defined in the documentation of the Regional Regulation of the Piedmont Region, updated to year 2021.

| **Node (Reservoir or Demand Site)** | **Priority** |
|---|---|
| Serrù Reservoir | 3 |
| Ceresole Reservoir | 5 |
| Teleccio Reservoir | 3 |
| Eugio Reservoir | 3 |
| Valsoera Reservoir | 3 |
| Ceresole Villa Power Plant | 2 |
| Ceresole Rosone Power Plant | 4 |
| Teleccio-Eugio-Rosone Power Plant | 2 |
| Caluso Consortium | 6 |
| Ovest-Orco Consortium | 7 |
| Est-Orco Consortium | 7 |
| Reirola San Marco Consortium | 8 |
| All Environmental Flow Requirements | 1 |
| Soana Reservoir | 5 |
| Soana Power Plant | 4 |

*Table 18: Representation of supply priorities for scenario 4.*

# 5) Results

## 5.1) Calibration Results

In this section, the results related to the calibration of the model are presented, based on the measured data described and defined in *Section 3*. Overall, the calibration procedure produced satisfactory results.

Given the results obtained, it is possible to provide a positive answer to the research question formulated in the Introduction, thus confirming that it is possible to achieve good calibration performance and to develop a reliable hydrological model even when the Hydrological Response Units are organized differently with respect to the methodology proposed by *Young et al. (2009)*.

Subsequently, the calibration results related to Snow Water Equivalent, streamflow, reservoir, and glacier calibration are presented.

### Snow Water Equivalent Calibration

The calibration of Snow Water Equivalent yielded overall satisfactory results for most of the snow measurement stations included in the model. The calculated Pearson correlation coefficients (r) spans within a range between 0,74 and 0,90, thus indicating a good correlation between observed and simulated data. Consequently, Snow Water Equivalent is well simulated within the valley.

As previously mentioned in *Section 3.4*, the Colleretto and Locana/Rosone stations exhibited less satisfactory results, with Pearson correlation coefficient values equal to 0,47 and 0,58, respectively.

However, despite the low correlation values observed for these stations, they do not exert a significant influence on the overall performance of the model, as they are characterized by very low Snow Water Equivalent values.

The calibration results obtained for the snow gauge stations are shown in the following figures (*Figure 21, Figure 22, Figure 23 and Figure 24*).

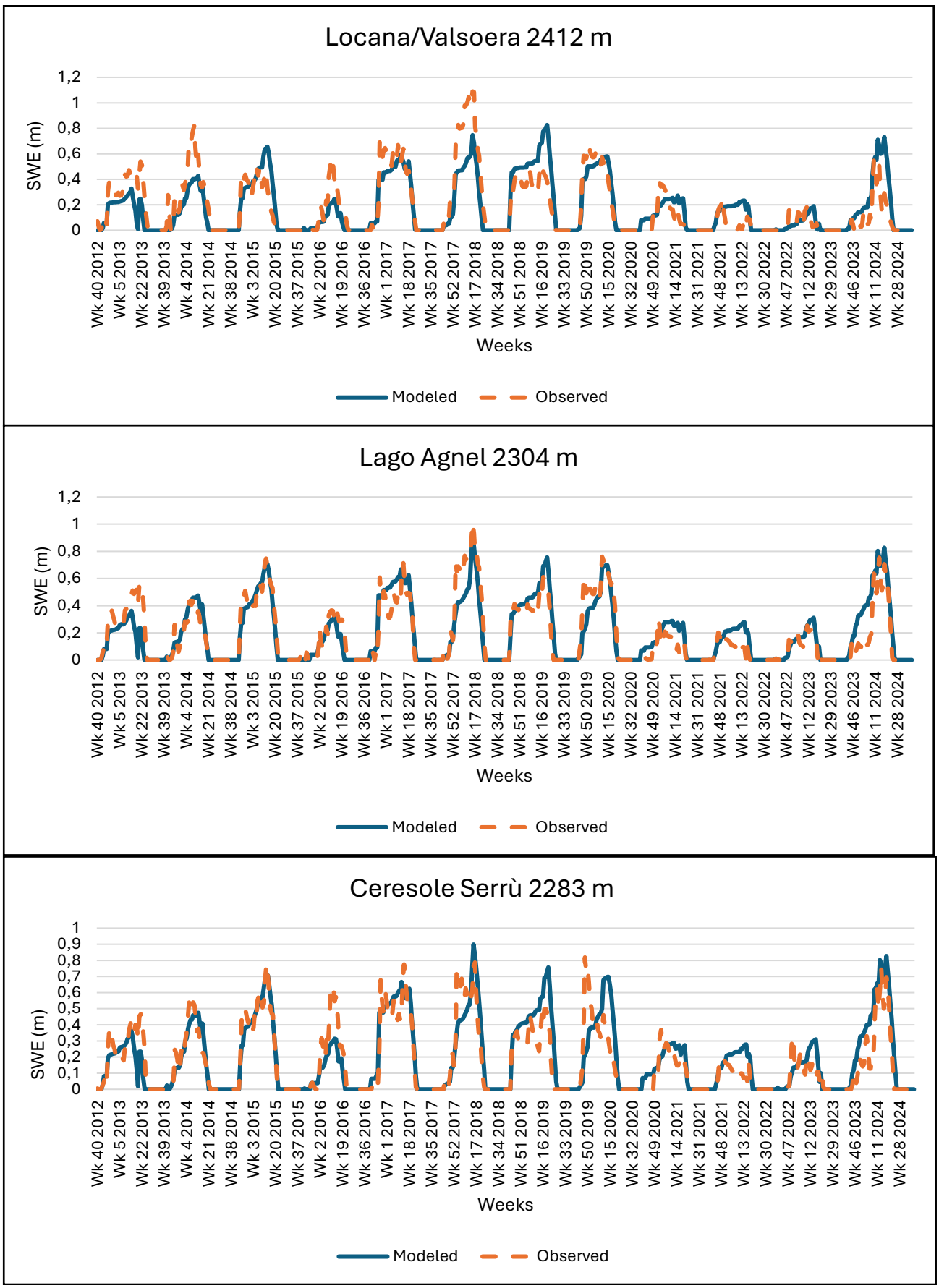


*Figure 21: Observed and Modeled values for Locana/Valsoera, Lago Agnel and Ceresole Serrù gauge stations.*

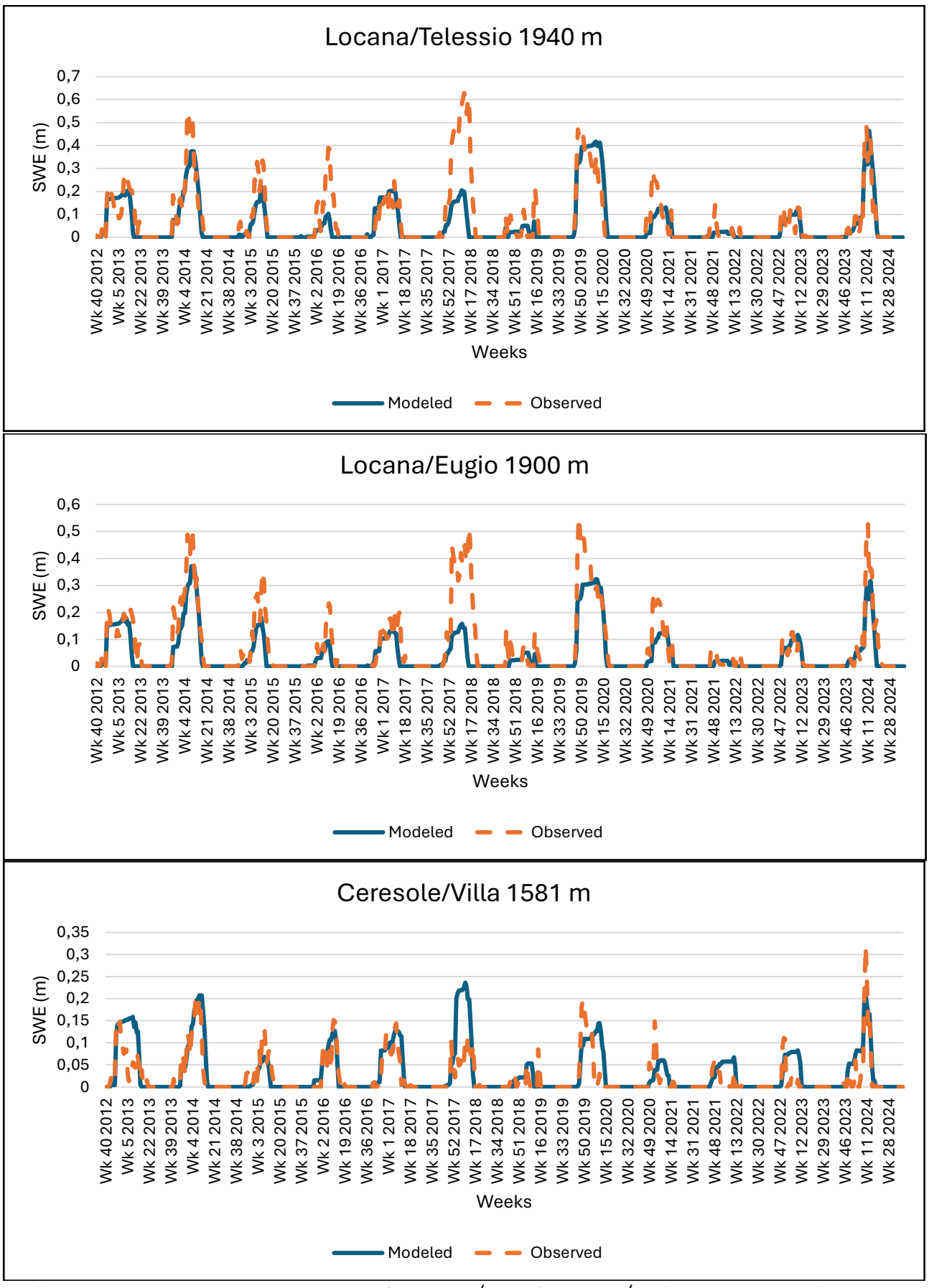


*Figure 22: Observed and Modeled values for Locana/Telessio, Locana/Eugio and Ceresole Villa gauge stations.*

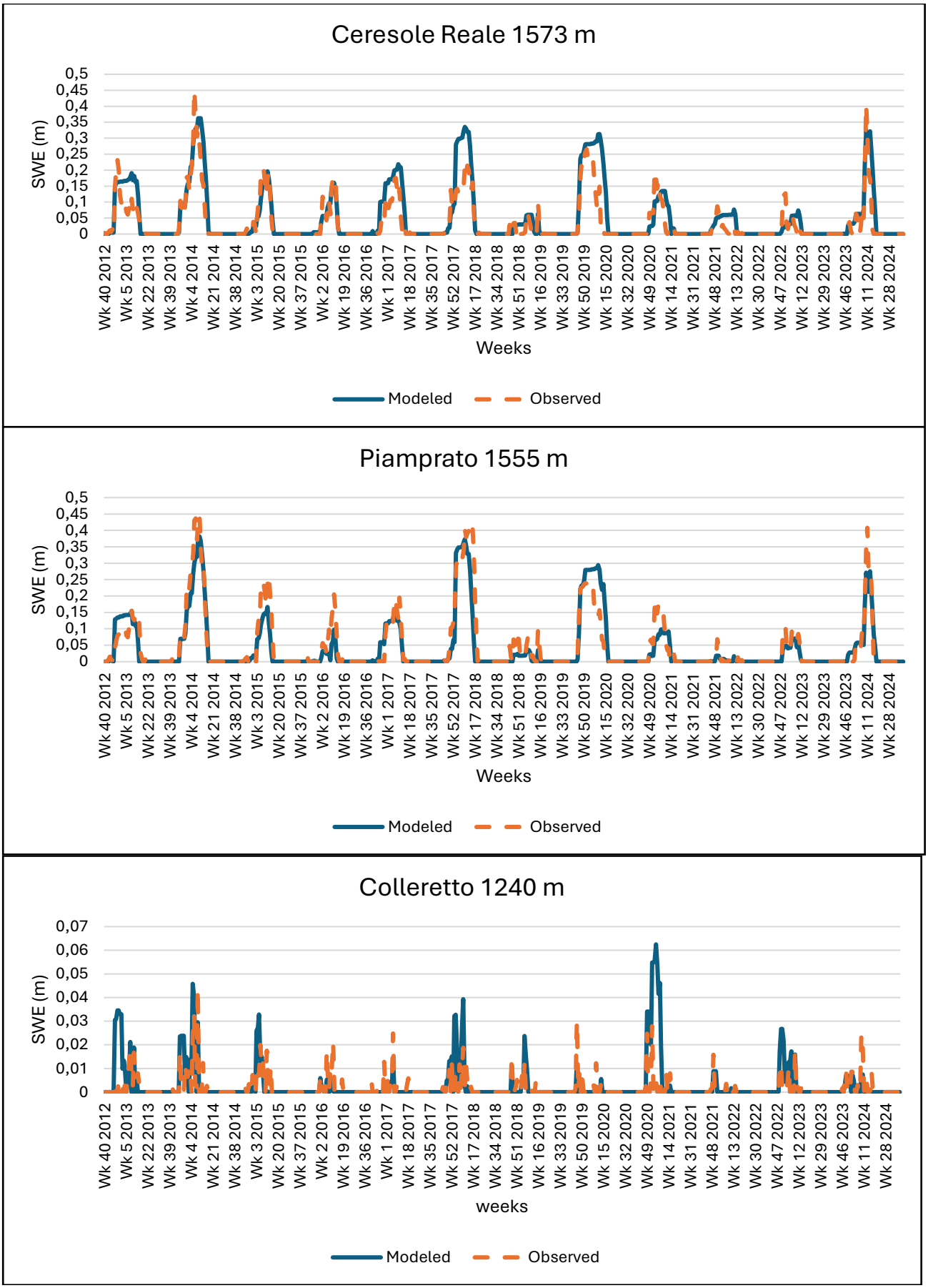


*Figure 23: Observed and Modeled values for Ceresole Reale, Piamprato and Colleretto gauge stations.*

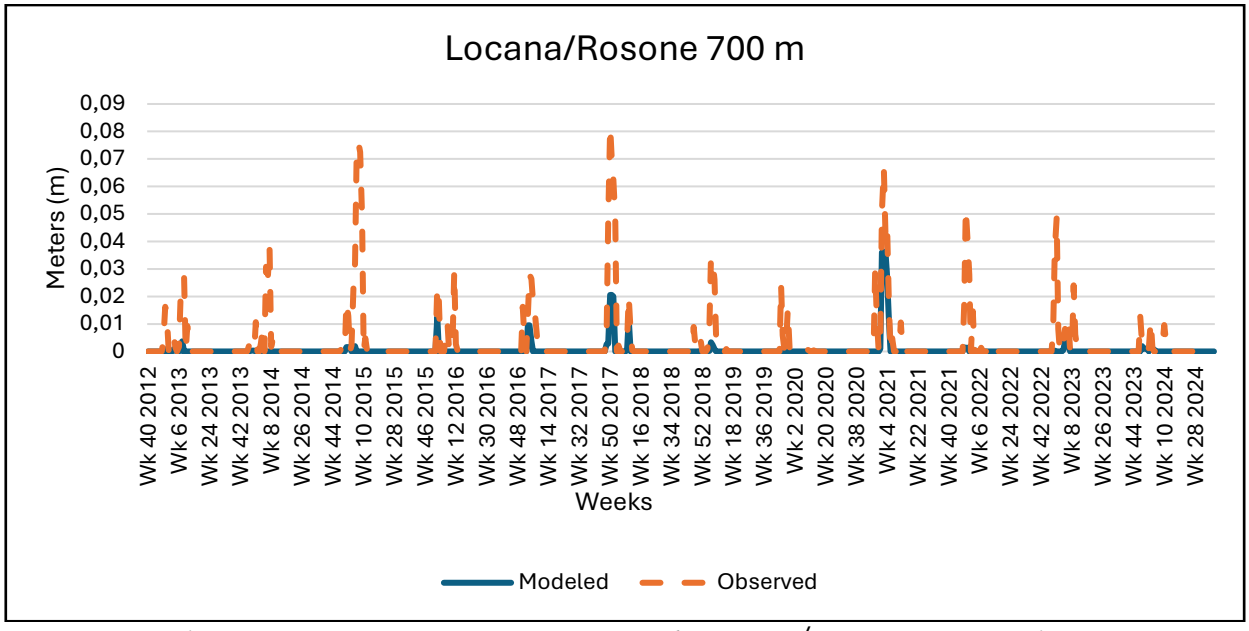


*Figure 24: Observed and Modeled values for Locana/Rosone gauge station.*

| Snow Gauge station | Pearson Correlation coefficient (r) | Root Mean Square Error (RMSE) |
|---|---|---|
| Locana/Valsoera | 0,82 | 0,14 |
| Lago Agnel | 0,9 | 0,1 |
| Ceresole/Serrù | 0,87 | 0,11 |
| Locana/Telessio | 0,8 | 0,081 |
| Locana/Eugio | 0,84 | 0,072 |
| Ceresole Villa | 0,74 | 0,037 |
| Ceresole Reale | 0,86 | 0,047 |
| Piamprato | 0,9 | 0,04 |
| Colleretto | 0,47 | 0,0078 |
| Locana/Rosone | 0,58 | 0,00096 |

*Table 19: Pearson correlation coefficients and Root mean square errors calculated for each gauge station*

### Reservoir and glacier calibration results

As previously defined in *Section 3.4*, the calibration of the Ceresole reservoir was carried out using the observed volume over the period 2012–2022 as reference. This procedure, in addition to verifying the correct calibration of the hydrological basin of the Ceresole reservoir, is also useful for evaluating the hydrological response of high-altitude basins (Agnel and Serrù sub-basins).

The model showed very good performance in reproducing the seasonal variations of the reservoir volume (NSE = 0,8; PBIAS = 6.1%; RSR = 0,47).
However, as shown in *Figure 25*, the simulated volume is underestimated during the summer periods of the years 2016, 2017, and 2020.
On the other Hand, the reservoir stored volume has been overestimated in 2014, between years 2015-2016 and in the first weeks of 2020.

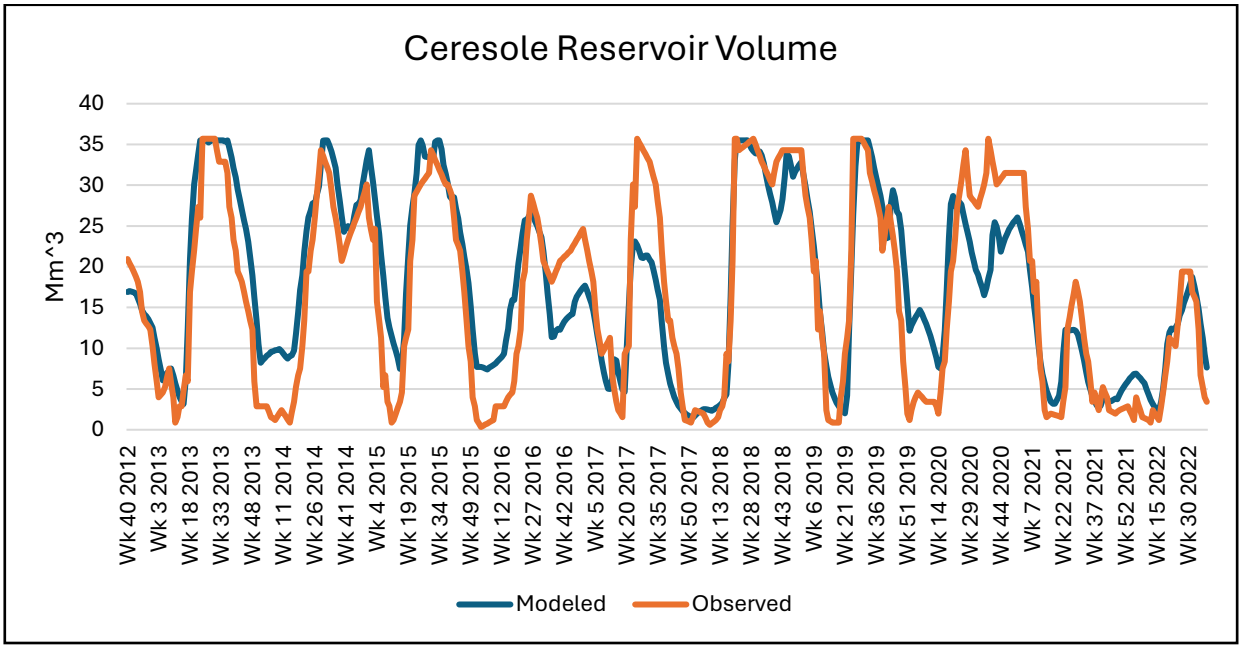


*Figure 25: Observed and Modeled volume of Ceresole Reservoir for period 2012-2022.*

Regarding the calibration of the glacier module, due to the limited glacierized area within the valley and its minor contribution to the overall hydrological mass balance, it was decided to verify only that the glacier thickness variation over the entire analysis period was consistent with the observed one. The comparison was performed using data from the Ciardoney Glacier.
The results indicate a total thickness reduction of 21,4 m, which is consistent with the observed value of 20,8 m.
Due to the lack of information for the other glaciers, the same parameters calibrated for the Ciardoney Glacier were adopted.

## Streamflow gauge calibration results

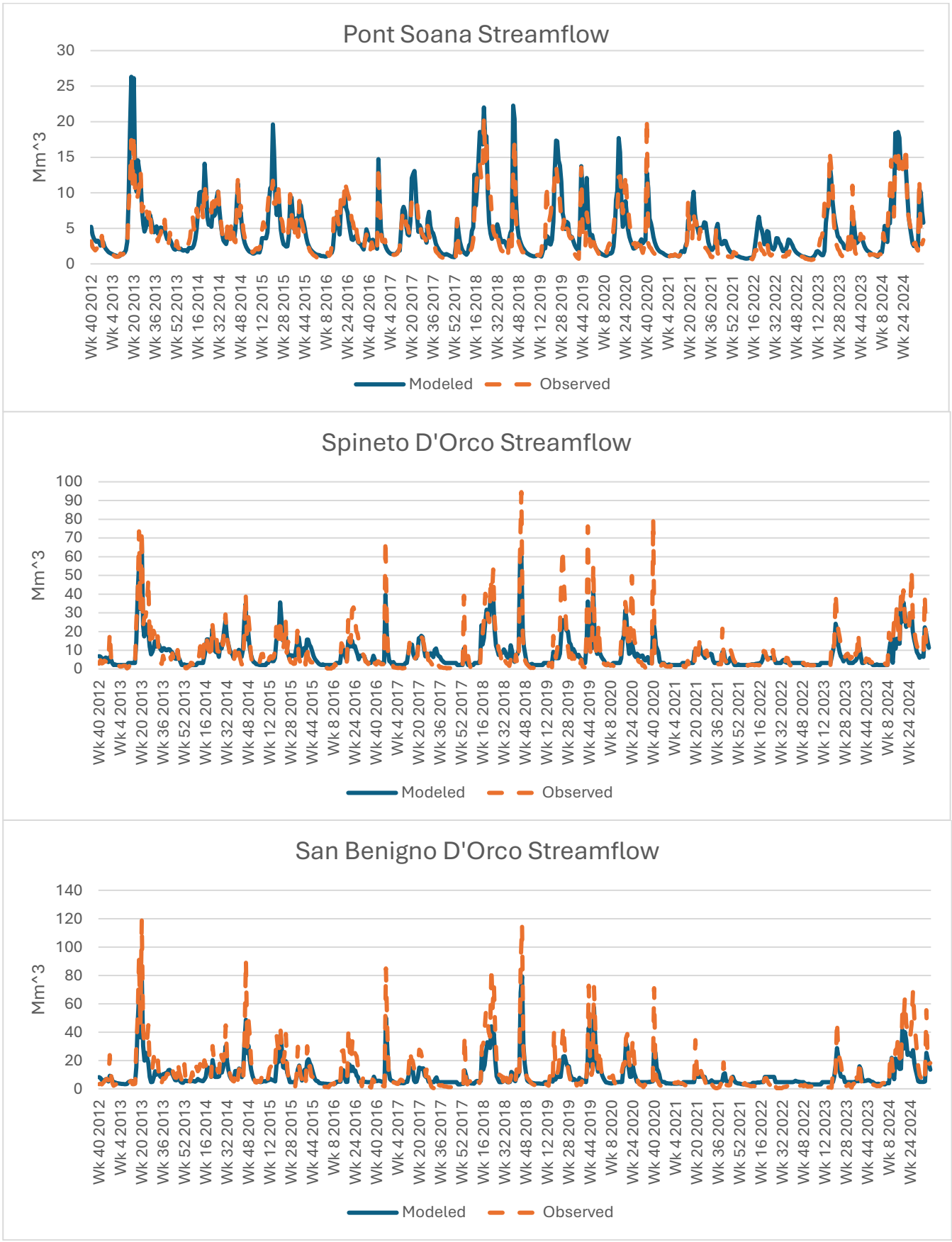


*Figure 26: Observed and Modeled values of streamflow obtained for Pont Soana, Spineto D'Orco and San Benigno D'Orco gauge station.*

*In Figure 26,* the results obtained for the streamflow gauge stations implemented in the model are shown.
Also in this case, the results calculated indicate a good agreement between the simulated and the observed values.

The Pont Soana gauge station played a key role for the whole calibration procedure.
This importance is mainly due to two determining factors:

- the measured flow rate corresponds to the Soana stream, which originates from and is fed exclusively by the homonymous basin as defined in the model;
- the Soana stream sub-basin currently does not contain infrastructures that cause alterations in the discharge.

Based on these considerations, it was therefore possible to adopt the Pont Soana gauge station as a reference point for the calibration procedure, by analyzing the discharge changes resulting from variations in the hydrological parameters.

By observing the results obtained for the Spineto d'Orco station and, in particular, for the San Benigno d'Orco station, it can be noted that the model tends to underestimate the peak flows that occurred in the years 2016, 2018, 2019, and 2020.

The observed underestimations are more pronounced at the San Benigno d'Orco station, probably due to the influence of water withdrawals related to the irrigation season of the consortia.

| **Gauge station** | **NSE** | **PBIAS (%)** | **RSR** |
|---|---|---|---|
| Pont Soana | 0,72 | 8,8 | 0,52 |
| Spineto D'Orco | 0,75 | -4,4 | 0,52 |
| San Benigno D'Orco | 0,73 | -19 | 0,52 |

*Table 20: Statistical metrics reported for the streamflow gauge stations.*

## 5.2) Results for scenario 1: Reference conditions

The results of Scenario 1 represent the baseline conditions of the Orco Valley under the current water resource management framework over the hydrological period 2013–2024.

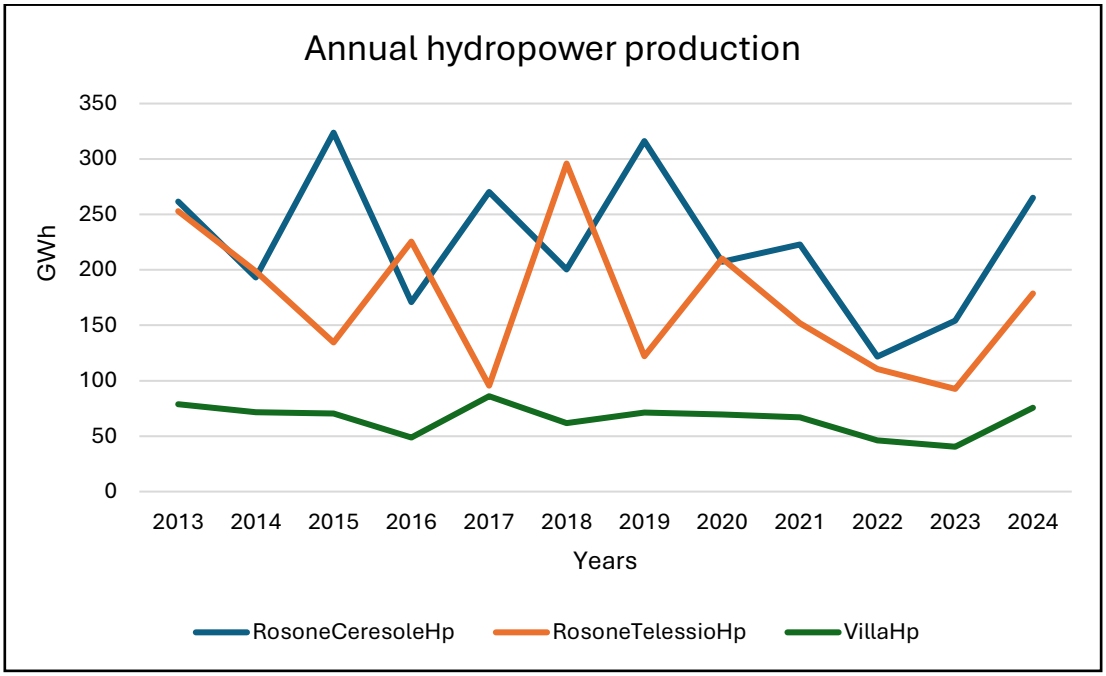


*Figure 27: Annual Hydropower production of each power plant for scenario 1.*

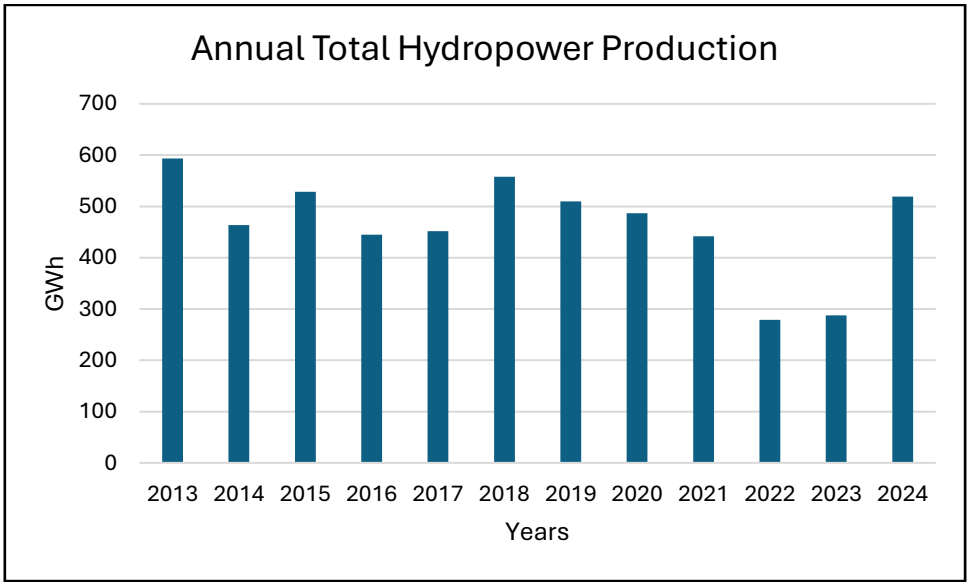


*Figure 28: Annual total hydropower production for scenario 1.*

*Figure 27* shows the annual hydropower production of the power plants implemented in the hydrological model.

The most relevant plant is Ceresole–Rosone, with a total energy production of 2707 GWh over the entire simulation period, while the Ceresole–Villa plant is the

least productive, with a cumulative value of 788 GWh. The Telessio–Eugio–Rosone plant recorded a total production of 2068 GWh.

In *Figure 28* the yearly total hydropower production is reported. The years with the highest energy generation were 2013, 2015, 2018 and 2024.
In particular, the highest production peak was recorded in 2013, reaching 593 GWh.
Conversely, the two-year period 2022–2023 showed a significant reduction in hydropower production due to the severe drought that affected the study area during those years.
In detail, the minimum value was observed in 2022, with a total production of only 278 GWh.
In *Section 9*, the modeled hydropower energy produced was compared with the values reported in the Iren S.p.A. technical reports (2022) for the available period (2013-2022), showing good agreement and consistency.

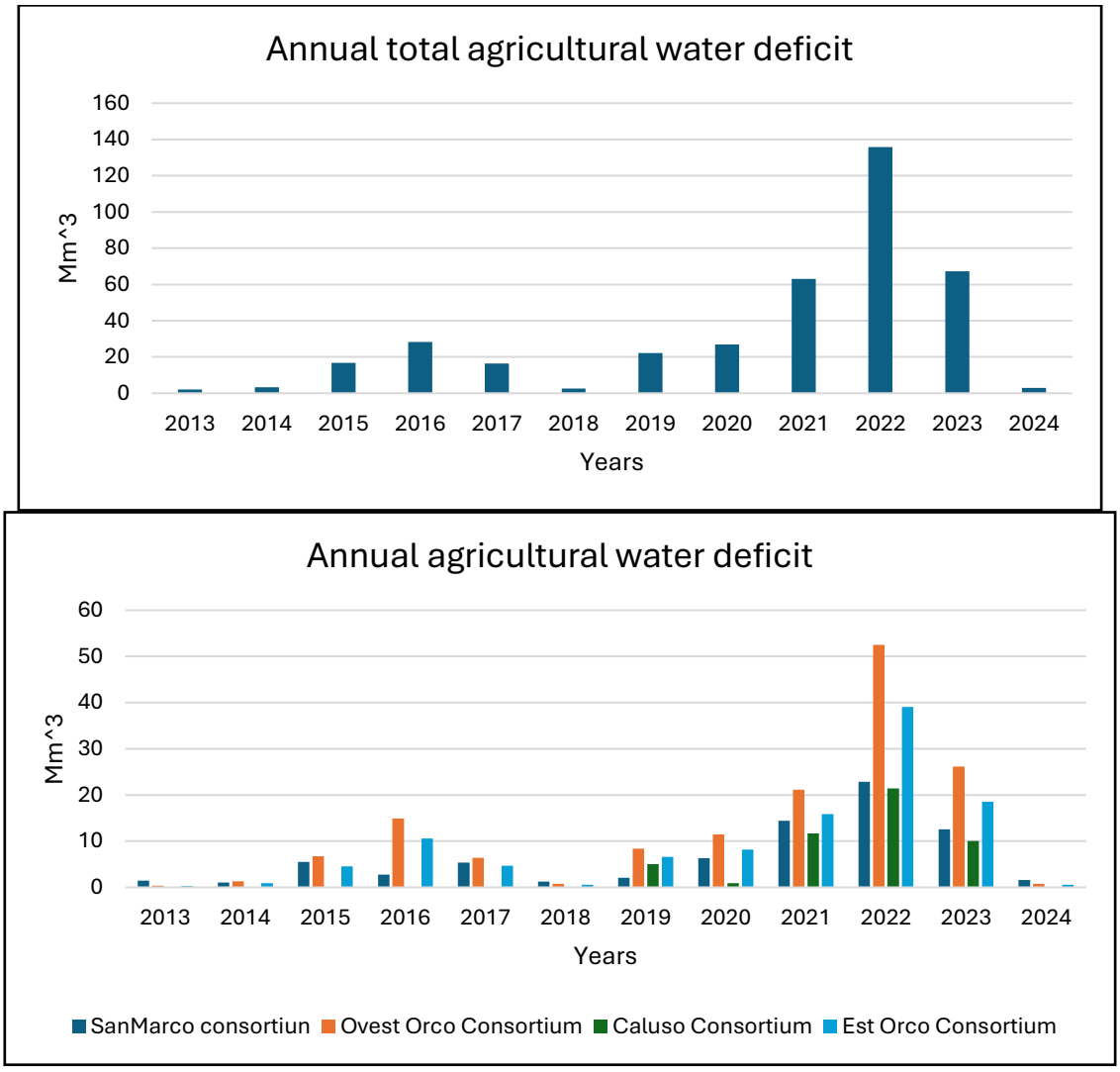


*Figure 29 and 30: Agricultural annual total water deficit (up) and consortia annual water deficit (down).*

In *Figure 29* the overall agricultural deficits that occurred during the simulation period are reported and calculated by WEAP.
It is noticeable that, throughout the entire simulated period, there were no years in which the irrigation water demand of the consortia was fully satisfied.
The years with the lowest total deficits were 2013, 2014, 2018, and 2024, whereas the most critical conditions occurred during the 2021–2023 period.
2022 was an extremely critical year from the irrigation point of view, with a total deficit of 135 million cubic meters.

*Figure 30*, instead, shows the annual deficit trends simulated for each consortium. The graph indicates that the Caluso consortium was the least affected, with its water demand fully satisfied in 2013, 2014, 2015, 2016, 2017, 2018, and 2024.
This condition can be attributed both to the spatial location of the consortium and to its higher supply priority compared to the other consortia.
By contrast, the Ovest Orco, Est Orco, and San Marco consortia exhibited greater vulnerability during periods of water scarcity, particularly in the 2021–2023 triennium.

Overall, the simulation of the baseline scenario highlighted a total deficit of 387,37 million cubic meters over the entire period.

| Caluso Consortium | Ovest Orco consortium | Est Orco Consortium | Reirola San Marco |
|---|---|---|---|
| 48,94 $Mm^3$ | 150,99 $Mm^3$ | 110,28 $Mm^3$ | 77,14 $Mm^3$ |

*Table 21: Total water deficit for each consortium.*

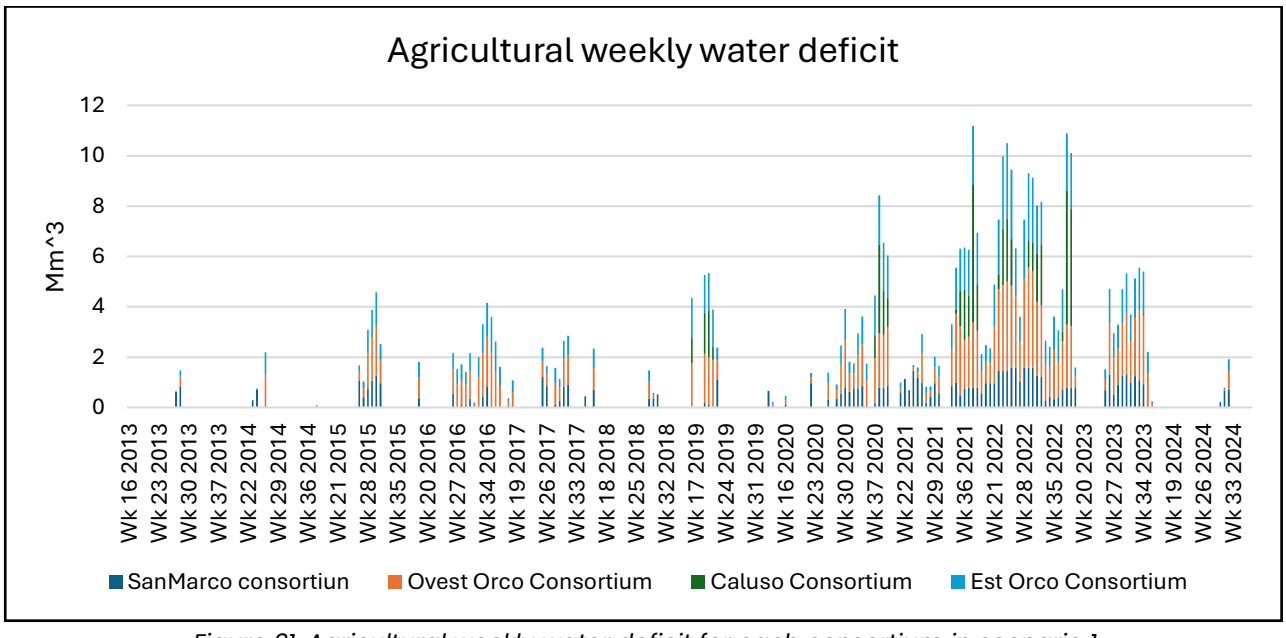


*Figure 31: Agricultural weekly water deficit for each consortium in scenario 1.*

## 5.3) Results for scenario 2: Introduction of the new Valle Orco aqueduct

Scenario 2 simulates the new Orco Valley aqueduct, which is currently under construction, in order to assess its impact on the water system of the study area.

Given the location where the infrastructure was implemented within the model, no significant variations in hydropower production were recorded.
Consequently, the results obtained for the baseline scenario remain unchanged.
By contrast, relevant effects emerged with regard to the downstream irrigation consortia.
As shown in *Figure 32*, an increase in the total agricultural water deficit occurred in all years of the simulation period. In detail, the most pronounced increase was recorded in 2022, with a total increment of 7,5 $Mm^3$, consistent with the hydrological critical conditions that characterized that year.

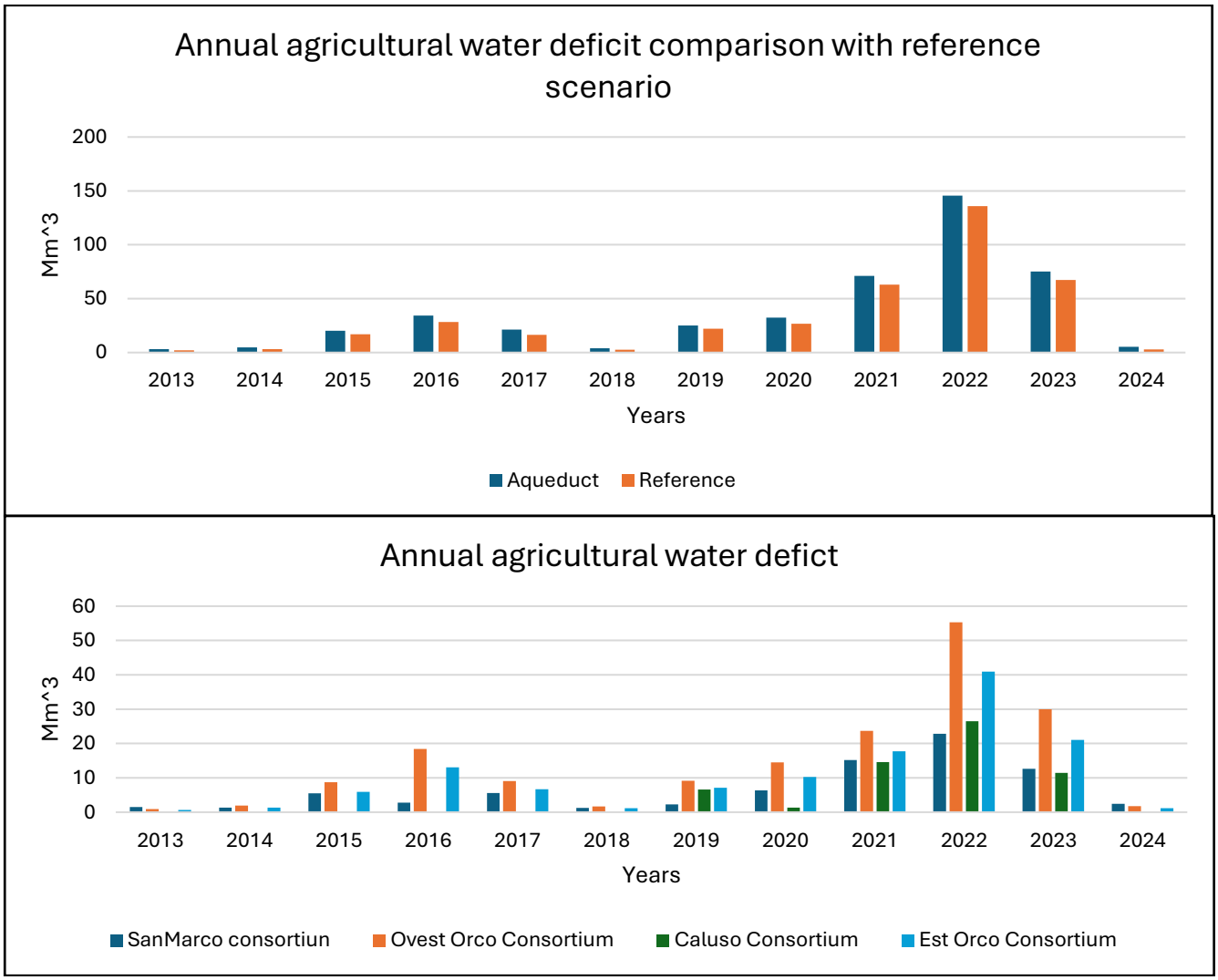


*Figure 32 and 33: Comparison for Annual agricultural total water deficit (up) and consortia annual water deficit (down).*

| Caluso Consortium | Ovest Orco consortium | Est Orco Consortium | Reirola San Marco |
|---|---|---|---|
| 60,41 $Mm^3$ (+23%) | 175 $Mm^3$ (+15%) | 127 $Mm^3$ (+15%) | 79,77 $Mm^3$ (+3,14) |

*Table 22: Total water deficit for each consortium in scenario 2 and the percentual increase with respect to scenario 1.*

From *Table 22*, it can be observed that the aqueduct had a particularly significant impact on the Caluso consortium, resulting in a 23% increase in irrigation deficit compared to the conditions reported in Scenario 1.
However, when the analysis is conducted in terms of absolute water volumes, the Ovest Orco consortium experienced the largest increase in total unmet demand.

It is noteworthy that the Reirola San Marco agricultural site, despite its more downstream location, recorded a smaller increase compared to the other irrigation consortia.
This is likely due to the fact that WEAP attempts to allocate water in a manner that avoids excessive discrepancies among the different components characterizing the valley's hydrological system.

*Figure 34* reported below shows the weekly unmet irrigation demand for each consortium under Scenario 2.

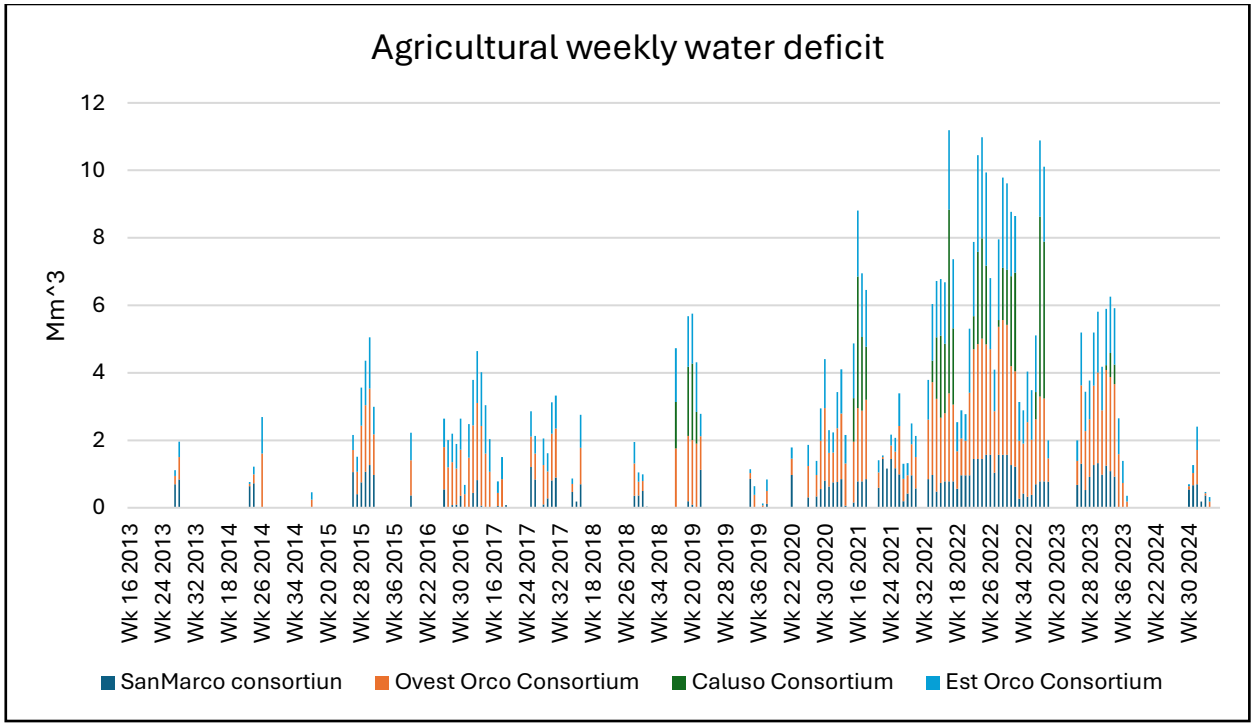


*Figure 34: Agricultural weekly water deficit for each consortium in scenario 2.*

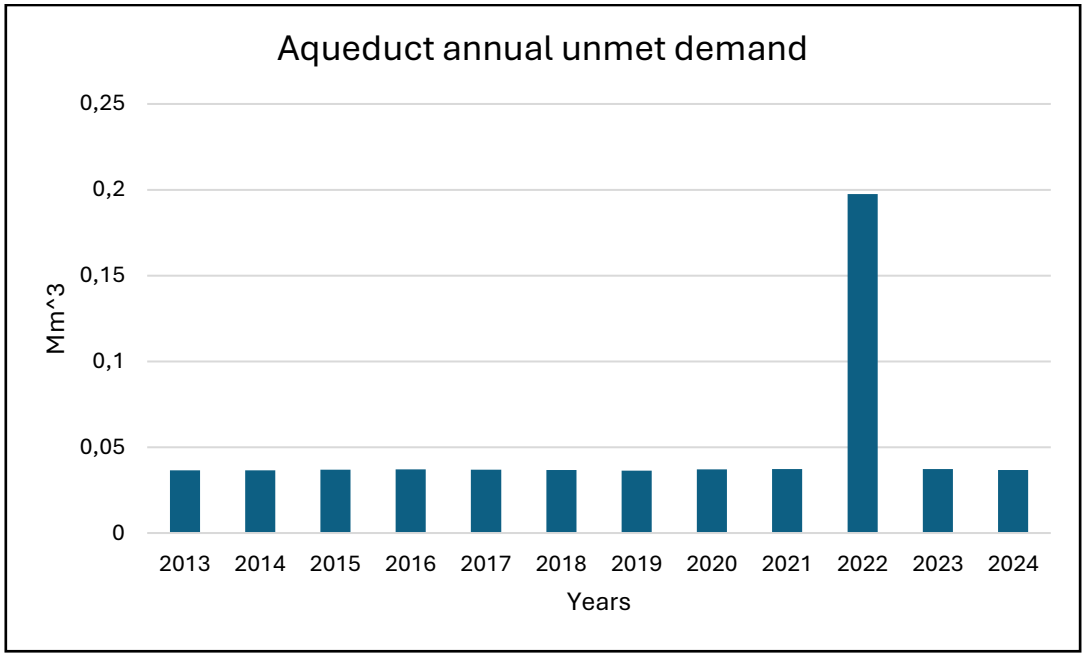


*Figure 35: Aqueduct Annual unmet demand.*

Although the aqueduct is assigned the highest possible supply preference, its demand is not always fully satisfied.
As shown in *Figure 35*, each year exhibits a relatively small but constant deficit of approximately 0,036 $Mm^3$, with the exception of 2022, when the maximum peak of 0,2 $Mm^3$ was reached.
This result indicates that the aqueduct was also affected by the extreme water scarcity that occurred in that year.
Conversely, the water shortages of 2021 and 2023 did not have a significant impact on the infrastructure.

Overall, the total unmet demand for the aqueduct over the simulated period amounts to 0,602 $Mm^3$.

## 5.4) Results for scenario 3: Different water allocation with aqueduct

The present scenario simulates a different allocation of water resources within the study area, with the aim of assessing its effects on the new infrastructure and evaluating the extent to which hydropower production and irrigation demand satisfaction are influenced.

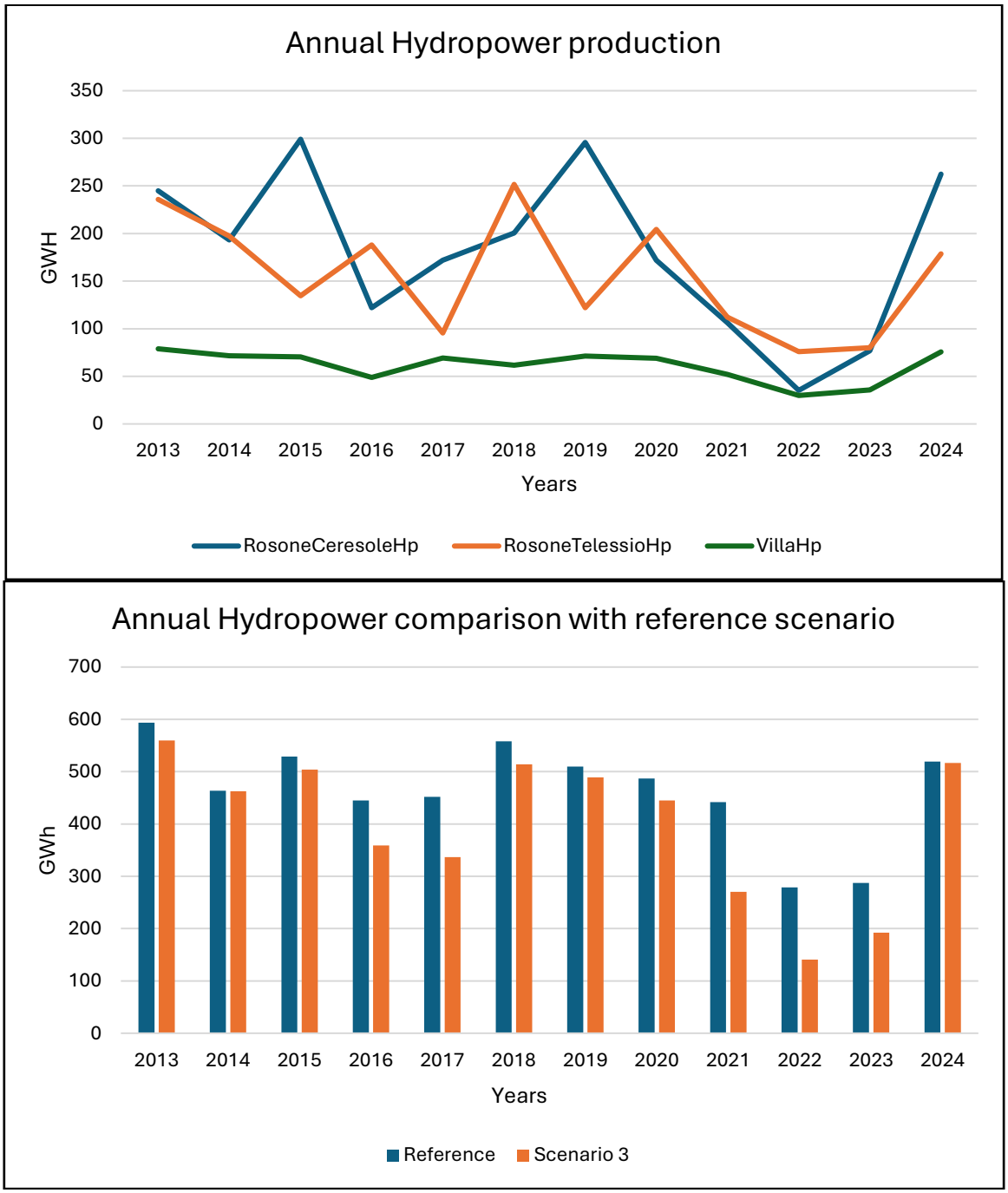


*Figure 36 and 37: Annual hydropower production for each power plant (up) and Annual hydropower production comparison with reference scenario (down).*

As can be observed from *Figures 36 and 37*, the change in water allocation within the valley led to a significant reduction in hydropower generation.
In particular, the most affected plant by this different configuration is Ceresole–Rosone, which recorded a decrease in total energy production from 2707 GWh in Scenario 1 to 2179 GWh in the present scenario, corresponding to a reduction of 19.51%.
The Telessio–Eugio–Rosone plant was also quite affected by the new allocation strategy, decreasing from 2068 GWh in Scenario 1 to 1876 GWh, thus registering a 9.92% reduction.
Conversely, the Ceresole–Villa plant appears to be the least penalized, with a reduction of 7.8% compared to the reference scenario.

*Figure 37* further shows that all simulated years experienced a decrease in energy production, with the exception of 2014 and 2024.
The years that exhibited the most significant reductions were 2017, 2021, 2022, and 2023.
Overall, the results indicate a total decrease of 13.9% compared to baseline conditions.

On the other hand, the agricultural consortia benefited from the change in water allocation, showing a substantial reduction in irrigation deficits during the irrigation season.

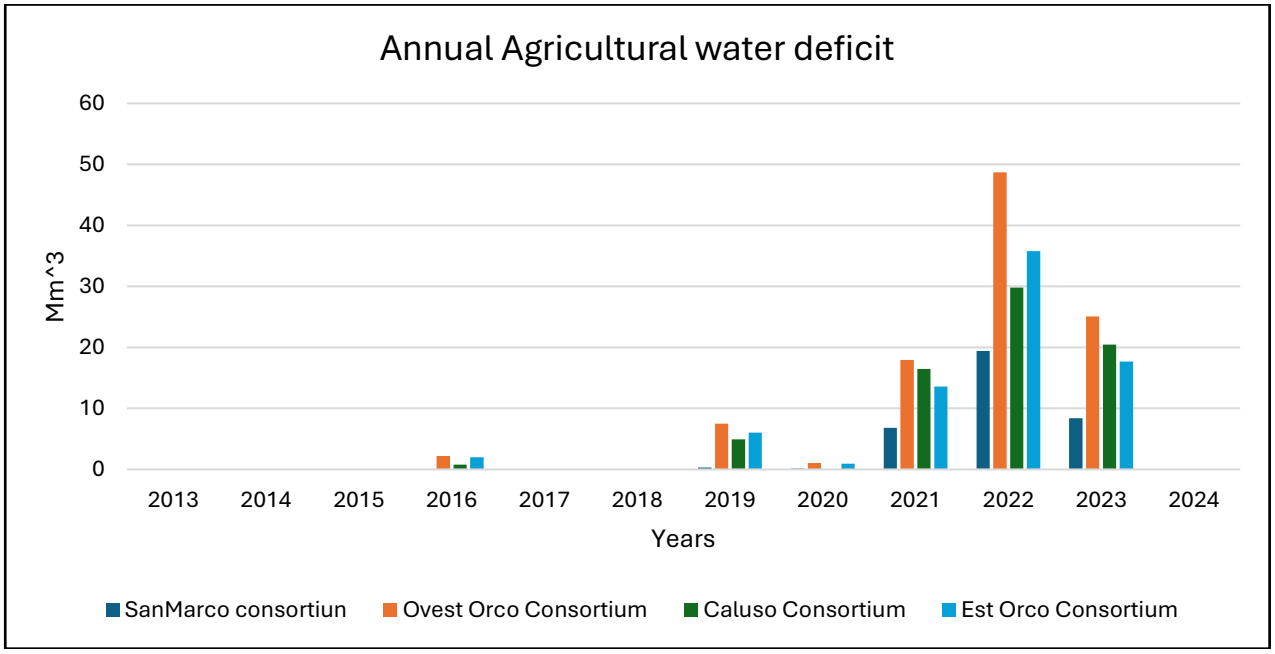


*Figure 38: Annual agricultural water deficit for each consortium in scenario 3.*

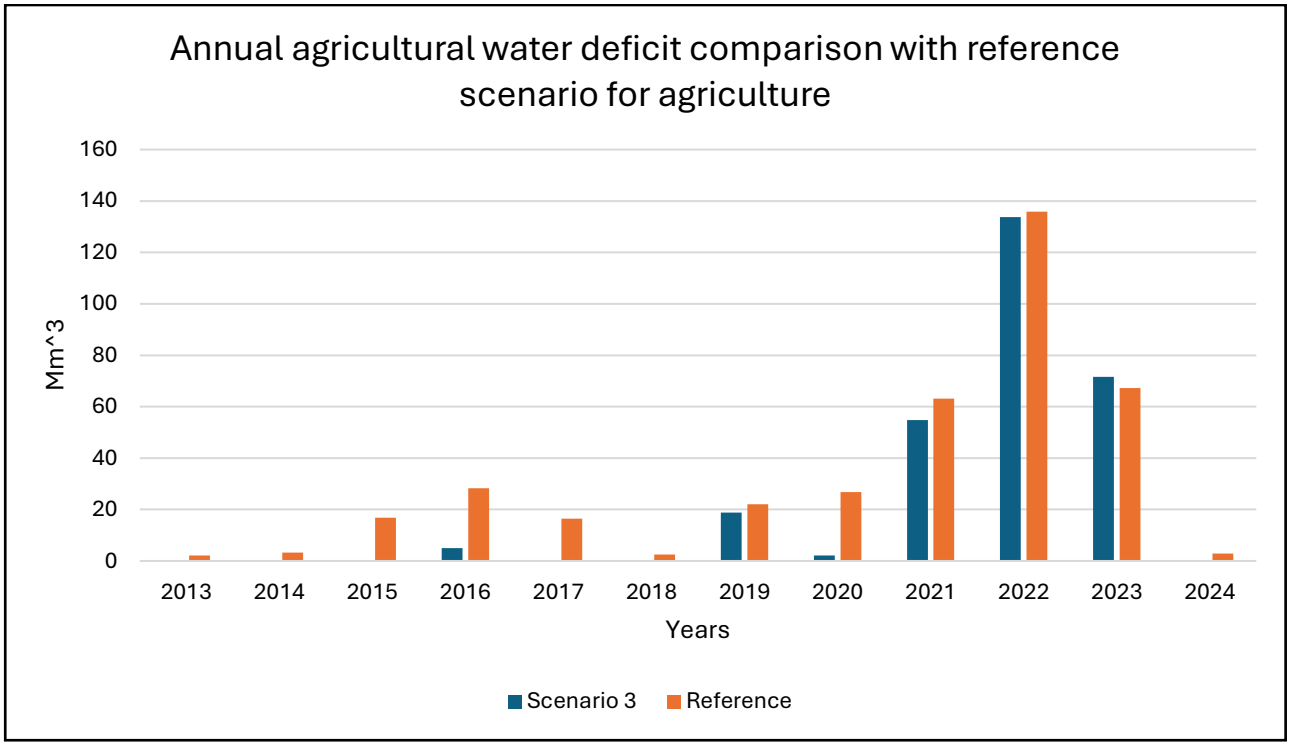


*Figure 39: Annual agricultural water deficit comparison with reference scenario.*

The results shown in *Figure 39* demonstrate that the different water management strategy led to the complete elimination of irrigation deficits during the irrigation season in the years 2013, 2014, 2015, 2017, 2018, and 2024, as well as a significant reduction in 2016 and 2020.
More limited changes were observed in 2019, 2021, and 2022, whereas a slight increase was recorded in 2023.
This behavior is due to the fact that the WEAP model released more water in order to satisfy irrigation demand as much as possible during the most critical years. Subsequently, because of the prolonged drought period, it was not possible to refill the reservoirs, thereby affecting both water supply in the following year and hydropower production, as highlighted in *Figure 37*.

| **Caluso Consortium** | **Ovest Orco consortium** | **Est Orco Consortium** | **Reirola San Marco** |
|---|---|---|---|
| 72,47 $Mm^3$ (+48%) | 102,44 $Mm^3$ (-32,8%) | 76,06 $Mm^3$ (-31,1%) | 35,094 $Mm^3$ (-54,6%) |

*Table 23: Total water deficit for each consortium and percentage variation with respect to scenario 1.*

*Table 23* reports the total irrigation deficit for each consortium and the corresponding percentage variation compared to Scenario 1.

It is noteworthy that all consortia experienced a significant reduction in irrigation deficit, except for the Caluso consortium, which recorded an increase of 48% of unmet demand.
As can be observed in *Figure 38*, the increase in unmet demand for Caluso is mainly concentrated in the 2021–2023 triennium.
This behavior can be attributed to the WEAP allocation logic, which, under conditions of limited water availability, reallocated part of the water originally intended for Caluso to the other consortia in order to prevent a further worsening of their deficits.

Overall, the total irrigation deficit over the simulation period decreased from 387 $Mm^3$ in reference scenario to 286,08 $Mm^3$ (-26.1%) in scenario 3.

*Figure 40* shows the weekly irrigation deficit values obtained for Scenario 3.

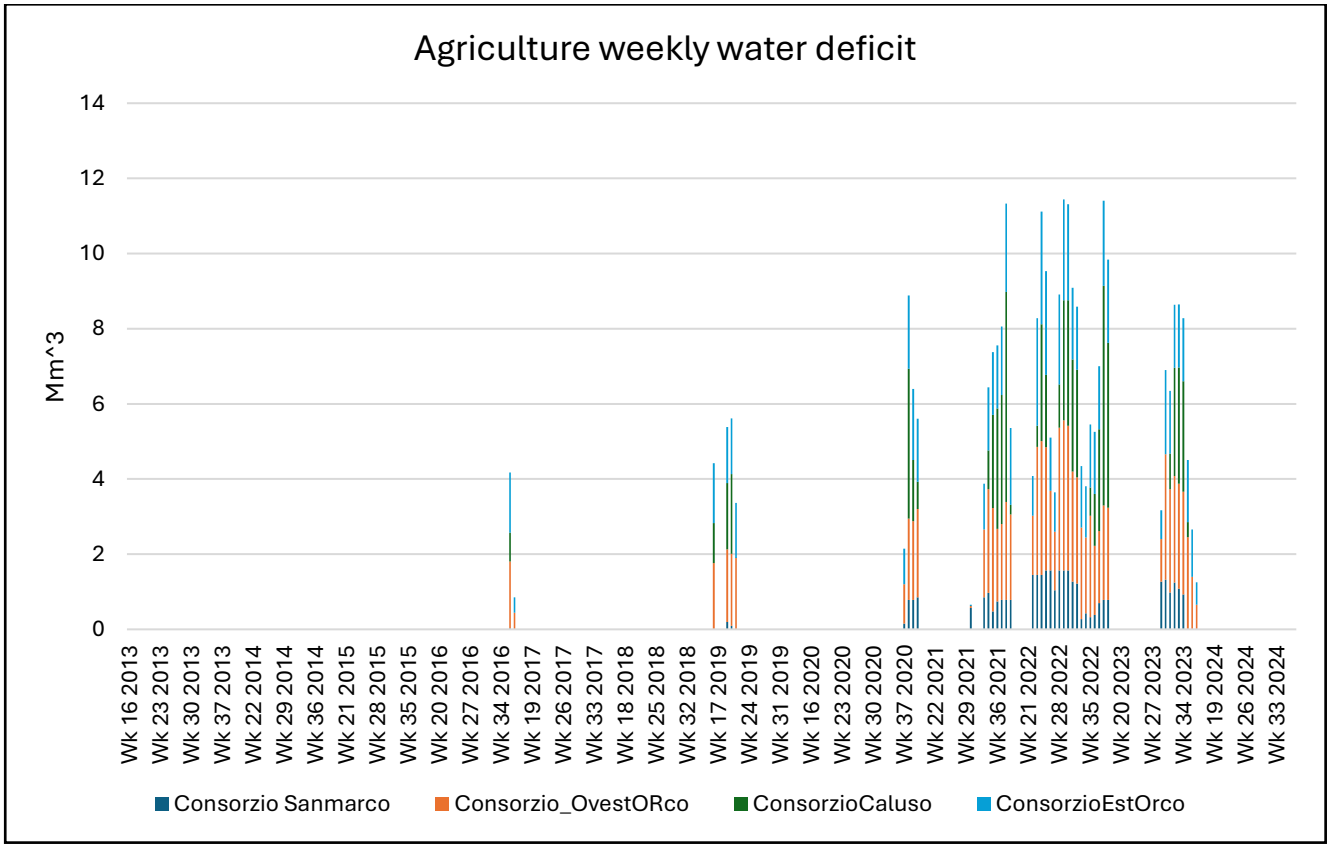


*Figure 40: Agricultural weekly water deficit for each consortium in scenario 3.*

After the analysis of the effects on hydropower production and irrigation demand, it is useful to evaluate how this allocation strategy has influenced reservoir storage conditions (*Figure 41*).

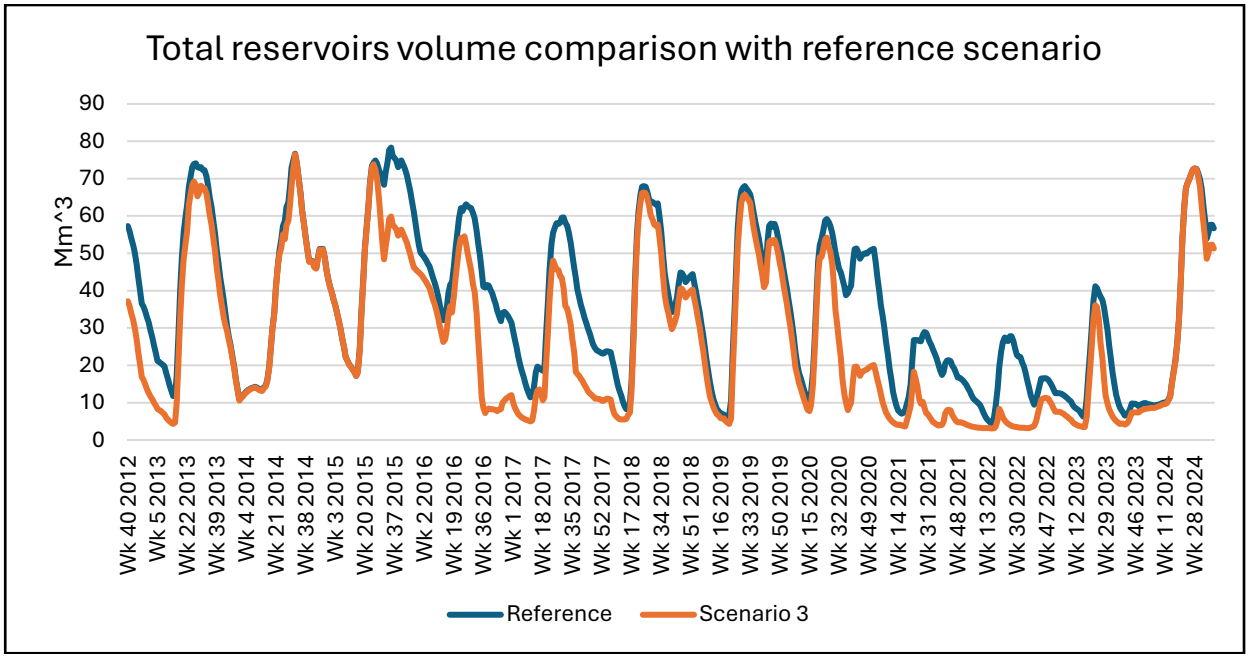


*Figure 41: Total Reservoir Volume comparison between reference scenario and scenario 3.*

The comparison of total reservoir volumes confirms what was anticipated in the discussion of *Figure 37*.
In order to satisfy irrigation demand as much as possible, the model released considerably more water than in the reference scenario.
Significant reductions in total storage volume are observed particularly in the years 2016, 2017, 2020, 2021, and 2022.
Particularly, from week 25 of 2021 to week 48 of 2022, the total reservoir volume remained below 10 $Mm^3$.

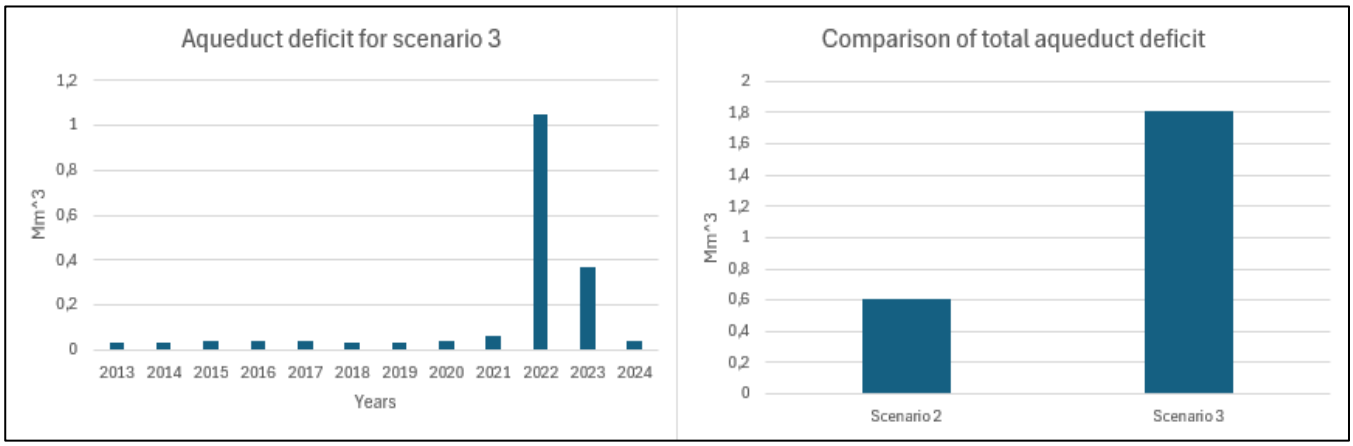


*Figure 42: Aqueduct annual deficit for scenario 3 (left) and Comparison of total aqueduct annual deficit between scenario 2 and scenario 3 (right).*

Finally, as shown in *Figure 42*, the aqueduct was also affected by the new water allocation strategy, exhibiting considerable increases in deficit, especially in 2022 and 2023. The overall deficit is tripled with respect to scenario 2.

## 5.5) Results for scenario 4: Influence of the new reservoir in Soana sub-basin.

In conclusion, the results obtained for Scenario 4 illustrate the effects generated within the study area by the addition of the new reservoir along the Soana stream.

Before proceeding with the discussion of the results, an important clarification must be provided regarding the withdrawal demand used for the new hydropower plant.
As previously stated in *Section 4.5*, the reservoir releases are calibrated according to the same logic adopted for the Ceresole reservoir, without accounting for the different location or the potentially different operational strategies that could be implemented for the new reservoir.

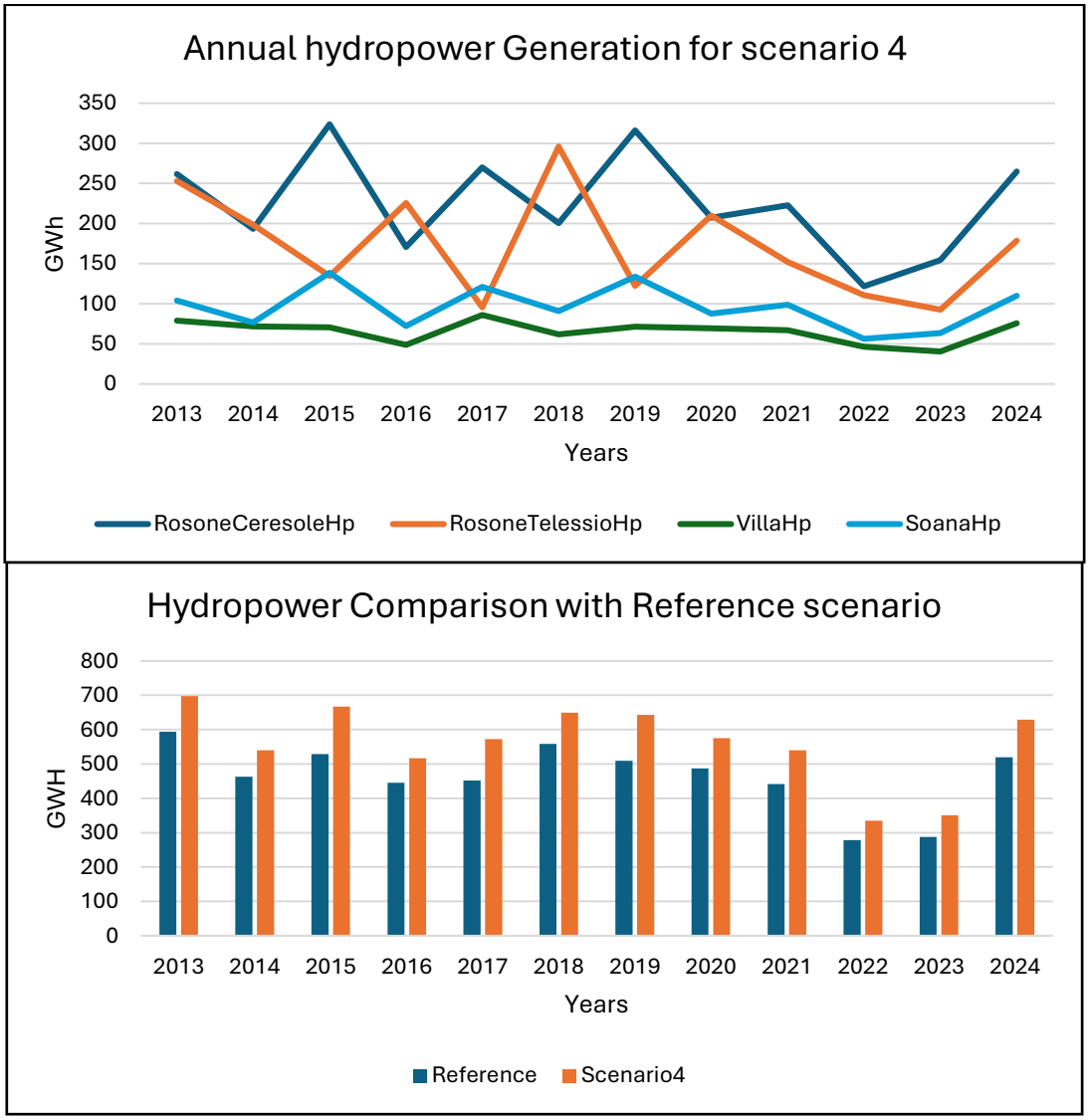


*Figure 43 and Figure 44: Annual hydropower production for each power plant (up) and annual hydropower production comparison with reference scenario (down).*

From the results shown in *Figure 44*, it can be observed that the addition of the new reservoir led to a rather significant increase in hydropower generation. However, this energy increase is considerably constrained by the limited hydraulic head available for the hydropower plant.
To enhance energy production, the plant would need to be constructed further downstream; nevertheless, such a solution would substantially increase the overall construction costs of the project.
As shown in *Figure 43*, the new plant would achieve a higher energy production compared to the Ceresole–Villa plant.

Overall, over the entire simulation period, the introduction of the new reservoir resulted in an increase of 1153 GWh in total energy production, rising from 5563 GWh in the reference scenario to 6717 GWh in the present scenario (+20.7%).

Regarding the agricultural sector, the results concerning changes in irrigation deficits are presented in *Figures 45, 46, and 47.*

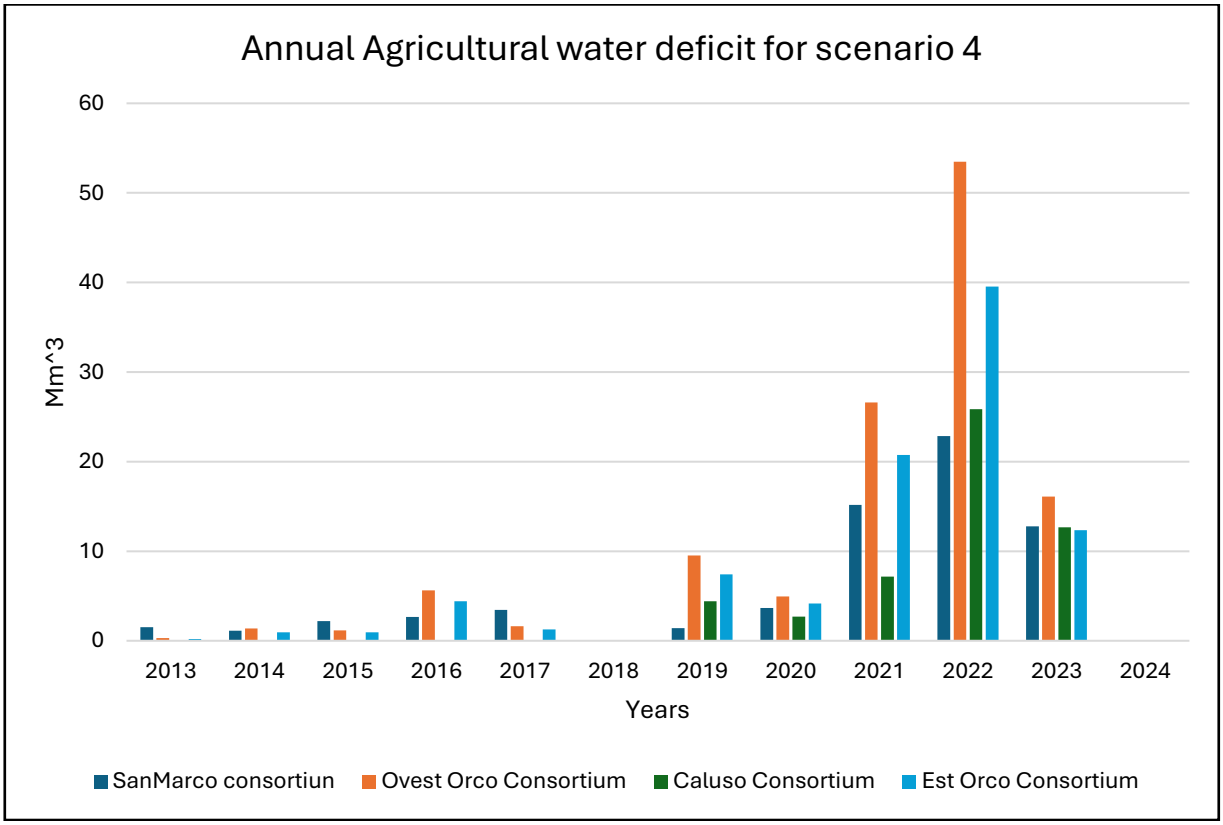


*Figure 45: Annual agricultural water deficit for each consortium in scenario 4.*

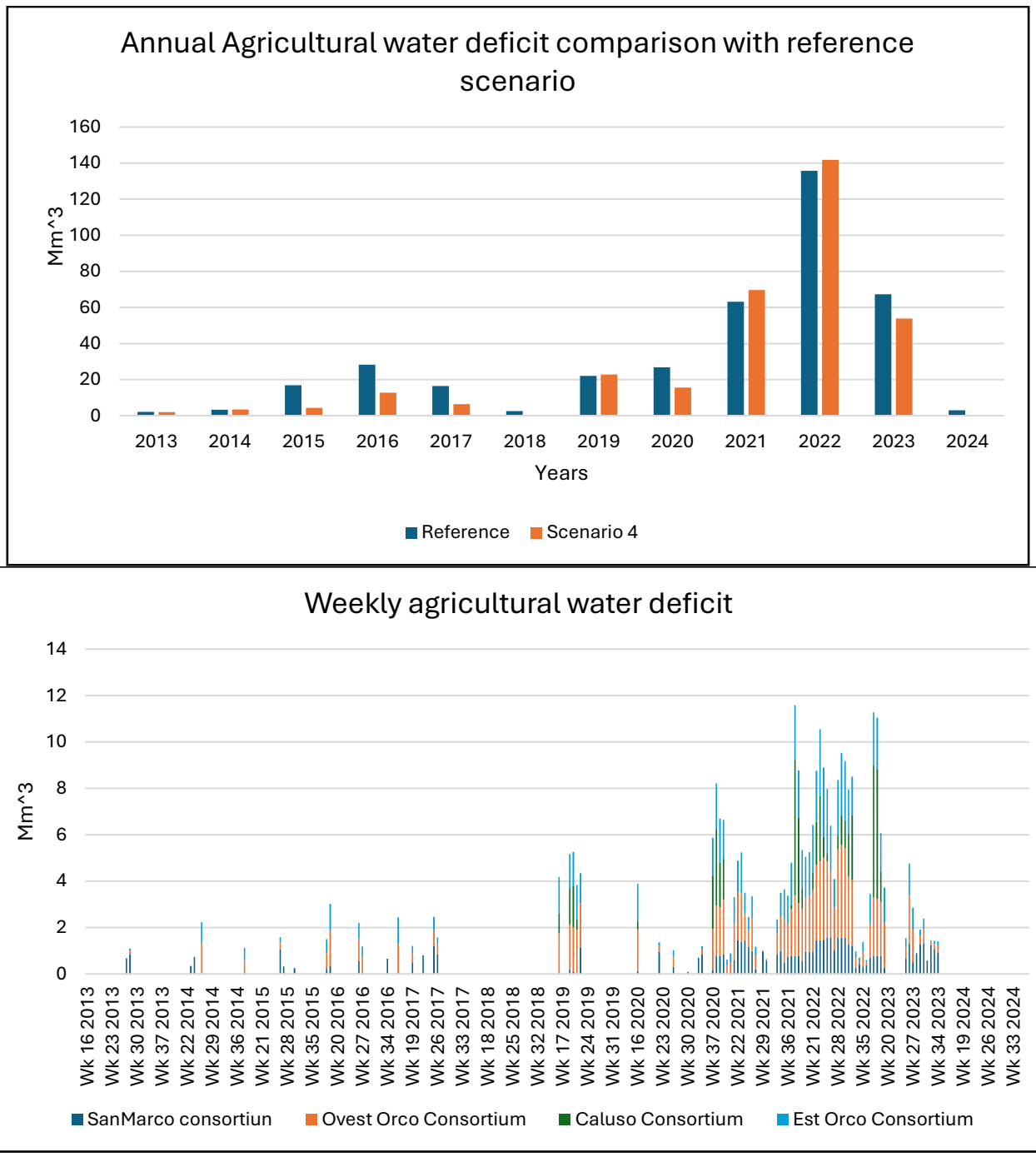


*Figure 46 and Figure 47: Annual total agricultural water deficit comparison with reference scenario (up) and weekly agricultural water deficit for each consortium (down).*

As can be observed from the graphs, the introduction of the reservoir, in addition to increasing hydropower production, also led to an improvement in irrigation deficits during the irrigation season.

In particular, *Figure 46* shows complete satisfaction of irrigation demand in 2018 and 2024, as well as a reduction in deficits in 2015, 2016, 2017, and 2020.

Conversely, increases were recorded in 2021 and 2022.

These results are consistent with the allocation logic described at the beginning of the paragraph.

For the years 2013, 2014, and 2019, deficits remained unchanged.

| Caluso Consortium | Ovest Orco consortium | Est Orco Consortium | Reirola San Marco |
|---|---|---|---|
| 52,81 $Mm^3$ (+7,3%) | 120,71 $Mm^3$ (-20,6%) | 91,95 $Mm^3$ (-16,6%) | 66,82 $Mm^3$ (-13,4%) |

*Table 24: Total water deficit for each consortium and percentage variation with respect to scenario 1.*

Similarly to the results obtained for Scenario 3 (*Table 23*), all consortia experienced an improvement in irrigation conditions, with the exception of Caluso (*Table 24*).

In this case as well, the WEAP model adopted the same allocation logic previously described in *Section 5.4*.
Overall, the total agricultural water deficit was reduced from 387 $Mm^3$ to 332 $Mm^3$(-14,2%).

Finally, after discussing the effects of the new reservoir on both the agricultural sector and hydropower production, *Figures 48* and *49* reported the simulated storage volume of the new reservoir and its contribution to the variation in total storage volume within the valley.

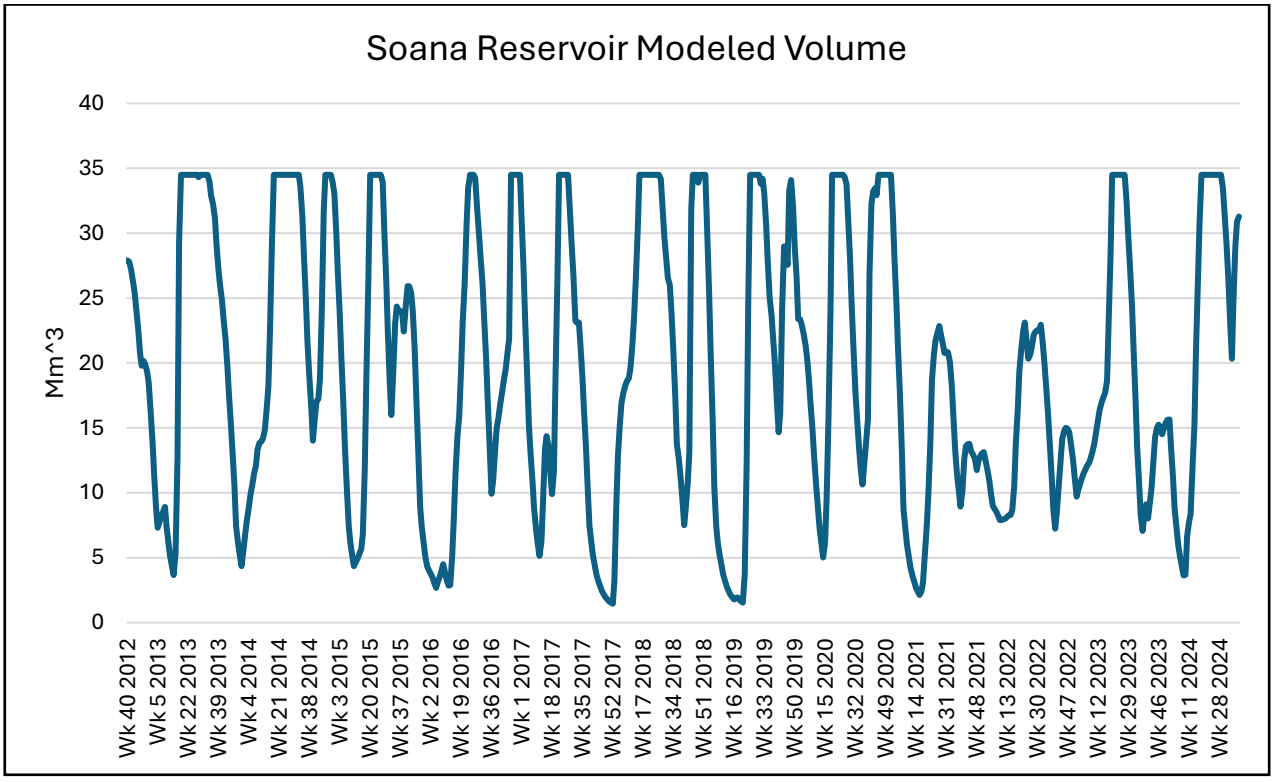


*Figure 48: Soana Reservoir Modeled Volume*

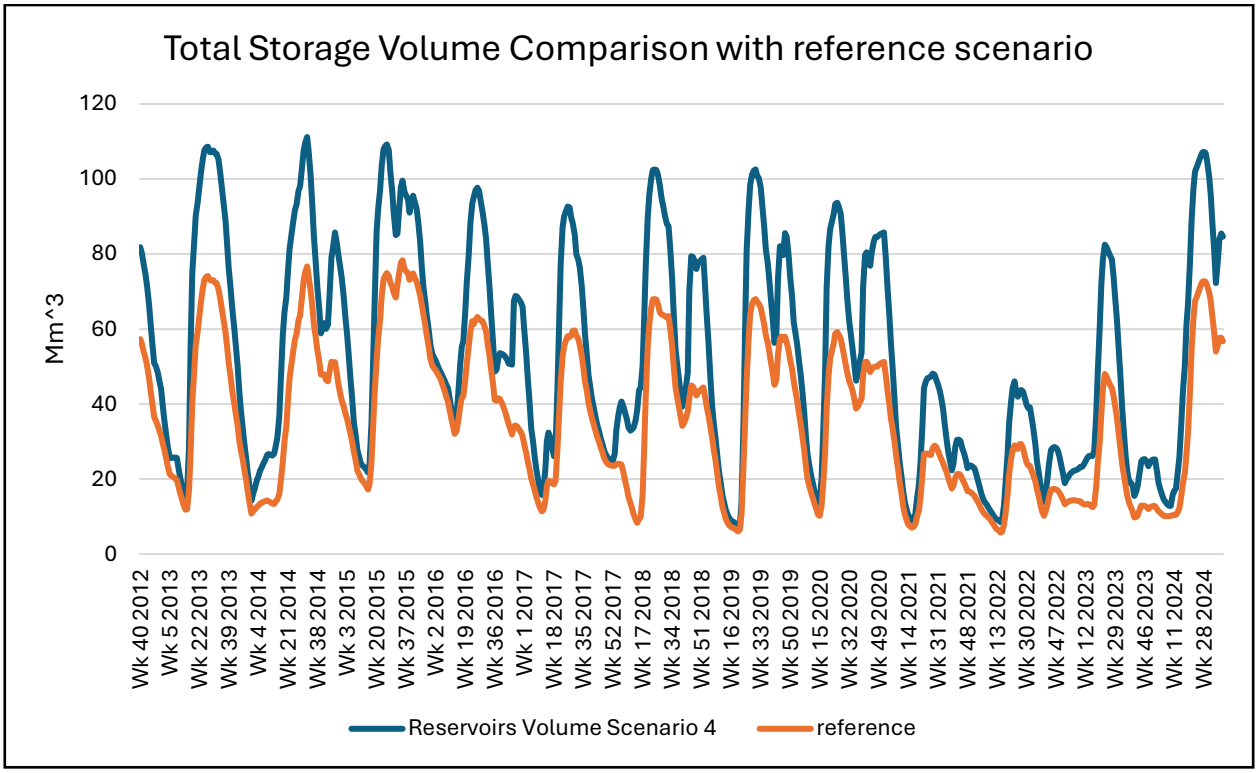


*Figure 49: Total Storage Volume Comparison between scenario 4 and reference scenario.*

# 6) Conclusions

The present thesis aimed to analyze the integrated water resource management of the Orco Valley watershed, assessing the effects resulting from the introduction of new infrastructures and the impacts derived from a different configuration of the hydrological model.
In particular, the validity of an alternative representation of hydrological processes was investigated through the implementation of Hydrological Response Units (HRUs), following the methodology adopted in the SWAT model.

To this end, a representative model of the study area was developed using the WEAP software.
The main components of the basin's water system were implemented within the model, including the five principal reservoirs, the hydropower plants, and the irrigation consortia located in the downstream portion of the area.
Subsequently, following the subdivision of the territory into sub-basins, the Hydrological Response Units identified through SWAT were assigned to the respective sub-basins according to their spatial distribution.

The model calibration procedure yielded overall satisfactory results, thus providing a positive response to the research question concerning the organization of the HRUs.
However, unsatisfactory results were obtained for two snow gauging stations, while the hydrological gauge stations located along the Orco stream showed an underestimation of modeled flow rates compared to observed flows during peak periods.
With regard to reservoir volumes, the model accurately reproduces the storage dynamics of the Ceresole reservoir, without significant underestimation or overestimation of the observed volume.

The results obtained from the scenario simulations highlighted the effects generated by the introduction of new infrastructures within the study area.
The implementation of the aqueduct within the model led to an increase in total irrigation deficit, primarily affecting the Ovest Orco and Est Orco consortia, with increases of 23% and 25%, respectively, compared to the reference scenario, while the Reirola San Marco consortium was the least affected.

Conversely, the change in water allocation implemented in the third scenario resulted in a significant reduction of irrigation deficits during the irrigation season, with an overall improvement of 26.1% compared to the reference scenario.
On the other hand, the hydropower sector was particularly impacted by the change of water allocation, reporting a 13.9% decrease in total energy production over the simulation period.
The results also revealed more issues concerning the aqueduct, as the baseline deficit recorded in the previous scenario was tripled, highlighting its vulnerability during periods of severe water scarcity, such as the 2021–2023 triennium.

Finally, the impact of the new IREN reservoir along the Soana stream showed an overall improvement in the valley's conditions, both in the energy and agricultural sectors.
Specifically, an increase in energy production of 20.7% and a reduction in agriculture unmet water demand of 14.2% were observed.
Nevertheless, the energy production of the new dam remains limited by the low available hydraulic head.
The results obtained demonstrate that the introduction of a new reservoir would contribute to a more effective management of water resources within the study area.

However, the hydrological model developed for this work presents several limitations, mainly related to the data collection process used for the simulations. The principal critical issues concern the lack of data about agricultural withdrawals for the downstream irrigation consortia, the presence of temporal gaps in the datasets obtained from meteorological stations and the absence of detailed information regarding the design of the new reservoir in the Soana sub-basin.

In conclusion, the results obtained demonstrate that WEAP is not only a valid support tool for the integrated analysis of water resources in complex contexts such as mountainous basins, but also an effective instrument for the preliminary assessment of the impacts deriving from the introduction of new infrastructures.

# 7) References


1. Yates, D., Sieber, J., Purkey, D., Huber-Lee, A., 2005a, *"WEAP21: A Demand-, Priority-, and Preference-Driven Water Planning Model. Part 1: Model Characteristics",* Water International, Vol 30(4), pp. 487-500;

2. Yates, D., Sieber, J., Purkey, D., Huber-Lee, A., 2005b, *"WEAP21: A Demand-, Priority-, and Preference-Driven Water Planning Model. Part 2: Aiding Freshwater Ecosystem Service Evaluation",* Water International, Vol 30(4), pp. 501-512;

3. Yates, D., 1996, *"WatBal: An Integrated water balance model for climate impact assessment of river basin runoff"*, Water Resour. Dev., Vol 12(2), pp. 121-139;

4. Sieber, J., Purkey, D., 2015, *"WEAP User Guide",* Stockholm Environment Institute, https://www.weap21.org;

5. Stockholm Environment Institute (SEI), 2023, *"WEAP Tutorial",* https://www.weap21.org;

6. Stockholm Environment Institute (SEI), 2025., Water Evaluation and Planning System (WEAP) [software], https://www.weap21.org;

7. Arnold, J.G., Kiniry, J.R., Srinivasan, R., Williams, J.R., Haney, E.B., Neitsch, S.L., 2012, "Soil & Water Assessment Tool: Input/Output Documentation, Version 2012", Texas Water Resources Institute;

8. Qgis Development Team, 2024, Qgis Geographic Information System, [software], Open-Source Spatial Foundation, https://qgis.org;

9. Regione Piemonte, n.d., Geoportale della Regione Piemonte, [Geographic dataset], https://geoportale.igr.piemonte.it;

10. Copernicus Climate Change Service (C3S), s.d., ERA5 Reanalysis Dataset, [Climatic dataset], https://cds.climate.copernicus.eu;

11. ARPA Piemonte, s.d., Banca dati storici ambientali ARPA Piemonte, [climatic dataset], https://www.arpa.piemonte.it;

12. Nistor, M.M, 2018, *"Projection of Annual Crop Coefficients in Italy Based on Climate Models and Land Cover Data"*, Geographia Technica, Vol 10(2), pp. 97-113;

13. Iren S.p.A., 2024, *"Val Soana, verificata la pre-fattibilità tecnica di un invaso ad uso plurimo"*, [press release];

14. Guyennon, N., Valt, M., Salerno, F., Petrangeli, A.B., Romano, E., 2019, *"Estimating the snow water equivalent from snow depth measurements in the Italian Alps"*, Cold Regions Science and Technology, No. 167, https://doi.org/10.1016/j.coldregions.2019.102859;

15. Smiraglia, C., Azzoni, R.S, 2015, *"Catasto dei Ghiacciai del Piemonte"*, Università degli Studi di Milano, https://sites.unimi.it/glaciol/wp-content/uploads/2019/02/3-piemonte.pdf;

16. Mercalli, L., Cat Berro, D., 2005, *"Climi, Acque e Ghiacciai Tran Gran Paradiso e Canavese"*, Ivrea, Società Meteorologica Subalpina;

17. Gray, D.M, Prowse, T.D., 1992, *"Snow and Floating Ice"*, in: Maidment, D.R. (Ed.), Handbook of Hydrology, New York: McGraw-Hill;

18. Zhen Hao, 2023, *"GDRL: Global Reservoir Area Storage-Depth Dataset through Reconstructed Bathymetry Using Deep Learning"*, https://doi.org/10.5281/zenodo.8306604;

19. Iren S.p.A., 2022, *"Impianto idroelettrico Agnel-Serrù-Villa. Rapporto di Fine Concessione-Parte seconda: Tecnico contabile. TO00003_Relazione Tecnica"*, [technical report];

20. Iren S.p.A., 2022, *"Impianto idroelettrico Ceresole-Rosone. Rapporto di Fine Concessione-Parte seconda: Tecnico contabile. TO01292_Relazione Tecnica"*, [technical report];

21. Iren S.p.A., 2022, *"Impianto idroelettrico Telessio-Eugio-Rosone. Rapporto di Fine Concessione-Parte seconda: Tecnico contabile. TO01290_Relazione Tecnica"*, [technical report];

22. Regione Piemonte, 2021, *"Regolamento regionale n. 14/R: Disposizioni per l'implementazione del deflusso ecologico"*;

23. Lucca, E., 2025, "The Water-Energy-Food-Ecosystems Nexus: concepts and application to address water scarcity in Northern Italy", PhD Thesis, Università degli studi di Firenze, Firenze;

24. Allen, R.G., Pereira, L.S., Raes, D. & Smith, M., 1998, "*Crop evapotranspiration – Guidelines for computing crop water requirements*", FAO Irrigation and Drainage Paper No. 56, Roma;

25. SMAT S.p.A., Servizio idrico integrato, [online website], 2025, https://www.smatorino.it/servizio-idrico-integrato/;

26. Regione Piemonte, Sezione Piano tutela delle Acque, 2025, https://www.regione.piemonte.it/;

27. Mekonnen, E.F., Getu, G.A., "Hydrological parameter sensitivity analysis for water evaluation and planning model calibration in the Borkena River Sub-basin", 2025, pp. 1-19, https://doi.org/10.1007/s43832-025-00247-5;

28. Loucks, D.P., van Beek, E., 2017, "Water Resource Systems Planning and Management: An Introduction to Methods, Models, and Applications", Springer.

29. Young, C.A., Escobar-Arias, M.I., Fernandes, M., Joyce, B., Kiparsky, M., Mount, J.F., Mehta, V.K., Purkey, D., Viers, J.H., & Yates, D., (2009), "Modeling the hydrology of climate change in California's Sierra Nevada subwatershed scale adaptation", Journal of the American Water Resources Association, Vol 45(6), pp. 1408-1423, https://doi.org/10.1111/j.1752-1688.2009.00375.x;

30. Ministero dell'Ambiente e della Sicurezza Energetica (2018). *Portale delle Valutazioni Ambientali – Scheda progetto ID 1732*. https://va.mite.gov.it/it-IT/Oggetti/Info/1732

31. Società Meteorologica Italiana, *"Il ghiacciaio Ciardoney"*, Nimbus, https://www.nimbus.it/moncalieri/ciardoney/ciardoney_ghiacciaio.htm;

# 8) Initial and calibrated parameters

| CROP COEFFICIENT (Kc) | | | | | | |
|---|---|---|---|---|---|---|
| ***Soil Use*** | ***Initial*** | | | ***Calibrated*** | | |
| | ***Kin*** | ***Kmed*** | ***Kend*** | ***Kin*** | ***Kmed*** | ***Kend*** |
| AGRL | 0,5 | 1,1 | 0,6 | 0,5 | 1,1 | 0,6 |
| BARR | 0,4 | 0,6 | 0,5 | 0,44 | 0,66 | 0,55 |
| FRST | 0,35 | 0,55 | 0,4 | 0,4025 | 0,6325 | 0,46 |
| RNGE | 0,7 | 0,7 | 0,7 | 0,805 | 0,805 | 0,805 |
| SWRN | 1 | 1 | 1 | 1 | 1 | 1 |
| URMD | 0,3 | 0,3 | 0,3 | 0,33 | 0,33 | 0,33 |
| WATR | 1,2 | 1,2 | 1,2 | 1,08 | 1,08 | 1,08 |

*Table 26: Initial and calibrated values for crop coefficient used in the model. The initial values are taken from Nistor (2018).*

| ***Soil Use*** | ***Reference RRF*** | ***Calibrated RRF*** | ***Slope (%)*** | ***Multiplying factor*** |
|---|---|---|---|---|
| AGRL | 8 | 12 | 0-10 | 1 |
| BARR | 4 | 6 | 10-20 | 0,8 |
| FRST | 20 | 28 | 20-25 | 0,6 |
| RNGE | 10 | 18 | 25-30 | 0,5 |
| SWRN | 4 | 3 | 30-35 | 0,4 |
| URMD | 4 | 3 | 35-50 | 0,25 |
| WATR | 1 | 1 | >50 | 0,1 |

*Table 27: Initial RRF taken from Young et al. (2009) and calibrated RRF.*

| Soil Water Capacity (Sw) | | | |
|---|---|---|---|
| **Soil type** | **Unit** | **Initial** | **Calibrated** |
| L | mm/time | 200 | 400 |
| CL | mm/time | 240 | 450 |
| C | mm/time | 230 | 370 |
| SL | mm/time | 150 | 320 |
| SCL | mm/time | 150 | 250 |
| SIL | mm/time | 250 | 450 |
| SICL | mm/time | 260 | 450 |
| SIC | mm/time | 260 | 490 |

*Table 28: Initial Soil water capacity values estimated from the Handbook of Hydrology (1993) and Calibrated values.*

| ROOT ZONE CONDUCTIVITY (RZC) | | | |
|---|---|---|---|
| **Soil type** | **Unit** | **Initial** | **Calibrated** |
| L | mm/time | 400 | 300 |
| CL | mm/time | 170 | 25 |
| C | mm/time | 40 | 85 |
| SL | mm/time | 1000 | 500 |
| SCL | mm/time | 230 | 120 |
| SIL | mm/time | 250 | 120 |
| SICL | mm/time | 120 | 60 |
| SIC | mm/time | 50 | 25 |

*Table 29: Initial Root zone conductivity estimated from the Handbook of Hydrology (1993) and Calibrated values.*

| **Parameter** | **Unit** | **Initial** | **Calibrated** |
|---|---|---|---|
| Deep Water Capacity (DWC) | Mm/time | 20 | 50 |
| Deep Conductivity (DC) | Mm/time | 1000 | 1500 |
| Z1 | % | 30 | 30 |
| Z2 | % | 30 | 40 |

*Table 30: Initial values defined in Sieber & Purkey (2015) and calibrated values.*

| ***Preferred flow direction (f)*** | | |
|---|---|---|
| ***Slope (%)*** | ***Initial*** | ***Calibrated*** |
| zero ten | 0,5 | 0,4 |
| ten twenty | 0,5 | 0,5 |
| twenty twentyfive | 0,6 | 0,55 |
| twentyfive thirty | 0,7 | 0,65 |
| thirty thirtyfive | 0,8 | 0,8 |
| thirtyfive fifty | 0,9 | 0,9 |
| fifty more | 0,95 | 0,95 |

*Table 31: Initial values estimated for preferred flow direction and calibrated values.*

# 9) Hydropower energy comparison between modeled and data records provided by Iren

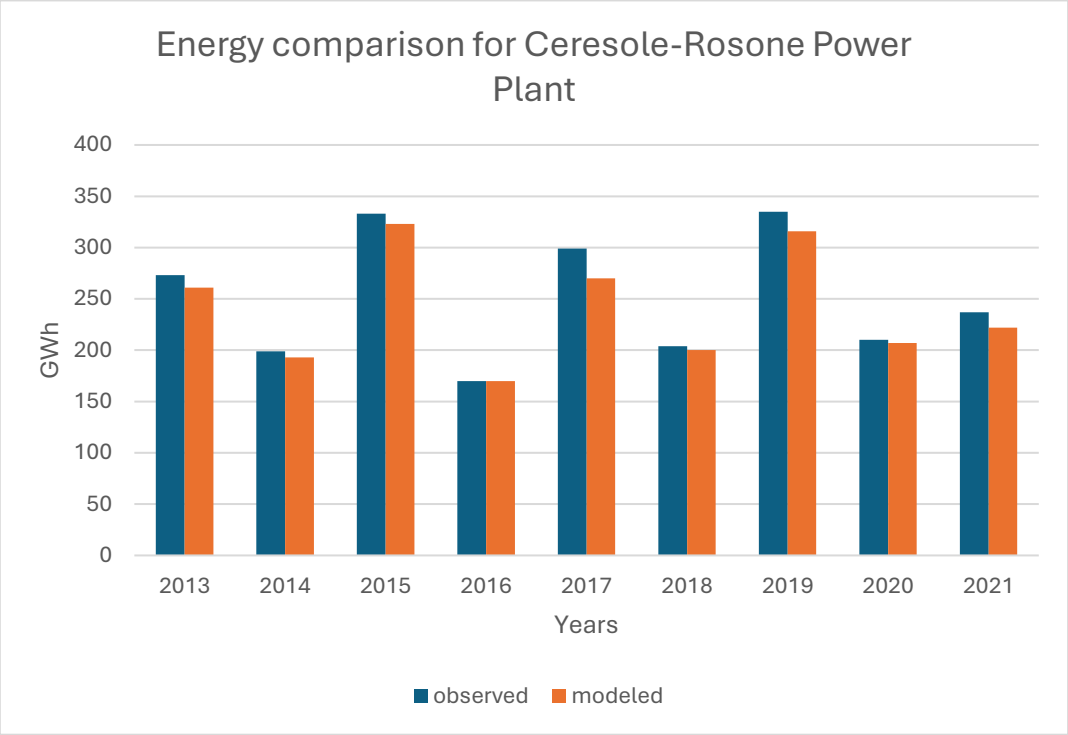


*Figure 50: Comparison between modeled and observed hydropower data recorded by Iren S.p.A. (2022) for Ceresole-Rosone Power Plant.*

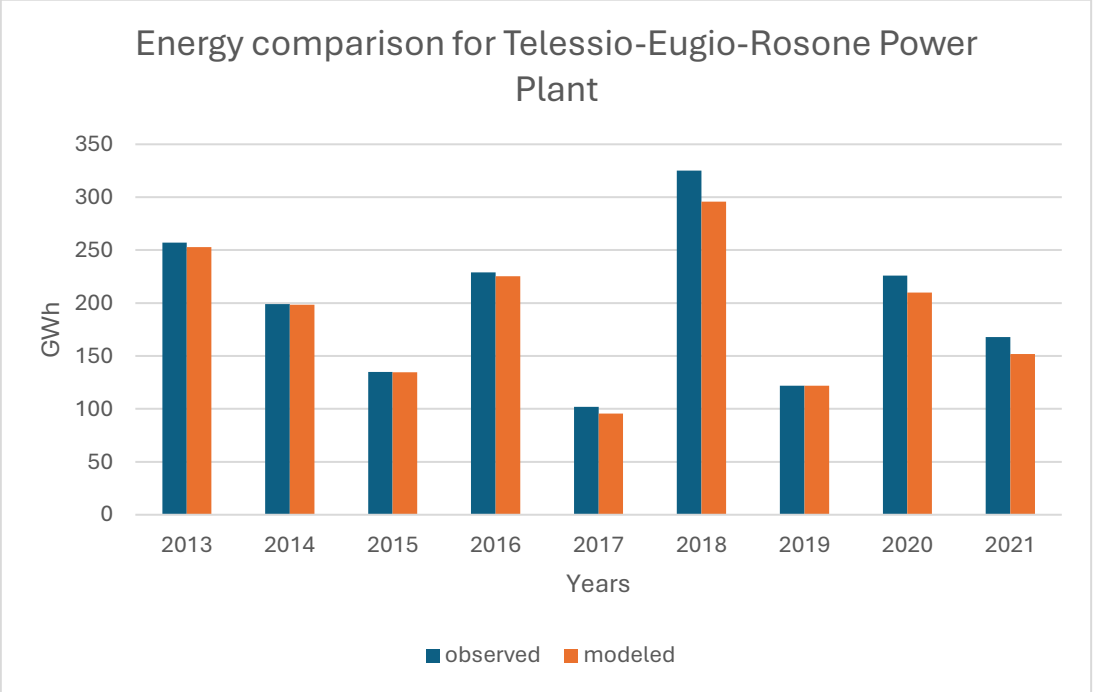


*Figure 51: Comparison between modeled and observed hydropower data recorded by Iren S.p.A. (2022) for Telessio-Eugio-Rosone Power Plant.*

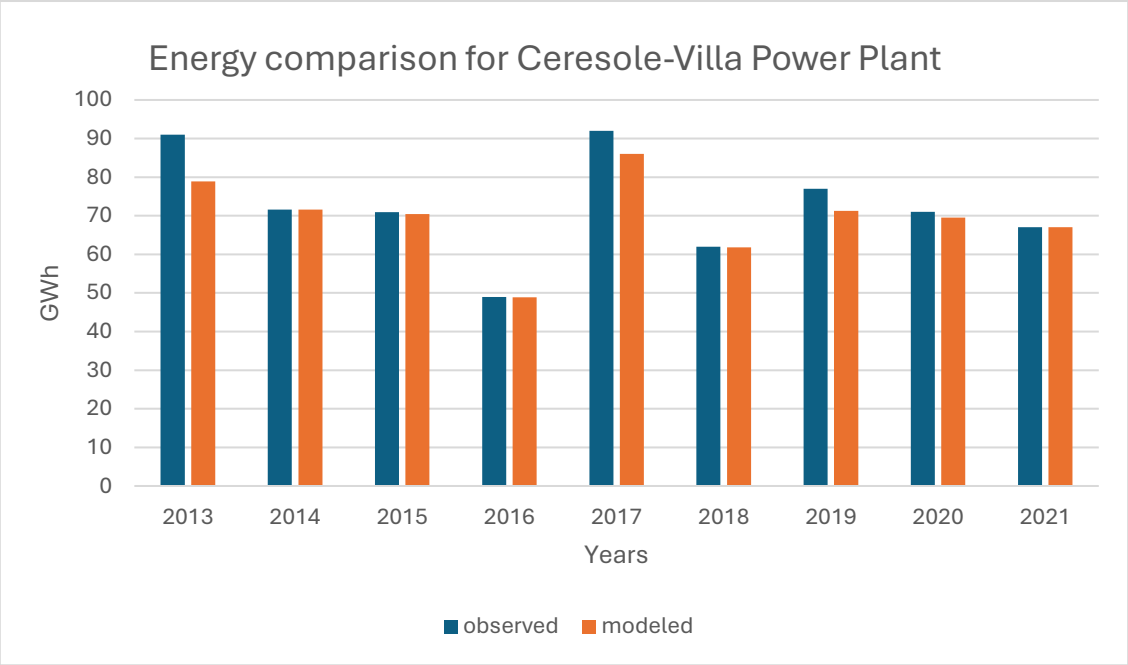


*Figure 52: Comparison between modeled and observed hydropower data recorded by Iren S.p.A. (2022) for Ceresole-Villa Power Plant.*